INTERMEDIATE STABLE PHASE LOCKED STATES IN OSCILLATOR NETWORKS

by

Alexander Darius Urban

Submitted to the Graduate Faculty of
the Department of Physics and Astronomy in partial fulfillment
of the requirements for the degree of

Doctor of Philosophy

University of Pittsburgh

2011

UNIVERSITY OF PITTSBURGH

DEPARTMENT OF PHYSICS AND ASTRONOMY

This dissertation was presented

by

Alexander Darius Urban

It was defended on

July 21th

and approved by

G.Bard Ermentrout, Deparment of Mathematics

David Jasnow, Department of Physics

Rob Coalson, Department of Physics

Joe Boudreau, Department of Physics

Xiao-Lun Wu, Department of Physics

Dissertation Director: G.Bard Ermentrout, Deparment of Mathematics

INTERMEDIATE STABLE PHASE LOCKED STATES IN OSCILLATOR NETWORKS

Alexander Darius Urban, PhD

University of Pittsburgh, 2011

The study of nonlinear oscillations is important in a variety of physical and biological contexts (especially in neuroscience). Synchronization of oscillators has been a problem of interest in recent years. In networks of nearest neighbor coupled oscillators it is possible to obtain synchrony between oscillators, but also a variety of constant phase shifts between 0 and π. We coin these phase shifts *intermediate stable phase-locked states*. In neuroscience, both individual neurons and populations of neurons can behave as complex nonlinear oscillators. Intermediate stable phase-locked states are shown to be obtainable between individual oscillators and populations of identical oscillators.These intermediate stable phase-locked states may be useful in the construction of central pattern generators: autonomous neural cicuits responsible for motor behavior. In large chains and two-dimenional arrays of oscillators, intermediate stable phase-locked states provide a mechanism to produce waves and patterns that cannot be obtained in traditional network models. A particular pattern of interest is known as an anti-wave. This pattern corresponds to the collision of two waves from opposite ends of an oscillator chain. This wave may be relevant in the spinal central pattern generators of various fish. Anti-wave solutions in both conductance based neuron models and phase oscillator models are analyzed. It is shown that such solutions arise in phase oscillator models in which the nonlinearity (interaction function) contains both higher order odd and even Fourier modes. These modes are prominent in pairs of synchronous oscillators which lose stability in a supercritical pitchfork bifurcation.

TABLE OF CONTENTS

LIST OF TABLES

LIST OF FIGURES

PREFACE

I am greatly indebted to both Dr. G Bard Ermentrout and Dr. David Jasnow. Without their support this dissertation would not be possible.

I owe a debt of gratitude to all the members of my committee:
Dr. Rob Coalson,
Dr. Joe Boudreau,
Dr. Xiao-Lun Wu,

Thank you, all.

1.0 NONLINEAR OSCILLATIONS AND THEIR IMPORTANCE IN NEUROSCIENCE

1.1 INTRODUCTION

In the past few decades, neuroscientists have discovered the importance of oscillations in the brain. For example, oscillating mitral cell activity in the olfactory bulb is thought to play a role in encoding information about specific odors, and oscillating neural circuits in the motor nervous systems of animals are known to be crucial in controlling movement. [1][2]. On the smallest scale of the nervous system, individual neurons can behave as complex nonlinear oscillators[3]. On a larger scale, oscillatory patterns in EEG (electroencephalographic) recordings have been shown to correspond to different cognitive states[3]. Oscillations most likely play an integral and indispensable role in normal brain function and even cognition. Gyorgy Buszaki noted that "oscillation based synchrony is the most energy efficient mechanism to temporally coordinate different parts of the brain"[3]. Thus, understanding networks of nonlinear oscillators lies at the forefront of current neuroscience research. Networks of nonlinear oscillators are described by systems of coupled first-order differential equations. This work is an exploration of different possible solutions to these equations based on the network connectivity and parameters which effect the intrinsic dynamic properties of each oscillator. Despite the emphasis on oscillations in neural models, many of the results of this dissertation can be generalized to any oscillatory network or nonlinear oscillator and may be applicable to more "traditional" systems found in physics such as networks of Josephson junctions, and oscillations in the luminosity of stars[4][5].

This first chapter is an introduction to the ideas and concepts from nonlinear dynamics and neuroscience that I will refer to throughout the rest of the dissertation. The first section

begins with some examples of nonlinear oscillations in physical systems, followed by a discussion of the two major types of neural models used in subsequent chapters. The theory of weakly coupled oscillators will be presented: this theory is one of the most widely used in the study of nonlinear oscillators. It involves condensing large systems of differential equations describing oscillations into one equation describing the phase of an oscillation. Finally, the last section of this chapter is dedicated to the experiments motivating our model networks.

1.1.1 Terminology

Imagine a typical harmonic oscillator with a weak nonlinear forcing (or damping) term that is described by the second order differential equation[1]:

$$m\ddot{x} + kx = \epsilon f(x, \dot{x}, \epsilon). \tag{1.1}$$

The solution to this equation is similar to that of a simple harmonic oscillator except the phase and amplitude vary slowly relative to the frequency of oscillation,

$$x(t) = A(\epsilon t)\cos(\omega t - \theta(\epsilon t)). \tag{1.2}$$

This oscillation consists of "two scales", the time scale of the slowly varying phase and the time scale of the oscillation. (in this equation $\tau = \epsilon t$ is referred to as slow time). Now, imagine that we have two such oscillators:

$$\begin{aligned} x_1 &= A(\tau)\cos(\omega t + \theta_1(\tau)) \\ x_2 &= A(\tau)\cos(\omega t + \theta_2(\tau)). \end{aligned} \tag{1.3}$$

In these equations, $\theta_{1,2}$ are phase shifts. If $\theta_2 - \theta_1 = constant$, then the oscillators are said to be "phase-locked" or "synchronous"[6]. In the event that $\theta_2 - \theta_1 = 0$, the oscillators are synchronous "in-phase". If $\theta_2 - \theta_1 = \pi$ then the oscillators are synchronous anti-phase. There is a third possibility, that is: $0 \leq \theta_2 - \theta_1 \leq \pi$. In this case, we say that the system

[1] In this equation ϵ is considered to be very "small".

is in an "intermediate stable phase-locked state". We are interested in intermediate stable phase-locked states because they can lead to interesting patterns of wave activity in networks that are not obtainable with the other types of phase locking. They may also be relevant in oscillating electrical circuits known as "central pattern generators" which are found in the motor nervous systems of many animals [1][7][8][9][10].

1.2 OSCILLATIONS ON MULTIPLE TIME SCALES

One of the defining features of many nonlinear oscillations (especially those found in neurons) is that they are generated by variables which evolve on different time scales. Relaxation oscillations are a prime example of this behavior and occur in systems in which there are at least two variables which operate on different time scales. That is, these systems of differential equations possesses both a "slow" variable and a "fast" variable. They are so named because normally there is a slow build up (like the membrane potential to threshold) followed by a sudden release, e.g., firing an action potential.

Consider the trajectory of a simple harmonic oscillator in phase space (the position vs. the velocity): the trajectory forms a closed circle. A closed trajectory is known as a *limit cycle* in dynamical systems theory, and it implies periodic behavior. In fact, when dealing with more complex systems, limit cycles can take on many complex shapes. For instance, the limit cycle of a relaxation oscillation consisting of two variables may appear more rectangular than circular due to the slow and fast branches of the trajectory which characterize its behavior. Consider a particularly simple example from mechanics: a bouncing ball between two walls. The ball's motion between the walls can be described by well known kinematics equations. However, when the ball reaches the walls, the velocity of the ball changes very abruptly. If one plots the trajectory of the system in phase space, it is roughly a rectangle. There is a point at which the acceleration appears to become infinite as the ball rapidly changes direction[11]. In fact one may analyze the system as if it were discontinuous[11]. This seemingly discontinuous or shock trajectory is the hallmark of the relaxation oscillation. Figure 1.1 illustrates non-sinusoidal limit cycle behavior in two different systems of differential equations. Figure 1.1 A

describes the Van der Pol oscillator which was introduced to describe oscillations in vacuum tube circuits[12][2]. Figure 1.1 B is a plot of the limit cycle of the Fitzhugh-Nagumo equations, which are a simplified description of oscillations in the membrane potential of a neuron derived from the Hodgkin-Huxley model (to be described in subsequent sections) [13][14]. It should be emphasized that the oscillations studied in this dissertation are not relaxation oscillations, in the sense that relaxation oscillations often exhibit shock-like behavior[3]. I am merely using relaxation oscillations as an example to demonstrate limit cycle behavior in nonlinear systems which is far from sinusoidal. Complex limit cycle behavior appears in a variety of research areas. Some of the more "modern" examples include oscillations in the luminosity of a star,[5] and oscillations in the intensity of a Raman or Brillouin scattered beam of light[15]. In neurons the fast and slow variables which describe complex nonlinear oscillations (or spiking behavior in general) may represent ionic currents through the cell membrane. These currents are controlled by voltage dependent gates which open and close at different rates. A neuron can be thought of as a nonlinear RC circuit where the lipid bi-layer of the cell acts as a capacitor. The Hodgkin-Huxley model, developed in 1954 to describe this process, is a fairly complex system of ordinary differential equations [16]. Its oscillatory behavior, however, may be understood qualitatively in terms of two major currents which flow across the cell membrane. These currents are the transient sodium and persistent potassium current. The sodium current is a "fast current" while the potassium current is a "slow current". Periodic spikes in membrane potential may be understood as a feedback effect between these two currents. First, a stimulus current depolarizes the cell enough to activate the sodium current. This current flows inward and acts to further depolarize the cell. Further depolarization inactivates the sodium current and activates the outward potassium current. The cycle continuously repeats itself as sodium depolarizes the cell only to have it repolarized by potassium. This model will be discussed in more detail in subsequent sections.

[2]The red arrow in Figure 1.1 denotes the region where $\frac{dy}{dx}$ seems to change discontinuously.

[3] The Van der Pol oscillator can be seen in Figure 1.1. The red arrow denotes the region where $\frac{dy}{dx}$ "seems to" change discontinuously (e.g., a shock).

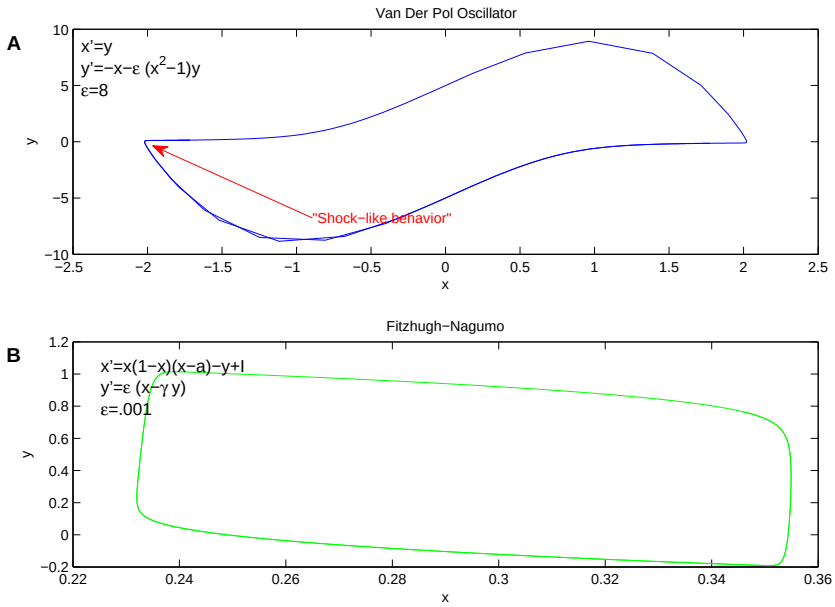

Figure 1.1: Two examples of relaxation oscillations. **A** shows a plot of a Van-Der Pol limit cycle. The equations are listed in the upper left hand corner. I chose ϵ to be large so that the system was strongly nonlinear. **B** is a plot of the phase portrait of the Fitzhugh-Nagumo system. It is a system of two equations which describe oscillations in the membrane potential of a neuron. Again, the equations are in the upper left corner of the plot. In this case, the two time scales are readily apparent from the sharp corners of the limit cycle: y is the "slow" variable.

1.3 DYNAMICAL SYSTEMS IN NEUROSCIENCE AND OSCILLATIONS IN THE BRAIN

One of the basic postulates of theoretical neuroscience is that the nervous system can be organized into interacting units. The architecture in these units is similar across many different speciesRevModPhys. In the late nineteenth century Ramon Cajal devised the neuron doctrine, essentially stating that the nerve cell is the fundamental unit of information signaling and processing in the nervous system [17]. Each nerve cell receives input from hundreds of other sources and these inputs are integrated at the axon hillock to produce the *action potential*. The action potential is the fundamental mechanism by which information is transmitted across the network. Once an action potential is generated, the disturbance travels down the axon of the neuron terminating at the synapse where it causes the release of various neurotransmitters. Neurotransmitters diffuse across the synaptic cleft to affect the post-synaptic neuron. Interactions between neurons can be classified as either *excitatory* or *inhibitory*. When one cell excites another it tends to depolarize the post-synaptic cell's membrane. When a presynaptic cell inhibits the post-synaptic cell, it hyper-polarizes the cell membrane. Strictly speaking, the type of interaction produced by the synaptic potential is not determined by the type of neurotransmitter released by the previous cell but rather is determined by which ion channels are gated by the post-synaptic cell [17]. Nonetheless, we can speak in general of two types of synapses. If the synapse releases the neurotransmitter glutamate, it is said to be *excitatory*. If the synapse releases the neurotransmitter gaba it is said to be *inhibitory*. There is also a third type of coupling known as a *gap junction*. A gap junction is equivalent to an ohmic link in circuit theory. It is essentially a channel connecting the cytoplasm of the two cells[17]. The potential difference between cells drives a current. In this section I will introduce two models for describing neurons and neuronal networks. Each class of models represents a different approach towards the study of neural systems[18]. The first class of models that we examine are *firing rate models* which represent a coarse-grained approach to network modeling. Firing rate models are probabilistic descriptions of neuronal

activity in a recurrent network[4].

The second group of models we examine are *conductance based* models. Conductance based models are more realistic in the sense that they provide a much more detailed description of the dynamics of an individual neuron in terms of the various voltage gated ion channels and currents which produce an action potential. The specific conductance based model that is used in this dissertation is the Wang-Buszaki model, which is derived from the Hodgkin-Huxley model[19].

1.3.1 The Ermentrout-Cowan model

Today, many theoretical neuroscientists believe that the brain encodes information in terms of the firing rates of populations of neurons. In order to determine these firing rates, experimentalists study the response of neurons to various stimuli. There are several methods to model and describe firing rates or neural activity. Neurons and neural systems in general are highly variable, meaning that even under carefully controlled experiments, the response of an individual cell varies from one trial to the next. Thus, many neural systems can at best only be described probabilistically. The ultimate goal of many experiments is to infer a stimulus and response probability distribution. A common measure used in neurophysiological experiments is the peri-stimulus response histogram (PSTH)[18][20]. The PSTH is essentially a cross-correlation between the stimulus spike train and the response spike train. The histogram is centered at the onset of the stimulus. The PSTH is calculated by defining time bins Δt. One then takes all possible combinations between stimulus and response spikes and computes the time differences between them. The results are binned appropriately [20][16]. The PSTH tells us the firing probability per unit of time. By computing the PSTH we are computing a transfer function relating the presynaptic stimulus with the probability of a post-synaptic spike. Thus, the firing rate is a probabilistic description of a neural response. There are several approaches to formulating firing rate models. One of the most famous was used by Wilson and Cowan in their 1973 paper[21]. The second model which is the model

[4]A recurrent network is one which possesses feedback connections between neurons in the network. The synapses of an individual neuron can project in any direction. This is in contrast to a *feed-foward* network, in which the synapses project in only one direction.

used in this dissertation, was derived by Ermentrout in 1980[22]. In the Ermentrout-Cowan approach, measuring the PSTH is central to formulating a firing rate model that describes a particular neural system [18]. The Wilson-Cowan derivation is slightly different and rests on measuring the distributions of firing thresholds in a neural population[21]. In the end, the results of the two derivations are almost identical; both approaches yield a system of differential equations describing the probability that a neuron is active at time t. Before discussing the derivation of the Ermentrout-Cowan model, I want to introduce some of the major assumptions in the Wilson-Cowan model as they are relevant to the Ermentrout-Cowan model as well. The Wilson-Cowan models are a caricature of a real neural system. In deriving this model vast simplifications are made. Nonetheless, even the simplified model can produce some very important features such as oscillations and hysteresis, which they presented as a mechanism for short term memory [21].Their derivations begin by comparing the human cerebral cortex to lower species, noting that the primary difference is not the thickness of the cortex, but rather, the increased surface area of the cortex. This observation leads to the hypothesis that computations are carried out on two dimensional sheets. In fact, Wilson and Cowan opine that the brain as a whole may be thought of as "a complex hierarchy of two dimensional neural sheets"[21]. There are several major assumptions that are used in the Wilson-Cowan model. One of the most important assumptions is the idea that even though the response of individual neurons is highly variable, the overall architecture is highly redundant. Since there exist nearly identical layers in the brain, the redundancy in the overall brain leads to reliability in "computations". Thus, although area provides "computational power", thickness provides reliability. Additionally, they assume that the cerebral "sheet" is isotropic and homogeneous and that neurons summate input linearly. In many neural systems, the assumption of linear summation is completely unrealistic but it makes the problem tractable. Finally, they assume that coupling is weak. A large number of pre-synaptic neurons firing simultaneously are needed in order to excite or inhibit a cell. This assumption implies that the probability distribution of the firing rates will be sharply peaked about their mean and allows us to treat the firing rate deterministically[21]. Using these assumptions, Wilson and Cowan sought to write down equations for the probability per unit time that either an inhibitory or excitatory cell is active.

Ermentrout's derivation begins by assuming that the nonlinearity as a function of the membrane potential is the firing rate (denoted x) of the post-synaptic cell:

$$\dot{x} = F(V). \tag{1.4}$$

There are several differences between Ermentrout's derivation and the derivation of the original Wilson-Cowan equations. For instance, Ermentrout derives his model using discrete numbers of neurons, not neural densities in masses of tissue. Furthermore, although Ermentrout's model contains a nonlinearity similar to the Wilson-Cowan model, this nonlinearity represents the probability of firing per unit time, not the number of neurons whose membrane potentials are at or above threshold. Ermentrout's nonlinearity is directly obtainable from the PSTH and represents the cross correlation between stimulus and response[18]. Starting from equation 1.3.1, we assume that we have a network of neurons where each neuron "j" in the network, projects to neuron "i". Each time a presynaptic cell fires, it elicits a unitary post-synaptic potential in the post-synaptic cell "i". We assume that these post-synaptic potentials are summed linearly and they are represented as some exponential function or combination of exponentials such as($\nu = \nu_0 e^{(\frac{-(t-s)}{\tau})}$). Thus, the total potential is the sum of all the *unitary post-synaptic potentials*[5]:

$$V_i = \sum_j \int_{-\infty}^{t} \nu_{ij}(t-t')F(V_j(t'))dt'. \tag{1.5}$$

The right hand side was obtained by substituting equation for the firing rate. Applying our expression for firing rate yet again, we obtain:

$$x_i = F(\sum_j \int_{-\infty}^{t} \nu_{ij}(t-t')\nu_j(t')dt'). \tag{1.6}$$

Where $\nu_j(t')$ is the voltage contribution from neuron "j". We assume that the time dependence of unitary post-synaptic potentials depend only on the pre synaptic cell. Therefore, we may write:

$$\nu_{ij} = g_{ij}\nu_j. \tag{1.7}$$

[5]A unitary post-synaptic potential is the depolarization in the post-synaptic neuron due to one presynaptic neuron or one synapse. Typically it takes many unitary post-synaptic potentials to elicit an action potential.

Here, g_{ij} is the amplitude of the post-synaptic potential and will have units of volts or millivolts. In a manner identical to the previous derivation we wish to time average x_j, where x_j is the probability per unit time that the pre-synaptic cell will fire. The resulting integral

$$X_j = \int_{-\infty}^{t} \nu_j(t-t')x_j(t')dt' \tag{1.8}$$

yields the mean probability that an impulses travels from cell "j". By introducing the time averaged variables:

$$\begin{aligned} \bar{x} &= \frac{1}{\tau}\int_{-}^{t} xe^{-\frac{t-t'}{\tau}}dt' \\ \bar{y} &= \frac{1}{\tau}\int_{-}^{t} ye^{-\frac{t-t'}{\tau}}dt' \\ \tau\frac{\partial\bar{x}}{\partial t} &= -\bar{x}+x \\ \tau\frac{\partial\bar{y}}{\partial t} &= -\bar{y}+x, \end{aligned} \tag{1.9}$$

we may derive the expression:

$$\tau_i\frac{dX_i}{dt} = -X_i + F(\sum_j g_{ij}X_j). \tag{1.10}$$

This is an equation for the time averaged probability that a presynaptic neuron will fire a spike (per unit time). It could also be interpreted as the fraction of cells firing in a large aggregate. This equation is almost identical to the Wilson-Cowan equation except it does not take into account the refractory period of the cell[6]. These equations are the firing rate equations that will be used in the second chapter. For our purposes, the nonlinearity used is the sigmoidal function introduced in the Wilson-Cowan equation. The coupling matrix g_{ij} will be, generally speaking, asymmetric. There have been other attempts at modeling firing rates with symmetric coupling. Cohen, Grossberg and Hopfield examined firing rate models with symmetric coupling[22][23]. Symmetric coupling produces fixed point behavior that can be described with Liapunov functions. Hopfield actually showed that under certain constraints, his model was identical to an Ising model[22][23]. These types of networks do not concern us, since ultimately we are interested in networks which demonstrate oscillatory and

[6]The refractory period of the cell refers to a time window during which the cell membrane is hyperpolarized and action potential generation is essentially impossible

wave-like behavior. Waves are not possible with a symmetric synaptic connectivity matrix since the eigenvalues are totally real.

1.3.2 Conductance Based Models: The Hodgkin-Huxley and Wang-Buszaki models

While the firing rate models are coarse-grained descriptions of large populations, conductance based models are much more biophysically detailed and are employed to model the dynamics of single neurons in order to to understand how single neuron dynamics affect large scale network behavior. A fundamental concept employed in neural modeling is that the neuron only fires when the membrane potential is pushed above some minimal threshold due to a stimulus. Thus, by injecting a current into the neuron, the neuron switches "on". If we remove the current the neuron "switches off" and returns to a rest state. This "switching" behavior is described mathematically by bifurcation theory. Bifurcation theory is used to describe how the possible solutions to a set of differential equations change as we vary parameters in the equations. Appendix B is a review of the key ideas of bifurcation theory and a description of the three major types of bifurcations discussed in Chapters 2-4.

A neuron at rest corresponds to a fixed point or steady state solution, and spiking behavior is seen as a bifurcation from a rest state. In most neural network theories, it is assumed that the neurons operate near to a critical point (near a bifurcation)[6]. Thus as we vary some parameter such as a stimulus current, there is a qualitative change in the overall network behavior [6]. In the neuron models which we study, the rest state can lose stability in one of two ways, a Hopf bifurcation or a saddle-node bifurcation. A neuron model whose rest state loses stability in a saddle-node bifurcation is referred to as a type I neuron. A neuron whose rest state loses stability in a Hopf bifurcation is referred to as a type II neuron. The manner in which the resting state of these models lose stability tells us about the resulting subthreshold dynamics in the spiking neuron. These subthreshold dynamics are very important in determining the manner in which the neuron integrates and processes input. The type I neuron is known as an integrator. The action potentials generated from this model are characterized by an exponential decay to rest. If two or more pulses perturb

the neuron with a high enough frequency (if the pulses are spaced closely enough), the neuron will fire. Thus, it "integrates" the signal of unitary post-synaptic potentials. By comparison, the type II neuron is known as a resonator. The subthreshold dynamics of the resonator exhibit oscillatory behavior. This system is more easily perturbed by a neuron firing at the same frequency as its subthreshold oscillation. A major feature of a type I neuron is that it can generate action potentials at arbitrarily low frequencies. The amplitude for a type I neuron, however, is relatively fixed. The frequency of firing is dependent on the magnitude of the current stimulus. This is in contrast with type II neurons, which tend to generate spiking behavior in a well defined frequency band. The amplitude of a type II neuron, however, can be arbitrarily small[6]. Some examples of type I neurons are the Wang-Buszaki model and the Conner-Stevens model[19][6]. Examples of type II neurons are the Hodgkin-Huxley model and the Morris-Lecar model[16][6][24]. The Hodgkin-Huxley model was first devised in 1952 by Alan Hodgkin and Andrew Huxley. It is a system of four equations describing the membrane potential of a neuron (originally a giant axon of a squid) in terms of three membrane currents: a persistent potassium current, a transient sodium current and a leak current[16][6].

1.3.3 Generation of Action Potentials

The resting membrane potential of the Hodgkin-Huxley system is normally taken to be $-65mV$ and one can make the mechanistic analogy that this resting potential is the "center of mass" of the conductances[6]. When a neuron is in a resting state, the outward potassium current and inward sodium current balance each other out . The potassium has a larger conductance, hence the center of mass lays towards its reversal potential. Action potential generation is the result of a positive feedback affect between the membrane potential and the sodium and potassium conductances. As the membrane potential rises, the sodium conductance increases, in turn increasing the inward sodium current flow. This current causes the membrane potential to rise further. The process continues until the slower potassium current gate turns on and increases the outward conductance. At this point, h, the inactivation gate for sodium, becomes inactivated ($h \to 0$) , switching off the sodium current. The potassium

current repolarizes the cell membrane. The h gate deinactivates and the cell membrane is now at a potential of $-65mV$ and is ready to fire again.

1.3.4 Generation Of Action Potentials Through Post-Inhibitory Rebound

A second mechanism for producing action potentials in a neuron or oscillatory behavior is post-inhibitory rebound. This behavior is important in some circuits responsible for locomotion in animals, which form the experimental motivation for the models presented in Chapter 2 [1][25][26][27]. Post-inhibitory rebound occurs when a neuron generates a spike after a hyper-polarizing current is removed. Many models, including the Hodgkin-Huxley model can exhibit post-inhibitory rebound. Wang and Rinzel [26] developed a minimalist model of a two neuron network exhibiting excitation by post inhibitory rebound. Furthermore, using this model, they distinguish two mechanisms by which a neuron may be excited through hyper-polarization. These mechanisms are known as *release* and *escape*. The minimalist model for post-inhibitory rebound consists of only two neurons coupled through inhibitory synapses. The synaptic current to cell i from cell j is represented as $-g_{syn}s_{\infty}(v_j)(v_i - v_{syn})$. The dynamics of each individual neuron are described solely through two currents, a leak current and a *depolarizing rebound current*[26]:

$$I_{pir} = gm_{\infty}^{3}(v)h(v - v_{pir}). \tag{1.11}$$

The activation and inactivation variables (m and h, respectively) are the same as in the Hodgkin-Huxley model[7]. In order to understand the *release* mechanism, consider the cells to be initially at rest. First, cell 1 receives a depolarizing initial "kick". As the cell is excited it will inhibit cell 2. As cell 2 is hyper-polarized the inactivation gate h will become deinactivated. Thus, I_{pir} (1.11) switches on to counter the inhibiting synapse. The greater the hyper-polarization, the greater h ($h \to 1$) and the larger the current. As the excitatory impulse in cell 1 decays, the synapse to cell 2 begins to switch "off" and V_2 climbs towards its rest state. The key mechanism in generating the subsequent action potential in cell 2

[7]These variables describe the probability that the ion channel gates are opened or closed. The equations describing these variables for the Wang-Buszaki model are listed in AppendixA or may be found in many textbooks such as [6]

is the synaptic threshold. The synaptic threshold θ_{syn} must be slightly more negative than the resting potential. In other words, the synapse abruptly turns off before h reaches 0. There is a time lag between the synapses turning off and I_{pir} turning off. I_{pir} pushes V_2 above the resting state at which point the activation gate m opens. Once this gate opens, the membrane quickly depolarizes and an action potential is generated. As cell 2 is excited, it inhibits cell 1 and the cycle repeats itself. The *escape* mechanism for post inhibitory rebound is somewhat more straightforward. It occurs when I_{pir} is sufficiently large it will overcome the synaptic current completely, quickly depolarizing the cell and producing an action potential[26].

1.4 WEAK COUPLING THEORY AND AVERAGING

We want to study oscillations in networks of both the conductance based model neurons as well as the firing rate models. Modeling these networks involves solving large numbers of differential equations. Analysis of these equations can be difficult. Weak coupling theory allows us to condense large systems of equations, which describe one oscillator, into one equation describing only the phase of the oscillation. This is extremely useful if one is interested in the relative timing between firing neurons. The theory of weakly coupled oscillators rests on two major assumptions. First, for the purpose of this dissertation, we assume that all oscillators are identical. The second assumption made is that the coupling between oscillators is sufficiently weak such that the coupling acts only to slowly shift the phase of each oscillator, not affecting the amplitude or frequency. This assumption is not bio-physically unrealistic. Its use in neural network theory has historically been motivated by two papers [6]. The first study, by McNaughton et al.[6][28] dealt with the synaptic efficacy of granule cells in rat *fascia dentata*. The authors wanted to study both the size of the post-synaptic potential elicited by a single presynaptic neuron and also the nonlinear summation of the contribution of all the presynaptic neurons in the net post-synaptic potential. The major question that was addressed was the number of synapses had to be active in order to initiate a granule cell discharge. The granule cells in question had a resting potential of

-69.0 millivolts ± 8.0 millivolts and requires a total post-synaptic potential of -24.0 ± 9.0 millivolts above the resting potential in order to generate a action potential. It was found that the average extracellular post-synaptic potential elicited by one presynpatic fiber was approximately 0.1 millivolts. Dividing the threshold value by this post-synaptic potential results in an estimate of the minimum number of presynaptic neurons needed to activate one granule cell (approximately 240). In fact, due to nonlinear summation effects the number or presynaptic neurons is closer to 400. A somewhat more recent study by Sayer et al [29][6] studies synaptic efficacy between CA3/CA1 pyramidal neurons in guinea pig hippocampal slices. In this study seventy one unitary post-synaptic potentials were recorded: the mean amplitude of the post-synaptic potential was 0.131 millivolts. These studies seem to indicate that the use of weak coupling theory is justified at least in some neural systems.

The method of reducing a system of differential equations into a phase model is essentially the same as the method of multiple scales in mechanics [30]. In the problems that we deal with we assume that only the phase, not the amplitude is time dependent. We begin by examining two weakly coupled nonlinear oscillators. Each oscillator is described by a system of first order ordinary differential equations:

$$\dot{X} = F(X). \tag{1.12}$$

Assume that there is a unique limit cycle solution; $X(t) = X_0(t)$, linearizing our system of ordinary differential equations about this limit cycle results in the equation:

$$\dot{X} = D_x F(X_0) X, \tag{1.13}$$

where $D_x F(X_0) X$ is the Jacobian matrix evaluated at the limit cycle solution. There exists an adjoint linear ordinary differential equation which satisfies:

$$\dot{X}^* + D_x F(X_0)^T X^* = 0. \tag{1.14}$$

If we define the operator $L^\dagger = \frac{d}{dt} + D_x F(X_0)^T$, we then see immediately that the adjoint X^* lies in its null space of $L^\dagger X^* = 0$. Next we couple two identical systems together:

$$\dot{X} = f(X) + \epsilon G(X, Y), \tag{1.15}$$

$$\dot{Y} = f(Y) + \epsilon G(Y, X). \tag{1.16}$$

$$\tag{1.17}$$

Here $G(x, y)$ is a coupling term. The effect of the coupling term is to introduce a time dependence in the phase of oscillation. This phase is slowly varying. We represent the solutions to each system as asymptotic expansions to first order:

$$\begin{aligned} X(t) &= X_0(t + \theta(\tau)) + \epsilon X_1(t) + ... \\ Y(t) &= Y_0(t + \theta(\tau)) + \epsilon Y_1(t) + ... \end{aligned} \tag{1.18}$$

In most applications the first order approximation is sufficient. In fact, to go beyond a first order approximation can be extremely difficult and with no clear improvement in the accuracy of the results [30]. Substituting these expansions into our equations and grouping terms to first order one obtains:

$$LX_1 = G(X_0(t + \theta_X(\tau)), Y_0(t + \theta_Y(\tau))) - \dot{X}_0 \frac{d\theta_X}{d\tau}. \tag{1.19}$$

In order for this system to have a nontrivial solution, the right hand side must not lie in the null space of the operator. Hence the vector comprising the right hand side must be orthogonal to the null vector of the operator $L^\dagger$. This observation is known as the Fredholm Alternative theorem. If we recognize the adjoint of the homogeneous solution to be the null vector of $L^\dagger$, then take the inner product of this null vector and the right hand side of equation 1.19, we obtain the solution:

$$\frac{d\theta_X}{d\tau} = \frac{1}{T} \int_0^T X^*(t) G(X(t + \theta_X), Y(t + \theta_Y))) dt. \tag{1.20}$$

Applying the change of variables:

$$t' = t + \theta_X, \tag{1.21}$$

the right hand side of equation 1.20 becomes:

$$H(\theta_Y - \theta_X) = \frac{1}{T}\int_0^T X^*(t')G(X(t'), Y(t' + \theta_y - \theta_x)))dt'. \tag{1.22}$$

$H(\theta)$ is called the interaction function. The same argument holds for the second equation, yielding:

$$\begin{aligned} \frac{d\theta_X}{d\tau} &= H(\theta_Y - \theta_X), \\ \frac{d\theta_Y}{d\tau} &= H(\theta_X - \theta_Y). \end{aligned} \tag{1.23}$$

These equations describe the dynamics of the phases of the oscillators. Ultimately, we are interested in studying patterns of activity in a large network. To this end it is useful to write the equations for phase (1.23) as equations for phase differences between oscillators. Making a change of variables, $\phi = \theta_X - \theta_Y$ we may rewrite the above system of two equations as one:

$$\begin{aligned} \frac{d\phi}{dt} &= H(-\phi) - H(\phi), \\ \frac{d\phi}{dt} &= -2H(\phi)_{odd}. \end{aligned} \tag{1.24}$$

The zeros of the right hand side of this expression correspond to phase locked solutions. Linearizing the system about these fixed points we see that the solutions are stable provided that $H'(\phi^*) > 0$. As a simple example, consider an interaction function that can be described with only two odd Fourier modes:

$$H(\phi) = b_1 \sin(\phi) + b_2 \sin(2\phi). \tag{1.25}$$

In this case the stable phase locked solutions can be explicitly found:

$$\phi^* = arccos(\frac{-b_1}{2b_2}). \tag{1.26}$$

These solutions are plotted in Figure 1.2. As we vary the ratio $\frac{b_1}{b_2}$, any stable phase between 0 and π is possible. The inset of Figure 1.2 shows the interaction function corresponding to

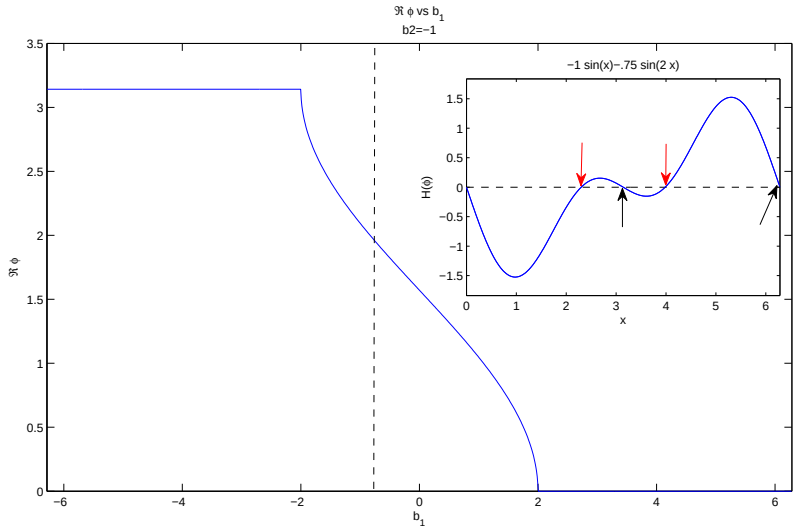

Figure 1.2: A plot of the stable phase difference between two oscillators as a function b_1, choosing $b_2 = -1$.

$b_1 = -1.0$,$b_2 = -0.75$. In order to determine the phase model describing a real neuron by experimental means, one must first compute the phase resetting curve. Consider a neuron which fires with some known period T: the phase resetting curve tells us the shift in the phase that a neuron fires in response to a stimulus. For instance, say that a neuron fires at some phase T_0 such that $V(T_0)$ corresponds to a spike. If an applied stimulus shifts this phase by ΔT , the *infinitesimal phase resetting curve* (PRC) is defined as the difference of these phases $\Delta(T) = T - T_0$. In electrophisiology experiments one can very precisely measure the voltage across the cell membrane and hence the timing between action potentials. Making the stimuli of sufficiently short duration and small amplitude one can achieve a good approximation of the (PRC) by fitting the phase data to a Fourier series. The PRC can be thought of as the sensitivity to a perturbation. As it turns out, the infinitesimal PRC is equivalent to the adjoint in equation 1.14 [31] .

1.4.1 Central Pattern Generators and the Unit CPG Hypothesis

The neurological inspiration for the analysis of oscillators in Chapters 2 and 3 is based on *central pattern generators*. A central pattern generator (CPG) is a neural circuit which is capable of producing patterns of rhythmic activity without rhythmic input. In other words, it is an intrinsically oscillating neuronal circuit.

In Chapter 2 we use central pattern generators as an inspiration for the types of firing rate models we seek to analyze. These circuits seem to be present in many species and responsible for a variety of behaviors such as breathing, flying, swimming, eating, walking, etc. There is strong evidence that in mammalian spinal cords there are various oscillating circuits that when activated coordinate muscle movements and locomotion. Grillner et al. [1] have claimed that the spinal circuits underlying locomotion in mammals can be activated even when all afferent input from higher brain regions or the body has been eliminated. It is known that oscillating activity exists in interneurons of the gray matter of the lumbar and sacral segments of higher mammals[17]. Little is known, however, about the connectivity of these circuits or how they are integrated together. The Unit Central Pattern Generator Hypothesis holds that individual central pattern generators help to make up the motor systems of various animals and that these units can be combined in such ways as to produce a large range of very complex motor behavior [1].

As a model of how central pattern generators may work in more complex mammals, many have studied the central pattern generators in the spinal cord of a lamprey (a parasitic fish). As a lamprey swims, an undulatory wave of muscle activity travels down its body. [1]. This wave of muscle contraction is generated and controlled by the central pattern generators in its spinal cord. Each half of the spinal cord can be thought of as segmented into central pattern generators. Each pattern generator is its own oscillator and initiates muscle contractions in the fish by activating a pool of motorneurons at the appropriate time. The ability of the fish to create these movements rests on the ability of the overall network to generate a variety of phase lags between consecutive central pattern generators along the length of the fish. For instance, the adult silver lamprey's spinal cord/notochord can consist of anywhere from 14 to 50 segments[25]. In each segment lies a central pattern generator which is composed of

two oscillating sub-networks. It has been shown that these oscillating circuits are connected via reciprocal inhibition through commisural interneurons[25]. Reciprocal inhibition between neurons in a central pattern generator is common. In fact, reciprocal inhibition is most likely indispensable for most central pattern generators. This statement is motivated by the simple observation that in order to execute motions such as swimming, as one set of muscles flex another group must relax. [8] As mentioned above, symmetric reciprocal inhibition has been shown to be a valid mechanism for generating anti-phase synchony between model neurons without tonic input, first by Perkel et al. [27] and then by Wang and Rinzel[26].

Initially, two hypotheses were set forth as to the nature of each central pattern generator. The first held that each oscillating subnetwork is an intrinsic oscillator. The reciprocal connections between these oscillators serve only to shift the phase of each oscillator between itself and it's contra-lateral partner. The second hypothesis holds that each segment is essentially the same as Wang and Rinzel's neurons which spike due to post-inhibitory rebound.

In lamprey, the second model may be a more accurate depiction of the CPG circuit. Buchanan showed that by hemisecting a lamprey spinal cord and showing that as the inhibitory connections were severed, the oscillations and the wave-like activity were destroyed[25]. In this experiment, there was no afferent input from the hindbrain and the entire system oscillated due to post inhibitory rebound. Despite this fact, we are still interested in autonomous oscillating circuits with reciprocal inhibition and will discuss such circuits in the next chapter. They may be a good description of a CPG in other contexts. Relatively simple examples of central pattern generators have been identified and studied in a variety of invertebrates[10][7]. Examples include the CPG which controls the *swimmerets* of the crayfish (appendages used to swim), the lobster stomatogastric system and the swimming pattern of the pteropod mollusk, *clione limancina*. The central pattern generators which control the Lobster stomatogastric system is the example which is most relevant to this dissertation. The lobster pyloric stomach undergoes a sequence of contractions lasting one second. These contractions are controlled by the bursting behavior of three groups of motoneurons PD, LP and PY. The system does not fire bursts "symmetrically"; they occur at

[8] The idea of a reciprocal inhibition model network may have originated with Brown's half centered oscillators in describing flexor/extension muscle movements [17].

$0, \pi$ and 4.89 radians of the cycle. [7]. The groups of neurons which control the CPG lie in the stromatogastric ganglion which contains roughly thirty neurons. Twelve of these neurons control the muscle contractions. The PY group contains eight neurons, the LP croup contains one neuron and the PD group consists of three neurons. [7]. This CPG may be modeled as a ring of inhibitory neurons.

1.5 CONCLUSION

This chapter introduced the importance of nonlinear oscillations in neuroscience using central pattern generators as a specific example. Both individual neurons and networks of neurons can generate a variety of complex oscillations. Many of these oscillations are similar to the classical examples of relaxation oscillators in physics. The primary mechanism for this behavior is the interplay of inter-cellular ionic currents which operate on varying time scales. There are two primary approaches to modeling this behavior. The first modeling method involves biophysically detailed conductance-based models, while the second method utilizes a probabilistic approach to derive a firing rate model. Because of the complexity of the equations used in either of these approaches, one must effectively apply weak coupling theory to simplify the analysis. Weak coupling theory can be used to condense a large system of nonlinear ordinary differential equations describing one oscillator into a differential equation describing the phase of that oscillator. This method is extremely useful in studying networks that generate precise timing differences between periodically firing neurons. The central pattern generator hypothesis in neurobiology holds that identical oscillating circuits in the spinal cords of animals can coordinate their activity in such a way to provide a variety of precise phase lags between each unit. This mechanism allows the animal to produce extremely complex sequences of motor activity. This hypothesis, as well as the network architecture of the motor nervous systems of invertebrates and fish is used as motivation for studying coupled subnetworks of inhibitory interneurons with reciprocal coupling.

In Chapter 2 we demonstrate oscillations in such networks and show that by adjusting the relative strength of connections between two sub-networks one may obtain any stable

phase between 0 and π. Chapters 3 and 4 demonstrate similar behavior between pairs of individual Wang-Buszaki neurons by tuning various parameters which affect the excitability of the cell membrane. In Chapter 4 the effect of this phase locking in larger networks is examined and we demostrate that one can obtain unique wave patterns termed *anti-waves*.

2.0 SEQUENTIALLY FIRING NETWORKS OF NEURONS

2.1 NETWORKS OF CIRCULANTLY COUPLED INHIBITORY NEURONS

The aforementioned central pattern generators produce precisely timed periodic firing sequences through inhibitory connections. This Chapter is an examination of generic firing rate model networks which are capable of producing sequential firing behavior with purely inhibitory connections. The main idea is that we want to analyze large networks or populations of neurons which behave as single oscillators. These networks are models of the *unit central pattern generators* which were discussed at the end of Chapter 1. Since most of our analysis is based on local bifurcation theory, the reader is encouraged to refer to Appendix refbifurcations, which is a summary of the main ideas of local bifurcation theory applied to systems of ordinary differential equations. Because different elements of the oscillator fire at different times, when we couple multiple oscillators together we will be able to produce different possible stable phase relations between oscillators. The oscillators or subnetworks which we couple together are identical and known as *motifs* [32, 33]. Hence the motifs act as building blocks which combine to form the larger network. Many nervous systems (in addition to central pattern generators) can be described as repetitions of simple motifs where the large scale dynamics can hopefully be inferred by understanding the interactions between individual neurons or subnetwork motifs. We start by examining systems of circulantly coupled neurons in which each group of neurons acts as its own (autonomous) oscillator. This type of coupling scheme has application to central pattern generation in the lobster stomatogastric system and may have applications to other invertaebrates (such as leeches). Central pattern generator motifs consist of as few as three neurons which, when coupled togther, produce the correct neural activity responsible for various motions (walking, eating,

etc.) [34, 35, 36, 37] [38, 39] [35]. Although common in invertebrates, these motifs are also found in some vertebrates[40]. Our choice of motifs was based on Winnerless-competition models (WLC). Winnerless competition describes a network in which neurons fire in cyclically and firing rate of one neuron never (permanently) dominates the others. The simplest of these models uses three neurons or homogenous neural populations. These neurons have bi-directional asymmetric inhibitory coupling. Their behavior is charachterized by sequential firing of neurons, in which one neuron turns on and then off as it is inhibited by the other two neurons. Many inhibitory networks produce WLC via heteroclinic cycles. A heteroclinic cycle is formed from three saddle points whose trajectories connect the stable and unstable manifolds of each saddle. The Guckenheimer-Holmes cycle is the canonical example of heteroclinic cycles. Rabinovich et al. have successfully modeled the dynamics of the olfactory bulb using inhibitory network motifs which generate heteroclinic cycles. However, this is not the only behavior found in inhibitory WLC networks.Terman et al [41] consider a class of motifs that are also dominated asymmetric inhibition. There, they consider networks of relaxation oscillators in which, the activity of one suppresses the activity of all other cells to which it is connected. Once the active cell turns off, some other cell or cells turn on and so on. Their motifs settle into attracting periodic orbits. "Winner-take-all" (WTA) networks use symmetric coupling and thus typically demonstrate fixed point behavior. That is, all solutions flow to some fixed point where the firing rate or activity of one neuron in the network dominates the rest. In our inhibitory models however, the coupling is asymmetric or random. These types of networks are more realistic models of biological neural networks[42, 43, 33] and are capable of generating much richer behavior such as limit cycles and chaos [44]. Furthermore, the relative coupling strengths can greatly influence the behavior of the network. Asymmetric motifs which are capable of chaotic and oscillatory behavior tend to be strongly influence by weak perturbations and interactions. This is compared to a symmetric winner-take-all motif producing fixed point behavior. In this case one must have strong interactions to produce behavior which changes from the uncoupled system.

We start our study of these systems by first examining motifs of inhibitory neurons which are capable of producing sequential behavior. The goal again, is to be able to produce pairs of coupled oscillators which posses intermediate stable phase locked solutions. in order to

analyse these motifs we apply bifurcation theory to examine the behavior of full firing rate models as well as Malkin's theorem and averaging to reduce these firing rate equations to phase models[2].

2.2 PURE INHIBITORY NEURAL MODELS.

Figure 2.1 shows a pair of coupled motifs, each of which is a network of five coupled cells. Suppose, that the isolated motif produces oscillatory but not necessarily synchronous behavior. That is, say that the cells within the motif have different (perhaps just time-shifted) waveforms. Then, we can ask, what happens when the two motifs are coupled and how does the resulting dynamics depend on the choice of connections, A or B or some combination of both of them. For example, the two motifs could represent the left and right sides of a bilateral central pattern generator (as in the lamprey spinal cord) with the dashed lines representing the cross coupling. In order to address this question, we analyze the dynamics within a single motif in which all connections are inhibitory.

We look for networks whose connectivities generate stable sequential dynamics and start by examining systems whose adjacency matrices are composed of normally distributed random numbers. It can be shown that these connectivity matrices can generate periodic dynamics and how these dynamics can be understood from the eigenvalue spectra of the matrices. The second class of systems we investigate are those whose connectivity matrices are circulant. Again, we explain how these patterned matrices can give rise to sequential periodic dynamics as the coupling strength between individual cells changes. Once we understand how interesting dynamics are generated from these motifs, we focus on pairs of the three-cell circulently coupled system. This system is common in neuroscience and is the basis of many central pattern generators.

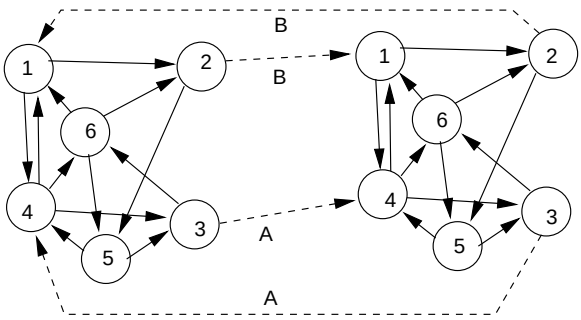

Figure 2.1: Two mutually coupled networks. Solid lines are intra-network connections and can be general. Dashed lines show two types of connections A,B which are reciprocal. Note that within the network, the coupling is "balanced": each cell receives the same number of inputs.

2.2.1 Random balanced coupling.

For ease of analysis we start by studying a simple Wilson-Cowan firing rate model where the connections between cells in each motif are are purely inhibitory. Thus each motif has the form:

$$\dot{x}_i = -x_i + F(I_i - \sum_{k=1}^{n} g_{ik} x_k), \tag{2.1}$$

where I_i is the input into the i^{th} cell, g_{ik} is the strength of interaction between cell k and cell i, and $F(u)$ is a monotonically increasing function; we will use $F(u) = 1/(1+\exp(-u))$. The coupling strengths, g_{ik} are non-negative. Even with a simple model as above (2.1) the general analysis of system is extemely difficult if not impossible if we do not make some simplifying assumptions. We assume that each network or motif is homogenous. That is, we assume that every cell recieves an identical stimulus and net connection strength is the same for each cell. Applying this condition, we say that the network is *balanced*. There are several ways to achieve balance in a network. In general a system will be balanced if the summed strength of all the inputs to a individual cell are equal.

$$\sum_{k=1}^{n} g_{ik} = g, \qquad \text{for all } i.$$

The homogeneity condition ensures that there is a unique homogeneous fixed point, $x_i = \bar{u}$ where

$$\bar{u} = F(I - g\bar{u}).$$

The network illustrated in figure 2.1 has the so-called *balanced* property. Balanced systems have been the subject of a great deal of recent work [45, 46]. In order to analyze these motifs, we want to perform a local stability analysis on our homogenous fixed point, $x_i = \bar{u}$.. We derive an expression for the eigenvalues of the system evaluated at this point as a function of two parameters. The coupling strength and the input current I. We write $g_{ik} = gG_{ik}$ where G_{ik} is now fixed and is such that $\sum_{k=1}^{n} G_{ik} = 1$. Thus, g and the input I are the two parameters in our network. The matrix entries G_{ik} are probablilities describing the presynaptic release of neurotransmitter. In other words it is the probability that the channels in the synapse is open or not.

Let $\alpha := F'(I - g\bar{u})$ where $F'(u)$ is derivative of the nolinearity F. $\bar{u}$ is itself a function of g and I: decreasing as a function of g and increasing as a function of I. Thus, α is also a function of g, I so that as g or I change, so does the parameter α. Since F is monotonic, α is always positive and is maximal at the inflection point of F. For our choice of F, the inflection point is at 0. Finally, we can always choose I so that $\bar{u}$ is at the inflection point, for our function, $I = g/2$ guarantees this feature.

With these preliminary remarks, we can write down the linearized equation

$$\dot{y}_i = -y_i - \alpha g \sum_{k=1}^{n} G_{ik} y_k.$$

Let μ_j be an eigenvalue of the matrix G whose entries are G_{ik}. Then, the eigenvalues of the linearized system above are

$$\lambda_j = -1 + \alpha g \mu_j.$$

As noted above, we can always move along a parameter path in g, I so that α is some fixed positive value. Thus, we can make the quantitity, αg as large as we would like by increasing

g and choosing I appropriately. The eigenvalues, λ_j are clearly negative for g sufficiently small.

G is the transpose of a probability matrix: all entries are non-negative and so the row sums are 1. We can conclude that the eigenvalue of G that has maximum magnitude is 1 with an eigenvector of all 1's. This gives, for the linearized system, an eigenvalue, $\lambda = -1 - g\alpha$ which is clearly negative. Let ν be the eigenvalue of G which has the most negative real part. Let us write $\nu = -r \pm i\omega$. Then as g increases, the linearized system has an eigenvalue

$$\lambda = -1 + \alpha g r - i\alpha g\omega.$$

If $g > 1/(\alpha r)$, then the real part of λ becomes positive. If this particular eigenvalue is complex ($\omega \neq 0$), then we generically expect a Hopf bifurcation to occur.

As mentioned in the introduction if the matrix, G is symmetric, then the only long-time solutions to (2.1) are fixed points. This would correspond to WTA behavior. Since we want sequential behavior, for purely inhibitory networks, we require that the matrix, G be asymmetric. This condition will be all but guaranteed using a random matrix. Using an asymmetric matrix will ensure limit cycle and possibly chaotic dynamics are possible. Figure 2.2 shows an examples of several 20×20 random matrices. Again, these the elements of these matrices are randomly chosen between 0 and 1. In general, for an $m \times m$ random matrix with entries taken from a uniform distribution and row sums normalized to 1, the $m - 1$ eigenvalues that are not 1, lie in a circle of radius $1/\sqrt{m}$ [47]. Thus, in order to get a hopf bifurcation, we need only choose those matrices whose eigenvalues with the most negative real parts are also complex. We see that in A, B, and C the eigenvalue with most negative real part is complex (red circles) while in D, the most negative eigenvalue is real. From our prior discussion, as g increases, we expect to see the loss of stability of the constant steady state via a Hopf bifurcation in examples 2.2 A,B, and C but a pitchfork bifurcation with the matrix example in D (see Appendix). The above linear theory can tell us how the homogenous fixed point looses stability and gives rise to a limit cycle. In order to actually see this behavior in the model we numerically compute a bifurcation diagram of the firing rate as a function of coupling strength g using AUTO. Figure 2.3 shows the bifurcation diagram for the system with the matrix in Figure 2.2A and $I = 20$. As predicted from the

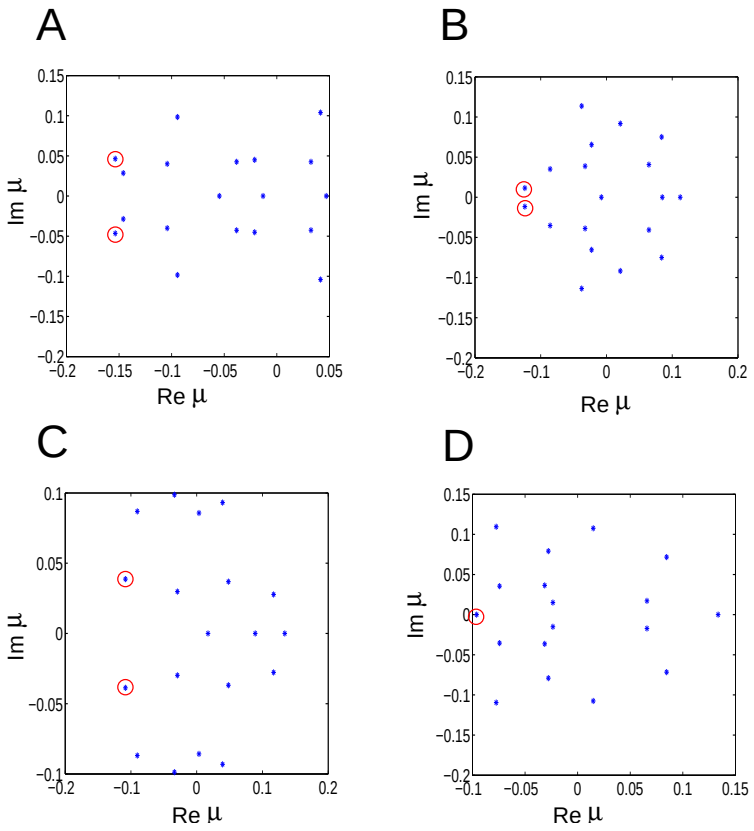

Figure 2.2: Eigenvalue spectra of several 20×20 random matrices with row sums equal to 1. In addition to the 19 eigenvalues shown, there is a simple eigenvalue, $\lambda = 1$ that is not shown. The entries of each matrix are chosen to be uniformly distributed on $(0, 1)$ and then each row is scaled so the row sum is 1.(A-D) are 4 such randomly chosen matrices.

spectrum of G, the uniform steady state loses stability through a Hopf bifurcation at a value of g near 30. There is a supercritical branch of periodic solutions that bifurcates (shown by the thick lines) which appears to terminate at a saddle homoclinic orbit. Figure 2.3C shows the frequency rapidly drops to 0 as g increases toward the homoclinic. The nearly vertical frequency drop suggests a saddle-homoclinic rather than a saddle-node on an invariant circle (SNIC) which, instead, shows a square root dependence of the frequency. Panel B shows a two-parameter diagram, that is, the curve of Hopf bifurcations as I and g covary. For quite a wide range of applied currents, we see that there is a Hopf bifurcation to periodic orbits as the linear analysis suggests. Figure 2.3D shows the projection of the trajectories of three different cells in the twenty cell network. One point that we would like to emphasize and is clear from Figure 2.3D is the sequential nature of the firing. That is, during a cycle, each of the three variables shown comes on at different phases.

Figure 2.4 shows additional bifurcation diagrams for twenty cell random networks. Figure 2.4A depicts the dynamics beyond the bifurcation for the coupling whose eigenvalue spectrum is shown in figure 2.2B. Like figure 2.3, the oscillation persists for a wide range of applied currents, I with apparently no additional bifurcations. This is in contrast to the behavior of the system whose eigenspectrum is shown in figure 2.2C and whose bifurcation diagrams are depicted in figures 2.4B-D for three different applied currents. First, we note that, as predicted from the linear theory, all three systems undergo Hopf bifurcations as the coupling strength, g is increased. However, the dynamics past the Hopf bifurcation depend very strongly on the applied current, I. When $I = 20$, then, like figure 2.4A, the oscillation persists for very large values of g, but the limit cycle undergoes some complex bifurcations for $g \approx 55$ before returning to a simple limit cycle. Choosing $I = 30, 10$ leads to dramatic differences in the global dynamics. For both $I = 10, 30$ but not, $I = 20$, the oscillation terminates at a saddle-node invariant cycle (SNIC) formed by a stable and unstable pair of fixed points (blue arrows). However, at low drive, ($I = 10$), there is a small regime of synaptic strengths where there are two small amplitude stable periodic orbits (green arrow).

Figure 2.5 shows that it is not even necessary that the initial bifurcation be a Hopf in order to get oscillatory dynamics. Figure 2.2D shows a connection matrix where the eigenvalue with most negative real part is real, so that a pitchfork bifurcation is predicted from the

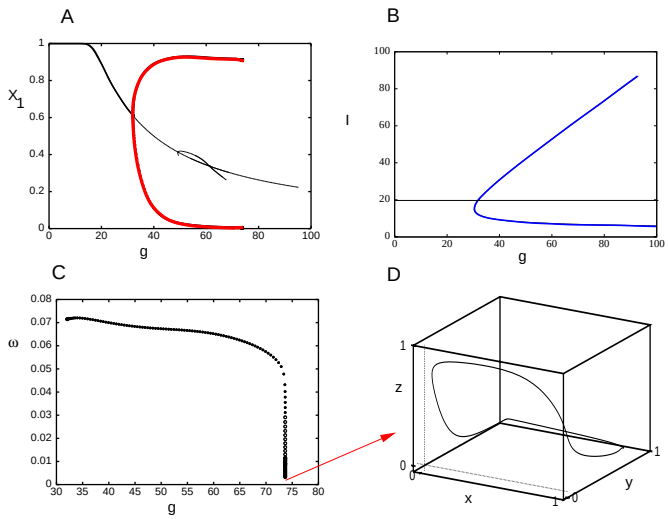

Figure 2.3: (A) Bifurcation diagram for a 20 neuron network as g varies with $I = 20$. Solid thick black line represents the symmetric stable equilibrium and red curve is the branch of periodic orbits. An unstable pitchfork bifurcation to unstable equilibria is partially shown between $g = 50$ and $g = 70$. (B) Two-parameter diagram with I and g as parameters The black line represents the parameters for (A). Blue curve is the curve of Hopf bifurcations. (C) Frequency of oscillation from (A). (D) projection of x_9, x_{16}, x_{18} near termination of the branch of periodic orbits in (C).

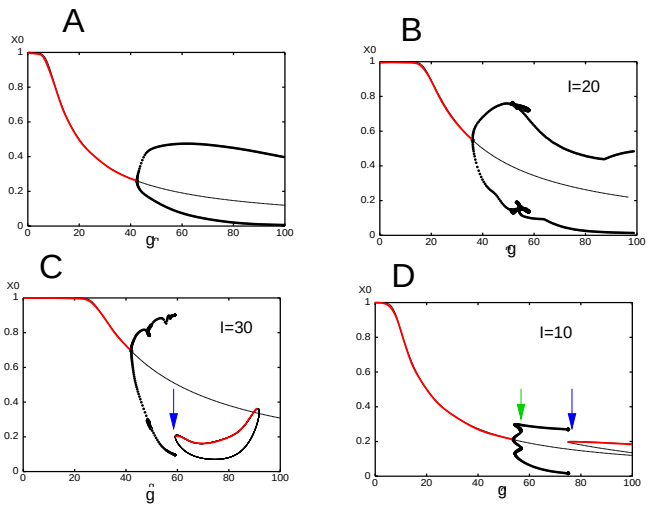

Figure 2.4: Different 20 neuron networks. (A) similar to figure 2.3 with the weight matrix from figure 2.2B; (B-D), weight matrix from figure 2.2C, with three different values of I. Red curves are stable fixed points, thin black are unstable and thick dark curves are limit cycles. Blue arrows mark SNIC bifurcations and the green arrow marks a pair of small amplitude stable limit cycles.

matrix. As can be seen in the bifurcation diagram, the uniform fixed point loses stability at a pitchfork bifurcation (a). The lower branch of fixed points undergoes a Hopf bifurcation (b) which terminates on a SNIC (c). The upper branch undergoes a Hopf bifurcation at two points (d,e). Another pitchfork emerges (f) which is unstable but the lower branch stabilizes at a saddle node (g) and produces a Hopf bifurcation (h). Thus for g between points c and h, there are three stable limit cycles. The green arrow shows the point which we will explore later in the next section as the oscillation is simple yet quite rich in structure. (By rich, we mean that it is not too close to a pure sinusoidal oscillation and has several large Fourier components.)

2.2.2 Circulant matrices.

As mentioned in the previous section, in order to get an oscillation or patterned state we assume that the coupling is asymmetric. In other words, the matix $G \neq G^T$. Another way of putting this is to say that the coupling matrix, G_{ij} is a function of $i - j$ only it is not a function of $|i - j|$. .Furthermore, for our purposes, we choose connectivity is topologically equivalent to a circle. This kind of system arises naturally in networks that have some type of spatial organization, such as the "ring model" [48]. Matrices of this form are called circulant. We write the first row of G as

$$R_1 := [a_0, a_1, \ldots, a_{N-1}]$$

and suppose that the second row is the same as the first row, shifted to the right:

$$R_2 := [a_{N-1}, a_0, a_1, a_2, \ldots, a_{N-2}].$$

We similarly shift the other rows to obtain the full matrix. For such matrices, the eigenvalues are explicitly computable:

$$\mu_k = \sum_{j=0}^{m-1} a_j e^{-2\pi ijk/m}. \tag{2.2}$$

Thus, if $a_j \neq a_{m-j}$, then we expect the eigenvalues will be complex (except, $k = 0$, the dominant positive eigenvalue). The number k is called the wave number for the eigenvalue. Figure 2.6 shows an example of the dynamics of a 20 neuron system with R_1 randomly

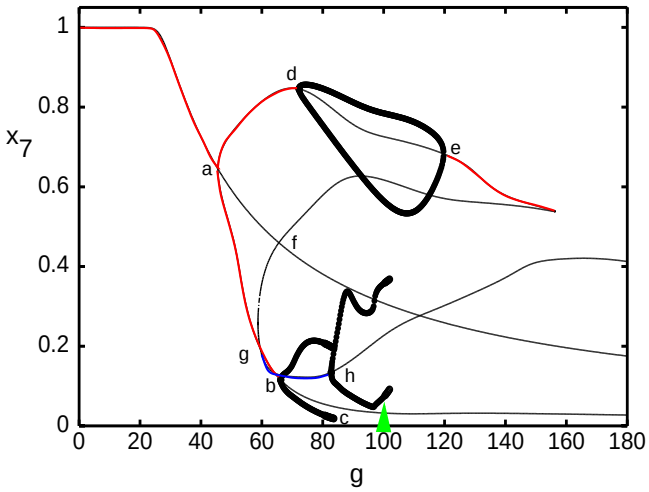

Figure 2.5: Bifurcation diagram of the system corresponding to figure 2.2D, where the first instability is at a zero eigenvalue resulting in a pitchfork (a) in the figure. Red curves are stable equilibria, thin black curves are unstable equilibria, and thick curves are stable periodic orbits. Here $I = 30$. Arrow denotes parameter used in figure 2.14.

chosen. Panel A shows the eigenvalue spectrum. The bifurcation diagram in panel B, shows a single stable branch of periodic orbits emerging from the uniform state. The pattern of oscillations is shown in 2.6C1. The spatial mode is $2\pi 3/20$, that is, $k = 3$. Since 3 and 20 are relatively prime, no two oscillators are at their maximum at the same time. The resulting pattern is a wave that has 3 oscillators near their maximum at any given time.

We are interested in sequential behavior; what we mean by this is not only that the system oscillate, but that different neurons (or groups of neurons) in our network will fire at different points in the cycle. In the example in figure 2.6C, seven groups of three oscillators occur in succession. The simplest network capable of producing sequential activity is a three cell system with a circulant coupling matrix:

$$\begin{aligned} x_1' &= -x_1 + F(I - g[ax_1 + bx_2 + cx_3]) \\ x_2' &= -x_2 + F(I - g[ax_2 + bx_3 + cx_1]) \\ x_3' &= -x_3 + F(I - g[ax_3 + bx_1 + cx_2]). \end{aligned} \tag{2.3}$$

Here a, b, c are non-negative parameters representing probabilities that a synapse is releasing neurotransmitter. Typically, we take.$0 < a < b < c$. Figure 2.7

Is the bifurcation diagram for this system. going from left to right in 3A shows that as we increase the coupling strength the homogeneous fixed point loses stability in a supercritical Hopf-bifurcation which gives rise to a branch of periodic orbits.

as we further increase the coupling strength this branch of periodics terminates in a SNIC bifurcation which gives birth to three pairs of saddles and nodes. The stable nodes correspond to states in which one of the three neurons becomes the "winner." Who becomes the "winner" depends on the initial conditions of the problem. If we tune g to a value slightly less than that neede to produce the SNIC bifurcation, we produce rich oscillations which contain many fourier components. These are contrasted with the nearly sinusoidal oscillations near the supercritical Hopf. (figure 2.7D) shows a projected orbit which illustrates how the "ghosts" of the three asymmetric fixed points perturb the original limit cycle from a pure sinusoid . (figure 2.7C) shows that as we increase g towards the SNIC bifurcation point, the period of the oscillation goes to infinity. The Frequency as a function of g has a square root shape which characterizes saddle-node on invariant circle bifurcations. The two parameter

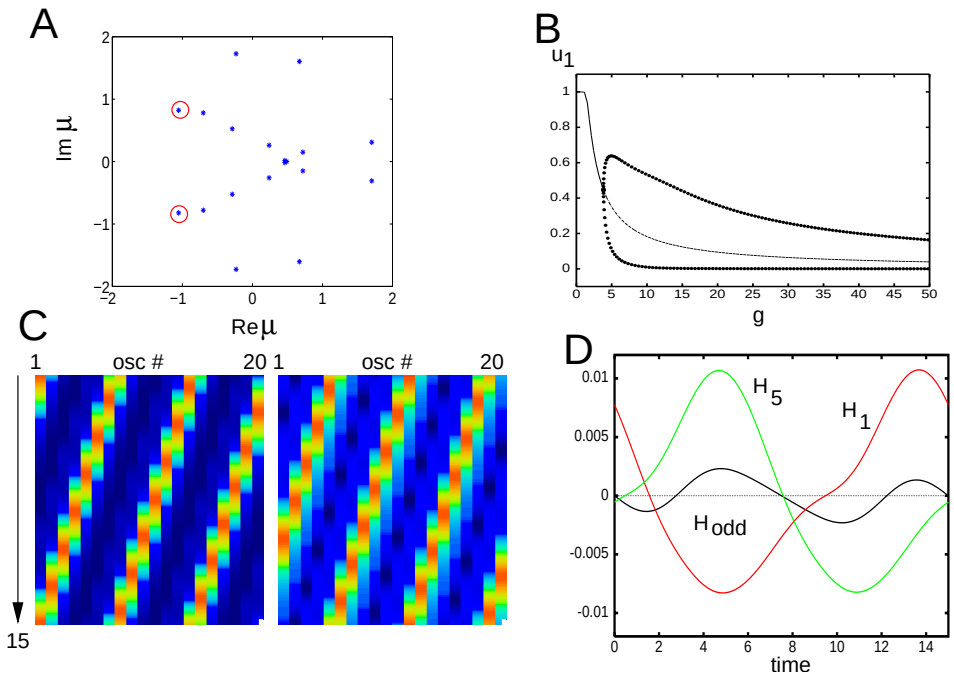

Figure 2.6: 20 neuron circulant system. (A) Eigenvalue spectrum; (B) Bifurcation diagram showing a single primary branch of periodic orbits ($I = 20$). (C) left: "Space-time" plot of dynamics for $g = 18$. Dominant spatial mode is $2\pi(3/20)$; right: Phase-sensitivity for one cycle of the oscillation; (D) Interaction functions when oscillator 1 receives inputs from oscillators 1 or 5 from the other motif. Black curve is the odd part of the interaction function when inputs from 1 and 5 are equal in strength. (See equation (2.4) for the definition of H.)

diagram (figure 2.7B) is almost the same as the 20 neuron network, but the termination is on a symmetric SNIC rather than a saddle-homoclinic. As mentioned above this three cell network is common in the CPG's of many animals from leeches to lobsters

In this section, we have shown that driven inhibitory networks of the form (2.1) generically produce limit cycle oscillations in which the cells in the network alternate their activity. In other words, like the three neuron model analyzed in [49], these more general networks produce repetitive sequential activity. Using such a network as our basic motif, we now explore the dynamical possibilities of coupling them together. Given that the cells are "on" at different parts of their cycle, we expect that there can be many different patterns of synchrony and locking depending on which cell is connected to which.

2.3 WEAK COUPLING THEORY.

The dynamics of generally coupled oscillators is a difficult problem, so that several approaches can be taken to make the problem tractable. One of the most general methods available is to restrict the analysis to the case where interactions between the oscillators are "weak." That is, coupling is not so strong as to distort the individual limit cycles. We first summarize the Malkin theorem for weak coupling which was proven in Chapter 1 [2].

Consider

$$\begin{aligned} X' &= Q(X) + \epsilon C_1(X,Y) + O(\epsilon^2) \\ Y' &= Q(Y) + \epsilon C_2(Y,X) + O(\epsilon^2). \end{aligned}$$

Here $Q : R^n \to R^n$ and $C_k : R^n \times R^n \to R^n$ are smooth functions. We assume that there is an asymptotically stable limit cycle, $X_0(t)$ for the uncoupled system, $X_0' = Q(X_0)$ with period, P. $C_{1,2}$ represent the coupling functions to order $0 < \epsilon \ll 1$. Let $X^*(t)$ satisfy

$$\frac{dX^*}{dt} = -D_X Q(X_0(t))^T X^*, \quad X^*(t) \cdot X_0'(t) = 1.$$

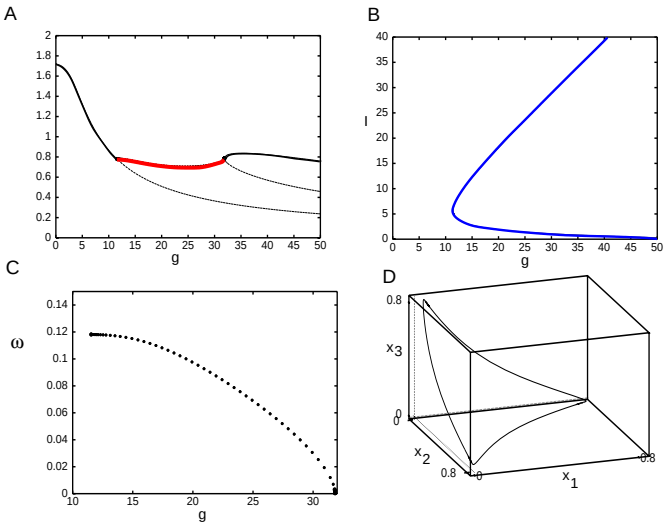

Figure 2.7: Three neuron network, $a = 0.1, b = 0.3, c = 0.6, I = 5$ with circulant structure. (A) Bifurcation diagram showing the L^2-norm. (B) Two parameter diagram showing curve of Hopf bifurcations. (C) Frequency of oscillations. (D) Three-dimensional projection for $g = 31$ near the termination of the branch of periodics.

Here $D_X Q(X_0(t))$ is the $N \times N$ Jacobi matrix (of partial derivatives of Q evaluated along the limit cycle, $X_0(t)$). Then $X(t) = X_0(\theta_X) + O(\epsilon)$, $Y(t) = X_0(\theta_Y) + O(\epsilon)$ and

$$\begin{aligned} \frac{d\theta_X}{dt} &= 1 + \epsilon H_1(\theta_Y - \theta_X) + O(\epsilon^2) \\ \frac{d\theta_Y}{dt} &= 1 + \epsilon H_2(\theta_X - \theta_Y) + O(\epsilon^2) \end{aligned}$$

where

$$H_j(\phi) := \frac{1}{P} \int_0^P X^*(t) \cdot C_j[X_0(t), X_0(t+\phi)] \, dt. \tag{2.4}$$

The function $X^*(t)$ is called the sensitivity function or the adjoint solution.

Before turning to the application of this theory to our motifs, we reiterate why understanding the interaction functions, $H_j(\phi)$ is useful. For reciprocally coupled identical oscillators, the Malkin theorem states (to order ϵ):

$$\begin{aligned} \frac{d\theta_X}{dt} &= 1 + \epsilon H(\theta_Y - \theta_X) \\ \frac{d\theta_Y}{dt} &= 1 + \epsilon H(\theta_X - \theta_Y). \end{aligned}$$

Let $\phi := \theta_Y - \theta_X$. Then

$$\frac{d\phi}{dt} = -2\epsilon H_{odd}(\phi) := \epsilon[H(-\phi) - H(\phi)].$$

Any continuous odd periodic function has at least two zeros, $\phi = 0$ and $\phi = P/2$. The former is the perfectly synchronous solution where both of the motifs follow the same exact trajectory and the latter is the "anti-phase" solution where the motifs are half a cycle apart. The existence of these solutions is independent of the of the nature of the coupling between two motifs, however, their stability does depend on the coupling, as we will show shortly. There is no reason why $H_{odd}(\phi)$, might not have other zeros besides, $0, P/2$. Such a zero would be very sensitive to the precise nature of the coupling and, if the zero is stable, would confer a great deal of flexibility in the range of stable patterns between two or more coupled motifs. Near the Hopf bifurcation, the limit cycles are very sinusoidal and thus, they have only a single Fourier component. Their sensitivity has a similar sinusoidal form so that their odd part of the interaction function is proportional to $\sin 2\pi\phi/P$ [50]. This means that the only possible patterns are $\phi = 0, P/2$. For this reason, we want to move away from the Hopf

bifurcation point so that the limit cycle, $X_0(t)$, and the sensitivity function, $X^*(t)$ have multiple Fourier modes. We conclude by remarking that perfect synchrony, $\phi = 0$ is stable if $-2H'_{odd}(0) = -2H'(0)$ is negative. That is, when $H'(0) > 0$. Similarly, the anti-phase solution, $\phi = P/2$ is stable when $H'(P/2) > 0$.

2.3.1 Weakly coupled motifs.

We now apply the weak coupling theory described in Chapter 1 to a pair of coupled motifs where the coupling strength, ϵ is small:

$$\begin{aligned} x_i' &= -x_i + f(I - g\sum_{j=1}^{m} G_{ij}x_j - \epsilon\sum_{j=1}^{m} C_{ij}y_j) \\ y_i' &= -y_i + f(I - g\sum_{j=1}^{m} G_{ij}y_j - \epsilon\sum_{j=1}^{m} C_{ij}x_j) \end{aligned}$$

We expand the inside of f in terms of ϵ to find

$$x_i' = -x_i + f(I - g\sum_{j=1}^{m} G_{ij}x_j - \epsilon\sum_{j=1}^{m} C_{ij}y_j) = -x_i + f(S_i) - \epsilon f'(S_i)\sum_{j=1}^{m} C_{ij}y_j + O(\epsilon^2) \quad (2.5)$$

where $S_i = I - g\sum_{j=1}^{m} G_{ij}x_j$. The equations for y_i are similarly defined with the y and x interchanged. For the remainder of the Chapter, we suppose the coupling between motifs is symmetric as in figure 2.1. Let $x_i^*(t)$ denote the components of $X^*(t)$ and $x_i(t)$ denote the components of $X_0(t)$. Then

$$H(\phi) = -\frac{1}{P}\int_0^P \left[\sum_{i,j=1}^{m} x_i^*(t)f'(S_i(t))C_{ij}x_j(t+\phi)\right]\, dt. \quad (2.6)$$

Let us define $z_i(t) = x_i^*(t)f'(S_i(t))$. This function determines the sensitivity of the oscillator to perturbations of the i^{th} cell. Then, we can write (2.6) as

$$H(\phi) = -\frac{1}{P}\int_0^P \left[\sum_{i,j=1}^{m} z_i(t)C_{ij}x_j(t+\phi)\right]\, dt.$$

Thus, the interaction function, H is dependent on the sensitivity of the oscillator being forced (the *reciever*) and the activity of the forcing oscillator (the *sender*). For example, if some of cells do not participate in the rhythm, that is, they are either suppressed or nearly

in the maximally active state, then they will be insensitive as receivers (since $f'(S_i(t))$ is close to zero) nor will they be useful senders since $x_i(t)$ is nearly constant and thus conveys no phase information. Generally speaking, in dealing with inhibitory motifs that have no special structure, some fraction of the cells will not participate in the rhythm in the the sense that their activities only fluctuate weakly. In circulant systems, all cells participate in the rhythm and their waveforms are just shifted versions of each other, so all of them are equally good at sending and receiving inputs from other motifs.

2.3.2 General results about synchrony.

Before our analysis of specific motifs and patterns of coupling, we look at synchrony with a particular kind of coupling. Consider

$$x_i' = -x_i + F(I - g\sum_j G_{ij}x_j - \epsilon\sum_j C_{ij}y_j) \tag{2.7}$$

The general interaction function is given by

$$H(\phi) = -\frac{1}{T}\int_0^T X^*(t)\cdot F'(I - gGX(t))CX(t+\phi)\ dt. \tag{2.8}$$

Here $F'(\cdot)$ means the vector formed from each of the components, $F'(I - \sum_j G_{ij}X_i(t))$. Synchrony is stable if $H'(0) > 0$, that is

$$M := -\frac{1}{T}\int_0^T X^*(t)\cdot F'(I - gGX(t))CX'(t)\ dt > 0. \tag{2.9}$$

Consider the equation:

$$X' + X = F(I - gGX). \tag{2.10}$$

Differentiate this with respect to t and we obtain:

$$X'' + X' = -gF'(I - gGX)GX'.$$

Integrate this against the adjoint $X^*(t)$ using the fact that $X'(t)\cdot X^*(t) = 1$ to obtain

$$1 + \frac{1}{P}\int_0^P X^*(t)\cdot X''(t)\ dt = -g\frac{1}{P}\int_0^P X^*(t)\cdot F'(I - gGX(t))GX'(t)\ dt \tag{2.11}$$

If the coupling to other groups, C is exactly the same as the coupling within groups, G, then we see that

$$gH'(0) = 1 + \frac{1}{T}\int_0^T X^*(t) \cdot X''(t)\, dt. \tag{2.12}$$

The term involving $X''(t)$ arises in many situations; for example, in the evolution of the phase for reaction-diffusion equations with scalar coupling [51]. It will be small or zero if the isochrons of the limit cycle are nearly radial (small "twist", see below). Thus, while it is not possible to declare that $H'(0)$ is positive, for a generic class of limit cycles, the twist is small. At a SNIC, the integral vanishes (see below). Thus, for our three oscillator circulant system (which is near the SNIC), we expect that synchrony will be stable if the coupling between groups exactly reflects the coupling within the group and is simply weaker.

We now prove that near a SNIC, the integral vanishes. The normal form near a SNIC is [52]

$$x' = 1 - \cos x + a^2(1 + \cos x).$$

We can solve this for the periodic orbit, $x(t) = -2\arctan(a\cot(at))$. As this is a scalar equation, the adjoint is $x^*(t) = 1/x'(t)$. Since $x'(t)$ is an even periodic function, the adjoint is also an even periodic function and $x''(t)$ is an odd periodic function. Thus, the integral of $x''(t)x^*(t)$ vanishes. Hence, near a SNIC, we have that $H'(0) > 0$ and synchrony is stable.

Near a Hopf bifurcation, $X(t) = (\cos t, \sin t)$ and $X^*(t) = (q\cos t - \sin t, \cos t + q\sin t)$ where q is dependent on the nonlinear coefficients of the normal form. If $q = 0$, the isochrons are radial; otherwise they have a twist. The desired integral is $-q$, so that if $q > 1$, then even with this special coupling, synchrony will be unstable. It is for this reason, we cannot say anything general about when synchrony is stable near a Hopf bifurcation except that for systems with nearly radial isochrons where we can say that synchrony is an attractor.

2.3.3 Interaction functions for circulant systems.

The general interaction function for two coupled motifs has the form:

$$H(\phi) = -\frac{1}{P}\int_0^P \left[\sum_{i,j=1}^{m} z_i(t)C_{ij}x_j(t+\phi)\right]\, dt,$$

where the functions $x_i(t), z_i(t)$ are very general and bear little relationship to each other. However, in a circulant system, the translational symmetry leads to the bifurcation to patterns of activity that are identical to traveling waves, c.f., figure 2.6C. This means that the only difference between, say, $x_i(t)$ and $x_j(t)$ is a temporal phase shift. That is, there exists an integer, k such that $x_j(t) = x_i(t + kP/m)$ where, m is the number of neurons in the motif and P is the period of the oscillation. Similarly, the sensitivities, $z_i(t)$ are related in the same way. Hence, to compute the interaction, we need only compute one integral and the rest will just be phase shifts. Specifically, let k_i be such that $x_i(t) = x_1(t + k_iP/m)$ and $z_i(t) = z_1(t + k_iP/m)$. Consider a term in the interaction function of the form:

$$-\frac{1}{P}\int_0^P C_{ij}z_i(t)x_j(t+\phi)\ dt.$$

We can rewrite this as

$$-\frac{1}{P}\int_0^P C_{ij}z_1(t+k_iP/m)x_1(t+k_jP/m+\phi)\ dt$$

which is then

$$-C_{ij}\frac{1}{P}\int_0^P z_1(t)x_1(t+(k_j-k_i)P/m+\phi)\ dt.$$

Let

$$h(\phi) := -\frac{1}{P}\int_0^P z_1(t)x_1(t+\phi)\ dt.$$

Then the general interaction function has the form

$$H(\phi) = \sum_{i,j=1}^{m} C_{ij}h\left(\phi + P\frac{k_j-k_i}{m}\right).$$

Thus, for circulant motifs, the composite interaction function is a weighted sum of the phase shift of the single $1 \to 1$ connection. In particular, we need only study coupled networks where a single cell in the motif (call it cell 1) receives all the inputs from the other motif. For example, in the simplest 3 cell motif, we need to look only at the cases where C_{11}, C_{12}, C_{13} are nonzero and thus

$$H(\phi) = C_{11}h(\phi) + C_{12}h(\phi + P/3) + C_{13}h(\phi - P/3). \tag{2.13}$$

where we use that fact that $2P/3 = -P/3$ modulo P.

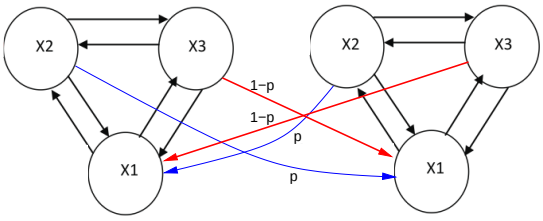

Figure 2.8: Example of a symmetric coupling motif with composite coupling.

2.4 SYNCHRONY AND LOCKING IN CIRCULANT SYSTEMS.

We start this section with an exploration of the dynamics of a pair of coupled three-cell motifs. From the discussion in the previous section and equation (2.13), we need only look at networks in which cell 1 receives all the inputs. Figure 2.8 shows an example system in which cell 1 receives input only from cells 2, and 3 in the other motif. When $p = 1$ coupling is just from 2 to 1 and when $p = 0$, it is from 3 to 1. We set

$$H_p(\phi) = ph(\phi + P/3) + (1 - p)h(\phi - P/3).$$

The phase difference between the two motifs satisfies

$$\frac{d\phi}{dt} = -2h_p^{odd}(\phi) := H_p(-\phi) - H_p(\phi).$$

Figure 2.9A shows h_p^{odd} for several different values of p. When $p = 1$ and connections are only from 2 to 1, the anti-phase solution is the only stable equilibrium and we expect that for weak coupling the two motifs will oscillate out of phase. In contrast, when $p = 0$ and coupling is only from 3 to 1, then perfect synchrony is an asymptotically stable solution; the two motifs will synchronize. For a mixture of the two types of coupling, the stable phase-difference between the two networks can take many values between synchrony and anti-phase. Thus, the timing difference (phase-difference) between the two symmetrically coupled networks can be arbitrarily prescribed by adjusting the ratio of the coupling strengths between different members of the motif. Figure 2.10A formalizes this idea by showing the stable equilibria for

the weakly coupled pair of networks as a function of the parameter p. When $p = 0$, synchrony is stable. As p increases, there is a super-critical pitchfork bifurcation for $p \approx 0.35$. The new branch of stable solutions represents a state in which the stable phase-difference between the two oscillatory networks is some intermediate value that increases from $\phi = 0$ in a monotonic fashion as p increases past 0.35. Starting at the other extreme, when $p = 1$, the anti-phase solution is stable. As p decreases, the anti-phase solution loses stability for $p \approx 0.65$. There is a subcritical pitchfork bifurcation which "turns around" to become supercritical where it joins with the solution branch emerging from the synchronous solution. Thus, except for a small interval of phases near the anti-phase solution, it is possible to achieve an arbitrary stable phase difference between the two networks by doing nothing more than varying the coupling ratio between the two connections. More generally, suppose we have two types of coupling, say $H_0(\phi)$ and $H_1(\phi)$ and consider $H_p(\phi) = (1-p)H_0(\phi) + pH_1(\phi)$. Suppose that $H_0'(0) = a_0 > 0$ and $H_0'(P/2) = -b_0 < 0$. This means that with $p = 0$, synchrony is stable and anti-phase is unstable. Suppose, in contrast, that $H_1'(0) = -a_1 < 0$ and $H_1'(P/2) = b_1 > 0$. That is, when $p = 1$, synchrony is unstable and antiphase is stable. Then we can compute the value of p for the pitchfork to occur on these branches. Synchrony ($\phi = 0$) is unstable for $p > a_1/(a_1 + a_0) := p_s$ and anti-phase is unstable for $p < b_1/(b_0 + b_1) := p_a$. Generically, the pitchfork will not be degenerate. (E.g., let $p = p_s$ be the value of p where synchrony loses stability. Let $h_{odd}(\phi)$ be the odd part of H at this value of $p = p_s$. Then, $h_{odd}'(0) = 0$ is the condition for the loss of stability. The condition for a non-degenerate pitchfork is $h_{odd}'''(0) \neq 0$. The sign of this quantity determines whether or not the pitchfork is sub- or supercritical. A similar condition holds at $p = p_a$.)

In our particular case, the new solutions which bifurcated from synchrony and anti-phase were stable and represented an intermediate phase-difference. However, it is not necessary for this to happen. Instead, for example, suppose that $p_a < p_s$. Then for $p_a < p < p_s$, both anti-phase and synchrony are stable. The coupled network is bistable. It turns out that in our canonical three cell circuit, the single reciprocal connection from 1 to 1 provides a bistable system with both synchrony and anti-phase stable as seen in figure 2.9B.

In sum, weak coupling analysis shows that *even with symmetric coupling of identical oscillators*, it is possible to modulate the phase-difference between coupled pair of networks

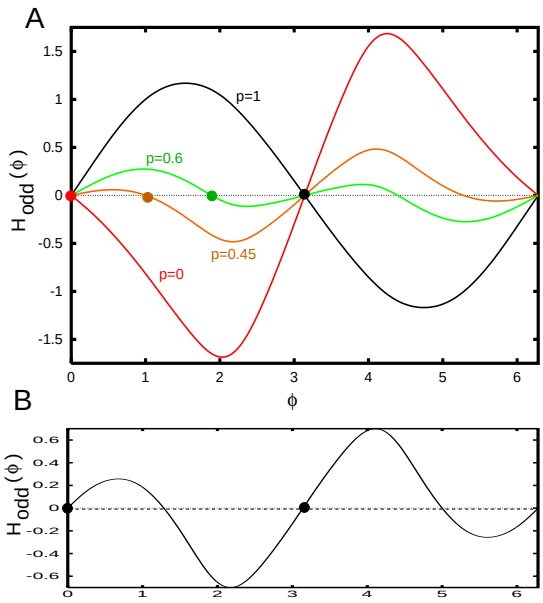

Figure 2.9: (A) $-2h_p^o(\phi)$, where h_p^o is the odd part of the weak coupling function for the composite coupling illustrated in figure 2.8. Filled circles show stable fixed points for 4 different values of p. (B) Odd part of the H function when the connection is #1 to #1.

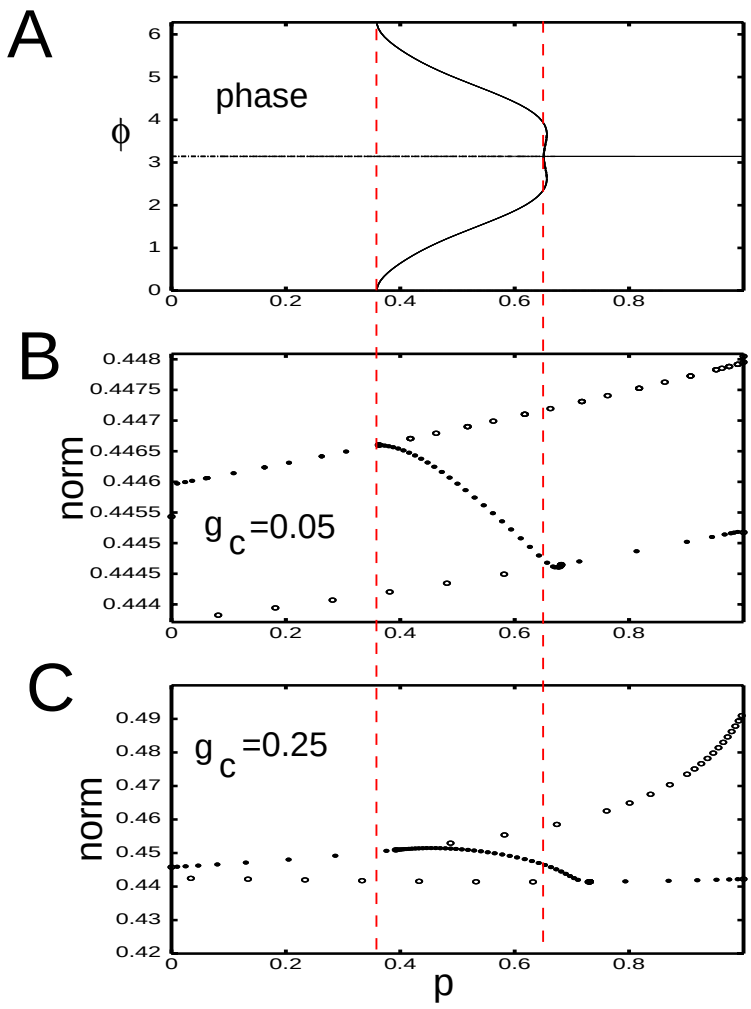

Figure 2.10: Behavior of the phase model and the full model as p varies. (A) Equilibria for the phase equation. (B,C) Norm of periodic solutions to the full model for two different coupling magnitudes.

by just varying the coupling ratio; that is, who is coupled to whom.

2.4.1 Beyond weak coupling

While the results for weak coupling show the rich possibilities of interacting circulant motifs, it is not clear how robust the timing/phase differences will be as the strength of coupling increases and the full oscillatory networks become more distorted due to the coupling. In figure 2.10B,C, we show bifurcation diagrams for coupling between units with strength $g_c = 0.05, 0.25$ as p varies. In both cases, synchrony is stable for p small and anti-phase is stable for p close to 1. As with the phase model, both the synchronous and anti-phase solutions lose stability via a pitchfork and the critical values of p are close to those predicted through weak coupling theory. Figure 2.11 shows the timing difference between the corresponding unit 1's in the two networks with moderate coupling strength. As predicted from weak coupling theory, synchrony and anti-phase disappear for p between 0.4 and 0.7 and the timing difference (or phase; details on how this is computed are in the figure legend) can take on any value. In particular, the timing is uniquely determined by p. Typical time series at three values of p are shown. For $p = 0.6$, the oscillation is somewhat distorted as the firing rates are not simply phase-shifts of each other, rather, their amplitudes are also different.

Figure 2.12 summarizes the global dynamics as the coupling strength, g_c increases. In A, stability of synchrony is lost through a pitchfork bifurcation as p changes for all coupling strengths, $g_c < 0.52$. For $g_c > 0.52$, synchrony is stable for all p. Furthermore, synchrony restabilizes as p increases for coupling larger than about $g_c \approx 0.3$. Panel B shows an analogous diagram for the fate of the anti-phase branch. Pitchfork bifurcations occur (with respect to the parameter p) for coupling strengths up to between 0.5 and 0.65. Beyond that, the anti-phase branch is lost to a saddle-node bifurcation.

One of the main points of this chapter is that an architecture in which cells within a motif come on at different times in the cycle can allow coupled networks to stably maintain specific phase relationships. However, it might be the case that these phase relationships (except synchrony and anti-phase) are very sensitive to the frequency of the oscillations. Thus, we consider the network shown in the last two figures, but, now, let the current input,

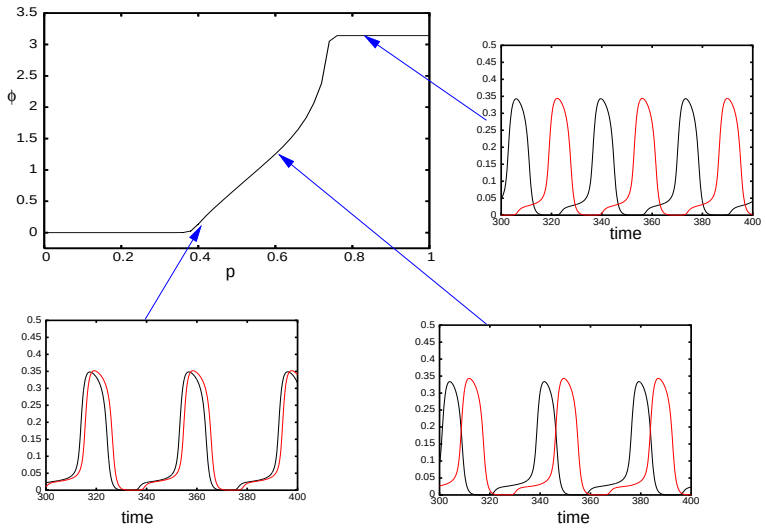

Figure 2.11: Phase shift between the two 3-cell systems as a function of p for $g_c = 0.25$. Phase-shift is defined as follows. Let t_1 be the time at which unit 1 in system X crosses 0.2; let t_2 be the time at which unit 1 in system Y crosses 0.2; let t_3 be the next time that unit 1 in system X crosses 0.2. The phase shift is $2\pi(t_2 - t_1)/(t_3 - t_1)$.

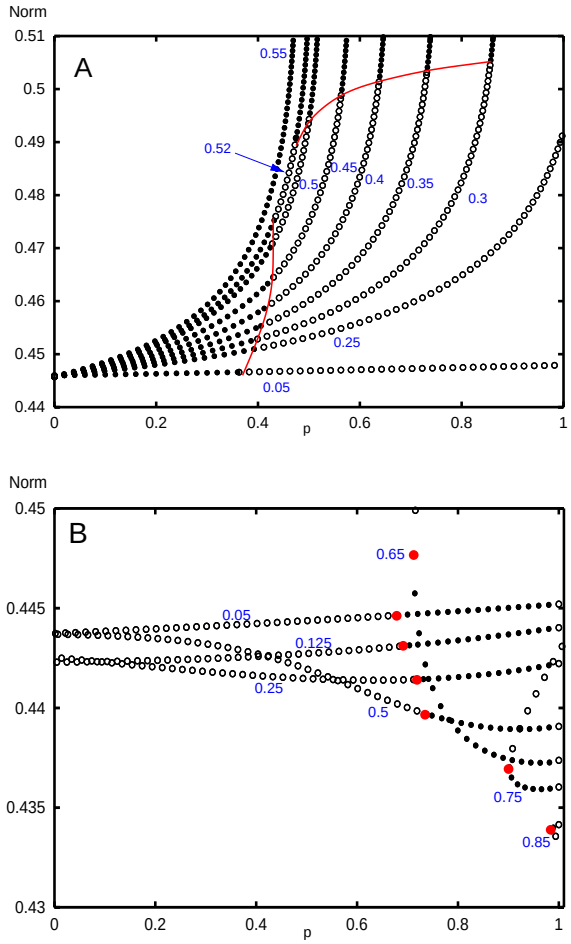

Figure 2.12: "Two-parameter" diagram for the full model. (A) Fate of the synchronous solution as p changes for different coupling strengths. Red curve is drawn through the values of the pitchfork bifurcation. (B) Fate of the anti-phase branch as p changes for different coupling strengths. Red circles show the bifurcation points at pitchfork or saddle-node bifurcations.

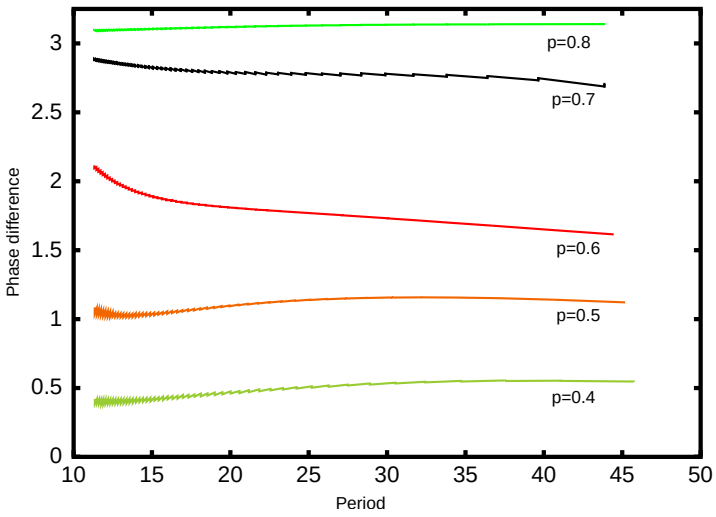

Figure 2.13: Robustness of the phase-difference as a function of the period of the oscillation. Phase shift between the two firing rate models when $g_c = 0.05$ and the input current I to each unit varies between $I = 1$ and $I = 2$.

I change between $I = 1$ and $I = 2$. At $I = 1$, the uncoupled system is near the Hopf bifurcation and the amplitude of the oscillation is very small, while when $I = 2$, it is close to the SNIC and the amplitude is quite large. The period ranges from about 10 to about 50. In spite of this large range in amplitude and period, for a fixed interaction between the two subnetworks (that is, for fixed p), the phase is remarkably constant. Figure 2.13 shows the phase difference (as measured in figure 2.11) as the period varies (achieved by changing the input, I). For each choice of p, the phase is almost constant over the entire range of periods.

2.4.2 Non-circulant systems.

Symmetric connectivity between circulant systems has been shown to yield the possibility for arbitrary time differences between pairs of the motifs. We explored in great detail the dynamics of a specific 3 neuron circulant system. However, the basic principle that underlies this, shared activity that occurs at different times during the cycle, should hold in any inhibitory network. For example, consider the random 20 cell network shown in figure 2.5 at the parameter value shown by the arrow. Figure 2.14 shows a summary of the dynamics predicted from weak coupling and the actual dynamics of a pair of two 20 neuron systems. Panel (A) shows the spatio-temporal pattern of dynamics over a period of time. The uncoupled period of the network is 8.4. While lacking the symmetry of a circulant system, it is clear that different neurons come on at different times during the cycle. Figure 2.14B shows the adjoint, $X^*(t)$ for the network over one cycle. The arrow marks the sensitivity for oscillator #4 and its time series is shown in figure 2.14C along with the activity profile of oscillator #7 (arrow in panel A). We compute the odd part of the interaction function when the two systems are coupled via a single symmetric interaction where unit #4 receives an input from one of several different units. Weak coupling theory predicts that if the interaction is from #1, then the two systems oscillate in anti-phase while if it is from #15, they will synchronize. Interactions mediated by #7 or #4 are predicted to lead to phase-locking at an intermediate phase-difference. (Recall that roots of the odd part of the interaction are possible phase-locked times and that the root is stable if the slope of the odd part of the interaction function is positive.) Figure 2.14E shows the dynamics of the full model

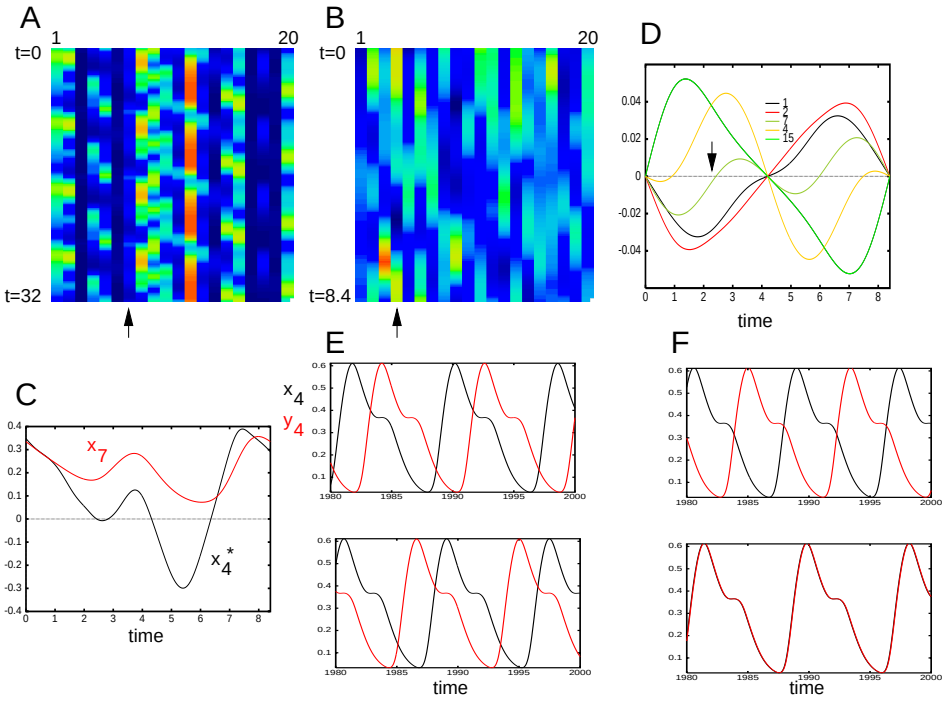

Figure 2.14: Dynamics of the network from figure 2.5. (A) Several cycles (time goes down) showing activity of neurons in the network. (B) Adjoint for one cycle of the oscillation in (A). (C) Plot of the adjoint $x_4^*(t)$ (shown by the arrow in (B)) and the activity $x_7(t)$ (arrow in (A)). (D) Odd part of the interaction function from weak coupling theory when one each of 5 different units is connected to unit #4. (E) Simulation of a pair of coupled 20 cell WLC systems ($g_c = 0.05$) where #7 connects to #4. Two different steady states are shown showing the symmetry of the system. (F) Coupling from #2 to #4 leads to anti-phase oscillations (top) and #15 to #4 leads to synchrony (bottom).

when coupling between the two systems is 0.05. Two different initial conditions lead to two different patterns corresponding to each of the two systems taking a small lead. (The curve in panel D marked by the arrow has two roots with a positive slope.) Figure 2.14F shows simulations for coupling between #1 and #4 (top, antiphase) and #15 and #4 (bottom, synchronous). Thus, we see that it is not necessary to have a circulant system in order for the ideas in this section to be relevant. What matters is not the symmetry but the mere fact that different components of the network turn on at different times during the cycle.

2.5 CONCLUSION

Many neural systems consist of repetitions of similar motifs that are then coupled together in order to form patterns of activity that may be useful for some types of computations or for creating desirable motor outputs. In this Chapter, we consider a specific type of motif that is dominated by non-symmetric recurrent inhibition. We showed that such networks were capable of producing wave-like repetitive activity even in absence of any spatial organization. We then showed that it is possible to design reciprocal symmetric coupling between pairs of these motifs such that they are able to produce arbitrary timing differences. Such timing difference are quite important in central pattern generators which are responsible for producing rhythmic patterned output to muscles used in locomotion and many other behaviors. For example, the crayfish swimmeret system requires a phase-difference of a quarter of a cycle between each of the four segments that comprise the pattern generator [53]. This phase-difference must be maintained over a wide range of swimming speeds corresponding to a similar range in oscillatory frequencies. Similarly, the lamprey spinal cord consists of about 100 segments, each of which consists of many reciprocally connected inhibitory neurons [54]. These segments must be coupled in such a way that they maintain a precise phase lag independent of the swimming speed of the animal [55]. Simple motifs of the type described in this chapter have exactly this property. As many CPGs are composed of networks of mutually inhibitory neurons, the architecture in this chapter could provide a simple robust mechanism for keeping a constant intersegmental phaselag over the entire range of physi-

ological frequencies. There have been other attempts at analyzing networks of inhibitorily coupled neurons. A recent paper, [56], considers the stability and dynamics of a large network consisting of coupled winner-take-all (WTA) systems. They, then, coupled these motifs and use contraction theory to analyze how the stability of the resulting patterns depends on the connectivity. [57] study clustering and other dynamics in coupled 5-cell motifs where each isolated motif generates rhythmic and cyclic dynamics. [41] use singular perturbation to analyze the global dynamics of networks of inhibitorily coupled neurons. [58] analyzes networks similar to our three-cell circulant system using harmonic balance and perturbation theory. Our approach has been to use weak coupling analysis of networks of motifs, each of which is an oscillator that depends on strong recurrent inhibition.

3.0 INTERMEDIATE STABLE PHASE-LOCKED SOLUTIONS BETWEEN PAIRS OF ELECTRICALLY COUPLED NEURONS

3.1 INTRODUCTION

In Chapter 2 we examined the mechanisms for producing intermediate stable phase-locked states between two populations of neurons. In this chapter we will study how these states arise in pairs of individual neurons using the conductance based models discussed previously. Intermediate stable phase locked solutions between pairs of neurons can be produced in a variety of neuron models by using a variety of coupling schemes as well as adjusting the parameters which affect the excitability of individual neurons. The first work examining this behavior in conductance-based models was by Vanvreeswijk et al.[59] In this paper, the authors studied integrate-and-fire as well as Hodgkin-Huxley neurons. The aforementioned models demonstrate both supercritcal and subcritical pitchfork bifurcations from the anti-phase state in pairs of neurons using two different models with different coupling schemes. Their research showed that one could achieve a subcritical pitchfork bifurcation from anti-phase synchrony by using integrate-and-fire neurons with inhibitory synapses. A supercritical pitchfork bifurcation was achieved using the integrate-and-fire model with excitatory synapses. Both supercritical and sub-critical bifurcations from synchrony were obtained in the Hodgkin Huxley model by using inhibitory synapses and increasing the synaptic time constant.

Over the last fifteen years there have been many publications which have studied the transition between synchrony in-phase and synchrony anti-phase behavior. For example, Ermentrout et al. showed that adding either a slow voltage-dependent or calcium-dependent potassium current to a pair of model neurons could produce a supercritical pitchfork bifurca-

tion from the synchronous solution [60]. Cymbalyuk has both modeled and experimentally demonstrated a pitchfork bifurcation in a system of two "silicon neurons"[1][61]. His silicon neurons are capable of intermediate phase locking. Mancilla et al. performed synchronization experiments on pairs of cortical fast-spiking neurons and also modeled their behavior using weak coupling theory[62]. The cells were electrically coupled and the transition between synchrony and anti-phase behavior was studied as a function of coupling strength. Their analysis demonstrated a subcritical pitchfork bifurcation and predicted bi-stability between synchrony and anti-phase behavior. Unfortunately, he was unable to experimentally demonstrate the bistable behavior in real cells.

Finally, we mention the work of Bose and Kopell, who studied pairs of Morris-Lecar neurons[63]. These model neurons operate on multiple time scales (three in this case). The authors were able to show that by adjusting a time constant parameter, they could achieve an "almost synchronous" solution with a small phase lag. The maximal phase difference or "lag" obtained was very small; 0.028ms or 8.4 ms for a pair of neurons with a period of 300 ms [63]. The analysis in this chapter is based on Wang-Buszaki neurons with gap junction coupling. This model and coupling scheme were chosen for several reasons. First, electrical coupling has been shown to be important in the spinal cords of developing vertebrates as well as the central pattern generators of some invertebrates. Second, no one has studied the loss of stability of the in-phase and anti-phase states of this system through a supercritical pitchfork bifurcation. My analysis shows that such bifurcations are possible by adjusting the maximal potassium conductance or by changing the temperature-dependent time constant (which is referred to as η) [62][64].[2] Third, since the emphasis of the dissertation is on large networks, it is preferable to vary the parameters affecting neural excitability as opposed to the coupling strength between neurons. As previously stated, weak coupling theory is valid when the coupling is sufficiently weak such that it does not affect either the frequency or the amplitude of the unperturbed oscillation. This condition may not always hold true if we try to obtain our intermediate stable phase-locked states by increasing the coupling strength.

[1] A silicon neuron refers to an electronic circuit designed to mimic a biological neuron

[2] We note that Pfeuty et al. have previously shown that adjusting the maximal synaptic conductance of model neurons with gap junction coupling can affect the neuron's ability to synchronize in-phase [64].

3.1.1 Excitability Of A Fast-Spiking Interneuron

The Wang Buszaki model is derived from the Hodgkin Huxley model. It was originally used to describe fast spiking interneurons in the hippocampus [26]. It is a system of nonlinear ordinary differential equations and is listed in the Appendix to this chapter. The Wang-Buszaki model exhibits type I dynamics, meaning that it is an integrator. Before discussing pairs of neurons with gap junction coupling, one must examine the manner in which firing properties of the cell change as the temperature-dependent time constant, η, and conductance parameter g_k are varied (see Appendix). When an action potential is generated, there is an influx of sodium which depolarizes the cell. This influx of sodium is controlled by two gates which are mathematically described by the gating variables n and h; these gating variables are time dependent. The constant η describes the rates at which the ion channel gates n and h open and close. It is exponentially dependent on temperature. The higher the temperature, the faster the switching rate:

$$\eta = Q_{10}^{(T-T_{base})/10} \tag{3.1}$$

Q_{10} is the ratio of rates for an increase of 10 degrees Celsius [65].

The variable h essentially determines when to "shut off" the inward current. Thus, the magnitude of h and the rate at which it decays to zero will have a large effect on the size of the action potential and also the after-hyperpolarization of the cell membrane.

Figure 1 illustrates the changes which take place in a model neuron as we increase the parameter η from 3.0 to 10.0 or decrease the maximal potassium conductance g_k from 8.0 μ S to 3.0 μ S. In this case, the neuron receives a constant excitatory input, $i_0 = 0.63$ nA. For smaller values of η, such as $\eta = 3$ the variable h has a larger amplitude, whereas the variable n has a smaller amplitude. As η increases, h noticeably decreases (see Figure 3.1A). Therefore, for larger η , h is smaller and the action potential is smaller as well. Figure 3.1B is a plot of the shape of the action potential of one cell as we vary η.

The most important consequence of varying these parameters is that the absolute refractory period decreases. The neuron is less hyperpolarized after the action potential for larger η or smaller g_K [64]. This has the consequence that the neuron becomes more sensitive to

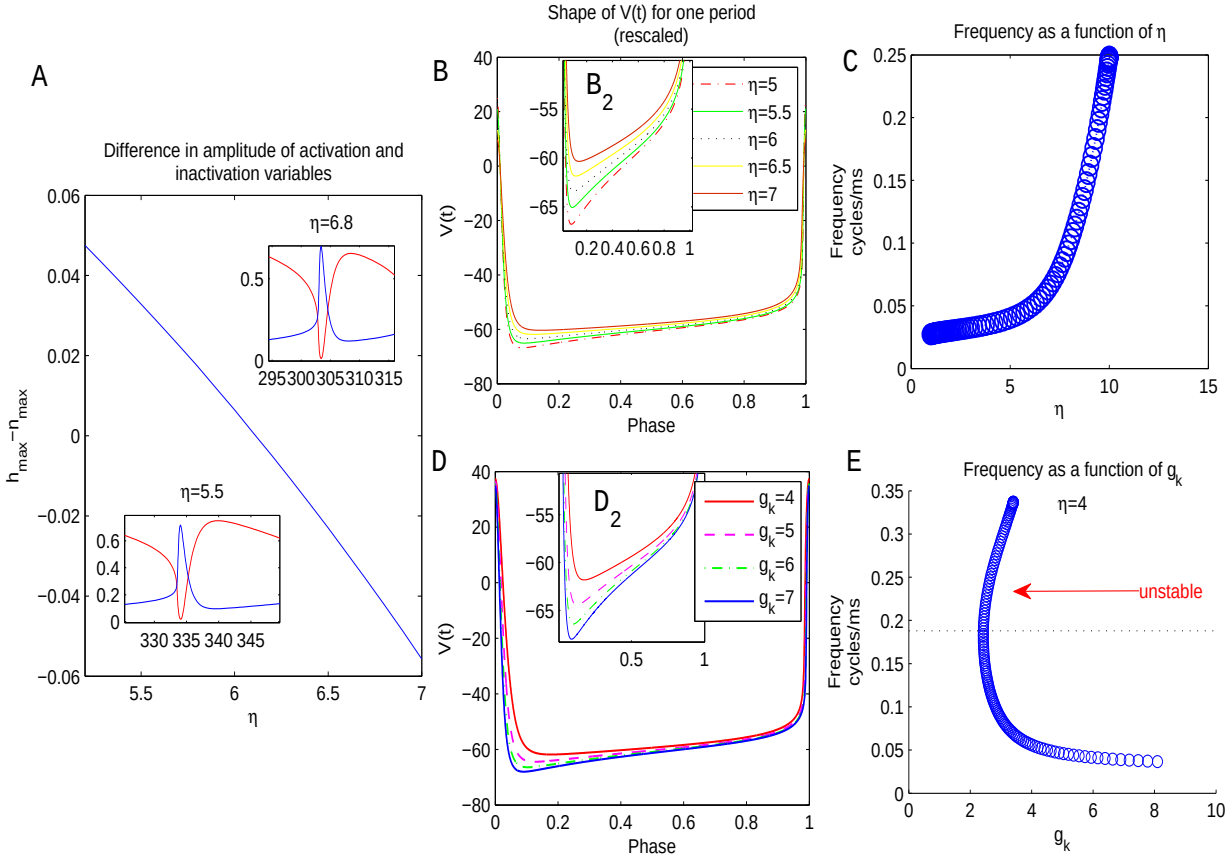

Figure 3.1: This plot shows changes in several features of the Wang-Buszaki model as we increase the parameter η. Namely, changes in the activation/inactivation variables lead to a smaller absolute refractory region, and a corresponding increased firing frequency **B.** is a rescaled plot of the action potential(full model) for varying values of η **C.** is a plot of the firing frequency as a function of η. **D.** is a rescaled plot of an action potential as a function of g_k. **E.** is a plot of the firing frequency as a function of g_k. The oscillations terminate in a subcritical Hopf bifurcation near $g_k = 3.4$

perturbations earlier in its cycle. In other words, this smaller absolute refractory region allows for the neuron to fire more quickly. As Figure 3.1C shows, as η increases, the frequency of the firing neuron also increases. As η approaches 5.80, the hyperpolarization region disappears and the neuron fires continuously above the resting potential of the equations. A similar affect is observed in Figure 3.1D: a decrease in the size of the hyperpolarization region corresponds to higher frequency firing. The frequency of firing increases as g_k is decreased until the system undergoes a subcritical hopf bifurcation at $g_k = 3.4$.

3.1.2 The Adjoint As A Measure Of Sensitivity To Perturbations

An effective way to quantify changes in neural excitability is through the phase resetting curve. Recall that the adjoint equation of a linearized system of odes is given by:

$$\frac{dV^*}{dt} = -D_V F(V_0)^T V^*, \qquad V^*(t) \cdot \frac{dV_0}{dt} = 1 \tag{3.2}$$

where $-D_V F(V_0)^T$ is the transpose of the Jacobian matrix evaluated along the limit cycle. It can be shown that the infinitesimal phase resetting curve (PRC) is a solution to the first component of the above adjoint equation [65]. In this case, the first component of the adjoint equation corresponds to the potential difference across the cell membrane. Within this dissertation we consider the adjoint and the infinitesimal PRC to be equivalent and the adjoint is to be a measure of sensitivity to an external stimulus. Figure 3.2 A and 3.2 B are plots of the adjoints as functions of the maximal conductance g_k and η, respectively.

From Figures3.2 A and 3.2B, we can see that as we increase η or decrease g_k the maximum region of V^* shifts from right to left. That is, the most sensitive region of the cycle shifts slightly but noticeably away from the depolarization towards the refractory period of firing. This is illustrated in Figures 3.2C and 3.2D which show the position of the maximum of the adjoint as a function of maximal conductance or temperature. This shift in sensitivity to perturbations corresponds to the emergence of the intermediate stable phase-locked states. In fact, for the special case of gap junction coupling, there is almost a direct relationship between the position of the maximum of the adjoint and a particular intermediate stable phase-locked state.

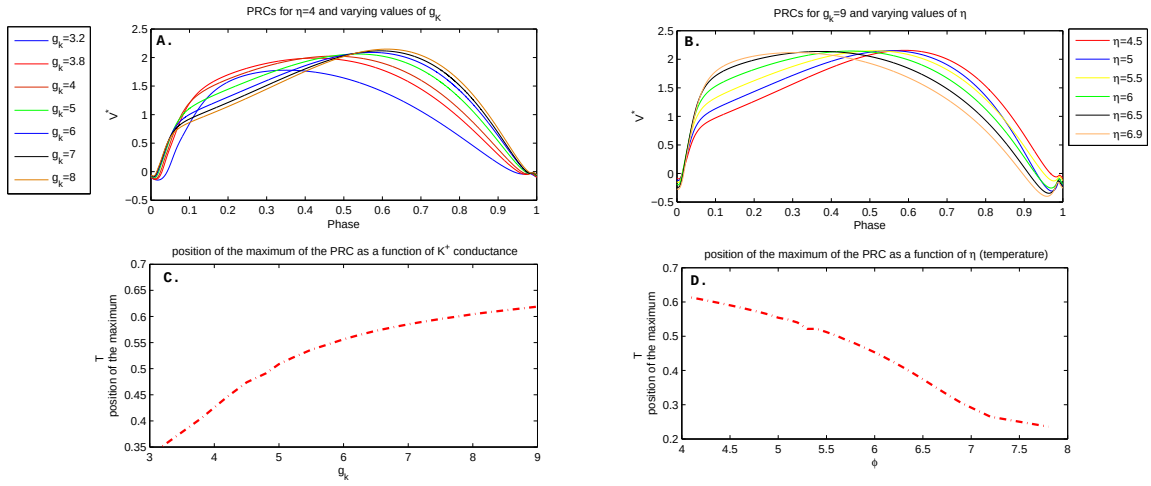

Figure 3.2: This plot demonstrates how the adjoint shifts as we vary the parameters of interest. Panels **A, B** show that the adjoint shifts from left to right as we either decrease g_k or increase η. Panels **C, D** show how the maximum shifts as the parameters are varied.

3.2 GAP JUNCTION COUPLING

Gap junctions are specialized ion channels connecting the cytoplasm of the pre and post-synaptic cell. A depolarizing ionic current is driven by the potential difference between the cells. Gap junctions are found throughout the brain and are critical components in many microcircuits which generate oscillatory and wave-like activity [66]. The structures in which they are found include the cerebello-olivary circuit, locus coeruleus, retina, olfactory bulb, hippocampal pyramidal neurons, neocortex and spinal cord [67][66]. As was previously stated, gap junctions also play key roles in central pattern generators[68] [66][9]. In several cases, gap junctions have been shown to act as a mechanism for switching synchronous behavior of spiking neurons between in-phase and anti-phase oscillations (normally in conjunction with inhibitory synapses). For example, it has been shown that the central pattern generator controlling the stomato-gastric mill in lobster, the structure which is responsible for "chewing" food, contains gap junctions[68]. In this CPG microcircuit, the synapses act to inhibit the cells, producing antiphase oscillations whereas the gap junctions tend

to synchronize the neurons firing behavior. The relative strengths of these two synapses can be modulated in order to switch between synchrony and anti-phase behavior[68]. In studying the Botzinger complex in rats (a central pattern generator controlling respiration), Rekling proved the existence of rhythmogenic type-I neurons with reciprocal gap junction coupling[9]. Bou-Flores et al. has found that gap junctions in this central pattern generator may aid in both neural synchronization and desynchronization in different contexts. In their experiment, Bou-Flores et al. found pharmacologically blocking gap junctions can actually increase the degree of synchronization in respiratory circuits [69]. Some of the most well-established and conclusive evidence for the role of gap junctions in rhythm generation comes from the study of spinal CPG circuits and motoneurons in neonatal and embryonic animals. In the zebra fish embryo, slow rhythmic bending of the trunk occurs just seventeen hours after fertilization[70]. This movement is triggered by a central pattern generator consisting of about fourteen neurons with gap junction coupling. This gap junction coupled network is the predecessor and proverbial backbone of the more complex system of central pattern generators composed of chemical synapses. The gap junctions tend to produce synchronized firing on the ipsilateral sides of the spinal cord. The contra-lateral portions of the cord are connected by a few reciprocal inhibitory connections. These oscillations persist even after the cord is severed at the hind-brain [70]. It is hypothesized that gap junction mediated oscillations are critical in shaping the development of the nervous system prior to sensory input[70]. Networks of electrically coupled neurons are not limited to the spinal cords of embryonic fish. Gap junctions play a major role in the spinal CPGs of adult aquatic animals such as the lamprey and the goldfish[9]. Similar gap-junction structures and oscillating network behavior is observed in the neonatal rat spinal cord[71]. Gap junctions are also prevalent in the neocortex of the neonatal mouse. Prior to the twelfth day of development of the neonatal mouse neocortex, waves have been observed which propagate over several millimeters[72]. These waves are a direct result of dendrodendritic gap junction coupling [72].

In order to understand the role that gap junctions play in rhythmically oscillating networks, consider just two neurons coupled with gap junctions. The coupled neuron equations

will have the following form:

$$\dot{V_1} = -\sum \bar{g} m_1^p h_1^q (V_1 - V_{eq}) + g(V_2 - V_1)$$
$$\dot{V_2} = -\sum \bar{g} m_2^p h_2^q (V_2 - V_{eq}) + g(V_1 - V_2) \tag{3.3}$$

where g is a conductance describing the strength of coupling. Intermediate stable phase-locked solutions are obtained in the full Wang-Buszaki model for two electrically coupled neurons. Furthermore, like the firing rate model results described in Chapter 1, these intermediate phase locked states are accurately described by a phase model. Previously, we demonstrated that by changing the temperature dependent time constant or the maximal potassium conductance in single neurons, the excitability of the neuron changed dramatically. Such parameters as temperature and potassium conductance play key roles in the behavior of central pattern generators and large scale oscillatory networks. Central pattern generators are seen as "flexible circuits" in the sense that they can produce very different patterns of activity under the influence of neuromodulatory transmitters such as dopamine [68]. Again, the lobster pyloric CPG is a primary example of this. In this circuit the neuromodulators dopamine and proctolin can act on different neurons to either increase or decrease the potassium conductance, producing different patterns of firing activity [68]. Temperature has also been documented to effect the synchronization properties of neurons. Specifically, it has been shown that cooling destroys synchronization in rat hippocampal slices and has even been proposed as a treatment for epilepsy[73].

To this end, consider Figure 3.3: Panels A and B are calculations of the phase difference between two neurons computed after 1500 ms of integration time for different values of g_k and η. The phase differences were measured from the points at which V_1 and V_2 are zero. Holding the stimulus current constant at $i_0 = 0.63$nA and varying either the parameter η or g_k, we are able to demonstrate the supercritical pitchfork bifurcation in the phase difference between neurons. Figure 3.3A and 3.3 B are calculations of the steady state phase difference between firing neurons as a function of η . Figure 3.3A illustrates the bifurcation of the system of two neurons from synchrony to anti-phase behavior as η is increased. For values of η between 5.0 and 7.0 the system passes through all possible stable relative phase-locked solutions varying between 0.0 and π. Figure 3.3B is a plot of the phase difference between

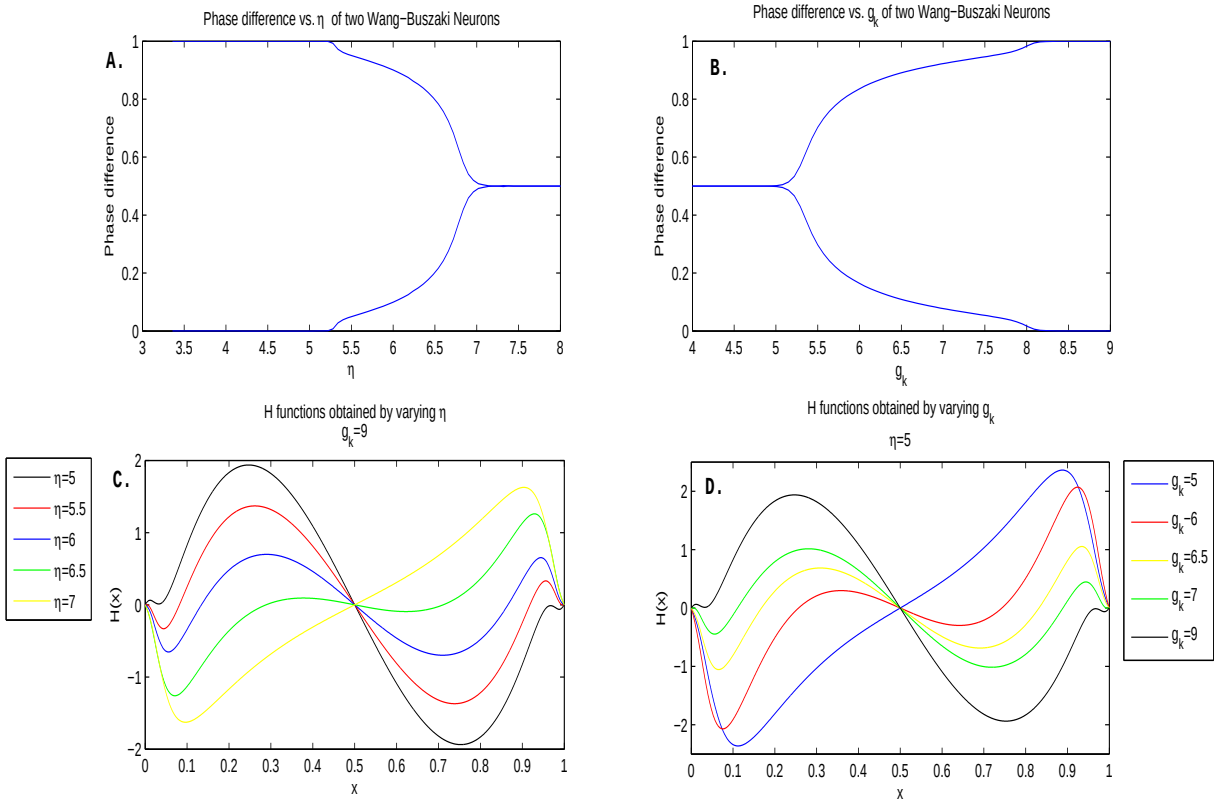

Figure 3.3: **A**. is a calculation of the phase difference between two Wang Buszaki neurons as a function of the parameter η. The diagram clearly illustrates a pitchfork bifurcation connecting the synchronous and anti-phase solutions. **B.** is a plot of the phase difference for varying values of g_k. **C.** is the calculation of the interaction function for different values of η (the dimensionless temperature dependent time constant) whereas **D.** is a calculation of the interaction function for different values of g_k. The zeros of these functions correspond to the stable phase locked solutions.

neurons as we decrease g_k. As we decrease g_k between 8.0 and 5.0 we obtain intermediate stable phase-locked solutions. By adjusting the parameters which affect the excitability of single cells, we can effect the ability of a large numbers of neurons in a network to sychronize. These intermediate stable states between pairs of neurons translate into wave behavior in larger networks.

3.2.1 Calculation Of The Interaction Function

In order to study large networks, it is necessary to derive a phase model which reduces the behavior of each individual neuron to one equation: This phase model reduction is identical to the procedure used in Chapters 1 and 2. The right hand sides of these phase model equations are described by interaction functions which are derived from the full model. One of the major results of the last two chapters is the derivation of phase models whose behavior is characterized by second and third order odd Fourier modes as opposed to a simple $\sin(x)$ function. It is important to note that in most of the previous work studying oscillator networks in neuroscience, the entire interaction function was approximated by a simple $\pm\sin(x)$ term.[3] In these systems, excitatory neurons were thought to have a synchronizing effect on neural populations, and have a "+1" coefficient. Inhibitory neurons, thought to promote anti-phase behavior, are given a "-1" sign [22]. Higher order terms were not included. We calculated the interaction functions for several values of g_k and η. Figure 1C and 1D shows the odd portions of the interaction functions. Once more, the phase-locked solutions correspond to the zeros of these functions and we approximate these functions by using Fourier series:

$$H(x) = \frac{a_0}{2} + \sum_{n=1}^{\infty} \Big(a_n \cos(nx) + b_n \sin(nx) \Big) \tag{3.4}$$

Table **??** shows the first few Fourier modes for $\eta = 6$.

Observe that the first two odd Fourier terms in Table**??** are the dominant ones. In the types of supercritical pitchfork bifurcations that we observe in both the conductance-based and firing rate models, the higher order Fourier modes become more prominent as we

[3]There are a few exceptions discussed in the next chapter

Table 3.1: Fourier Coefficients of the Wang Buszaki H-function with $\eta = 6$

$a_0 = 5.1974931$	
$a_1 = -2.9970722$	$b_1 = 0.47408548$
$a_2 = -0.92187762$	$b_2 = -0.36833799$
$a_3 = -0.44113794$	$b_3 = -0.2577318$
$a_4 = -0.25482759$	$b_4 = -0.15762125$
$a_5 = -0.16416954$	$b_5 = -0.09083201$
$a_6 = -0.11295291$	$b_6 = -0.048487604$

approach the bifurcation point. For instance, consider Figure 3.4 C which is a plot of the first two odd Fourier modes of the interaction function computed for different values of η. At lower values of η, $\sin(x)$ is the dominant term. Thus, synchrony is a stable solution. As we increase the value of η, the magnitude of the first term approaches zero. This continues for increasing values of η until the sign of the first order term switches and becomes negative. If we compare the magnitude of the first mode with that of the second mode, we see that even though the first mode becomes very small as it approaches zero, the second mode is always negative ($-0.3 \leq b_2 \leq -0.8$). Thus, there is a region corresponding to our intermediate stable states where this second mode becomes the dominant term. In these parameter regimes, it is reasonable to approximate the interaction function as:

$$H(x) = b_1 \sin(x) + b_2 \sin(2x) + a_1 \cos(x) \tag{3.5}$$

This interaction function will be used in the analysis throughout the next chapter.

3.2.2 Interaction Functions Composed of Higher Order Fourier Modes

Finally, it may be possible to use various coupling schemes to obtain phase models in which even higher Fourier terms are dominant. Introducing adaptation into a model can lead to higher-order terms. Recently, this has been demonstrated by Kilpatrick et al. in networks

of globally inhibitory networks[74] Alternatively, Crook et al. demonstrated that phase lags can be produced between spatially extended models of cortical oscillators by varying the axonal resistance [75]. It may be possible to use conduction delays to produce interaction functions with dominant third and fourth order Fourier modes. Furthermore, it is important to realize that because combinations from different coupling terms may be added linearly, we may build more "complex" interaction functions with different coupling combinations. This is essentially what we did in Chapter 1, when we varied the relative coupling strength of connections between two networks of three neurons. The relative contribution of the (even or odd) Fourier modes changes as we vary parameters such as coupling strength, conductance and synaptic reversal potentials. Therefore under some circumstances, combinations of synapses with different reversal potentials and/or different relative coupling strengths, can be used to eliminate the lower order modes of the interaction function. For instance, consider panel A of Figure 3.4. This interaction function was computed with a Wang-Buszaki neuron with both inhibitory synapses and electrical coupling[4]: By adjusting the relative coupling strength of the synapse and a gap junction, one can eliminate the second order term in the interaction function which in turn leads to an expression in which the higher Fourier modes are dominant. In this particular case, there is bi-stability between the intermediate stable phase-locked state and the synchronous solution (denoted by the red arrows). Similarly, Figure 3.4B is the interaction function computed for the Hodkin-Huxley neurons with just inhibitory synapses. This interaction function demonstrates bistability between synchony in-phase and the intermediate stable state.

3.3 CONCLUSION

In this chapter we analyzed a system of Wang-Buszaki neurons with gap junction coupling and studied phase locking behavior as a function of the maximal potassium conductance and the temperature dependent time constant. One can obtain intermediate stable phase locked states over a wide range of conductances and time constants. This builds on previous

[4]The system is near the supercritical pitchfork bifurcation.

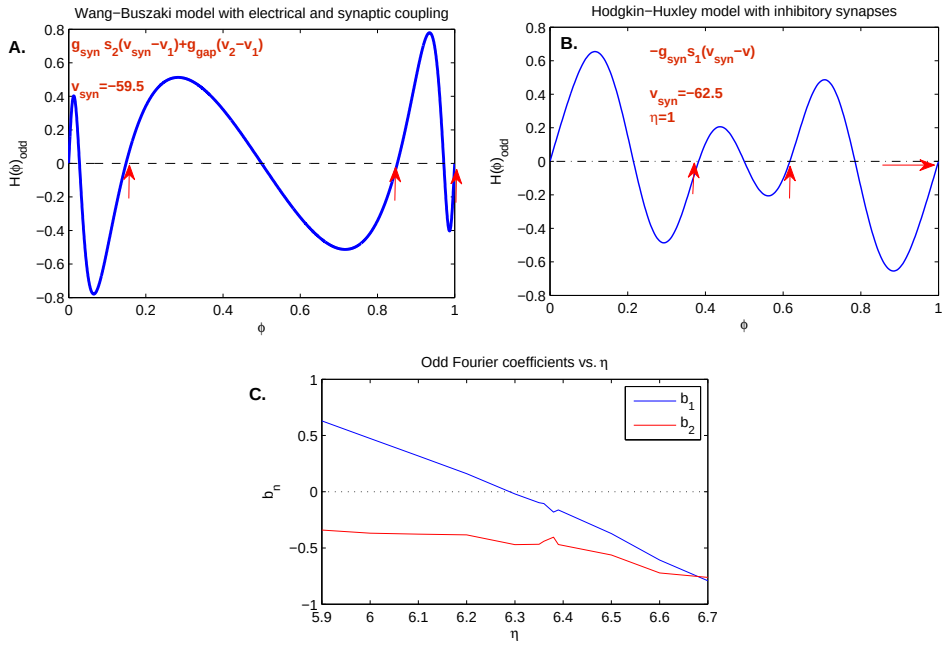

Figure 3.4: **A.** A plot of the odd portion of an interaction function with both electrical and synaptic coupling ($g_{syn}/g_{gap} = 10$). The prominence of Higher order Fourier terms lead to bi-stability between the synchronous and intermediate phase locked states. **B.** A plot of the odd portion of the interaction function of the Hodgkin-Huxley model with inhibitory synapses $\eta = 1, i_0 = 10$ and $v_{syn} = -62.5$. The intermediate stable phase-locked state is bistable with in-phase synchrony. **C.** a plot of the first two odd coefficients of the interaction function as a function of the temperature dependent time constant η.

work by Pfeuty [64] who studied a similar system and noted that changing the conductance properties of model cells has a great impact on their ability to synchronize. Gap junction coupling is very important in central pattern generators in both the stomatogastric system of lobsters as well as the developing nervous systems of many animals, including fish, mice and rats. It is well known that central pattern generators are flexible circuits whose conductance properties and activity patterns can be modified with neuromodulators such as dopamine. Dopamine lowers the potassium conductance in some interneurons and so our models most likely have relevance in real CPGs [68]. Using Weak Coupling Theory and Malkin's Theorem, phase models are derived describing our system of neurons. The interaction functions of these phase models consist of at least two dominant odd Fourier modes: Historically, many network phase oscillator models include only the lowest odd mode. In the last two chapters we have demonstrated methods for obtaining these interaction functions both between two populations of neurons and pairs of neurons. In both chapters, the models we studied are inspired by neural microcircuits which give rise to oscillatory and wave-like dynamics. However, each model represents an entirely different approach to modeling neural systems. This fact underscores the generality of the phase model reduction. Two almost identical phase models were derived from different neural systems. We approximate our interaction function by two odd and one even Fourier term. Chapter 4 is an analysis of chains and two dimensional arrays of phase oscillators coupled with these higher mode interaction functions. It is a study of waves and oscillatory patterns which can be obtained only by these intermediate phase-locked states. Because of the generality of the phase oscillator model, the approximate interaction function can describe a variety of coupling schemes and may be relevant to other oscillator systems in physics.

4.0 WAVES IN LARGE NETWORKS

4.1 INTRODUCTION

Wave activity is ubiquitous in the brain. Traveling waves of electrical activity in the brains of animals have been observed in a variety of species and occur in a diverse set of structures. These structures include the retina, olfactory cortex [76], peri-geniculate nucleus[77], neocortex [72] and spinal cord [1], among others [78],[77],[72],[76],[76][79][77]. Wave activity is generated by a variety of mechanisms and may serve different purposes in different contexts. In order to understand the different mechanisms by which waves are generated and their function in neural networks, consider the waves in the procerebral lobe of the slug, *limax*, as well as spindle waves in the lateral geniculate nucleus of the ferret. If the olfactory cortex of *limax* is injected with a voltage sensitive dye, wave activity can be observed to propagate across the procerebral lobe [76]. These waves are associated with the creation of odor memories which are apparently stored as bands of active cells in the procerebral lobe. It is hypothesized that these waves influence the ability of the animal to discriminate between two chemically similar odors[76]. Destroying the waves with pharmacological agents appears to also destroy the animals ability to distinguish between similar smells [76]. The cells of the procerebral lobe are autonomously oscillating[76]: this has been determined experimentally by severing the lobe into pieces and observing that the oscillations in these pieces were not destroyed[80].

A second well-studied example of wave activity is spindle waves which occur in the perigeniculate nucleus and lateral geniculate nucleus of the ferret[77]. Spindle waves have generally been associated with the transition between waking and slow-wave sleep and are a component of oscillations in the thalamocortical network [77]. These waves are created by

the interplay of inhibitory interneurons and thalamic relay neurons. Interneurons inhibit the thalamic relay cells which subsequently spike via post-inhibitory rebound. It is important to note the differences between these waves and those generated in *limax*. Because spindle waves are generated by post-inhibitory rebound, the cells which comprise the network are not autonomously oscillating. If the connections between cells were severed, the oscillations would cease. The function of spindle waves is unknown, but it is hypothesized that they calibrate synaptic connections throughout the thalamo-cortical network [77]. In order to characterize different types of waves and understand their functions in real nervous systems, several authors have attempted to develop simplified mathematical models which are capable of producing waves.

There are several mechanisms and network architectures for producing wave-like activity in neural models. In feed-forward networks, wave activity is modeled by synfire chains: pools of neurons with feed-forward excitatory connections [81][82]. In recurrent networks, waves can be generated by phase-locking between neurons or neural oscillators[78]. Alternatively waves may be generated by post-inhibitory rebound such as the slow waves of Rinzel, Ermentrout and Terman [83]. In this chapter, we focus on the generation of waves though phase-locking between neurons and neural oscillators. The models that we study are phase oscillator models, a class of models which has been studied extensively throughout the last thirty years by Ermentrout, Kopell and many others [84],[85],[86],[87]. As discussed in Chapter 1, chains of phase oscillators have been successfully used to model the spinal cords of the lamprey[8]. Ermentrout et al. have successfully modeled the olfactory cortex of *limax* using a combination of two dimensional arrays of oscillators and populations of all-to-all coupled oscillators[80].

This chapter is a study of wave behavior in both chains and two dimensional arrays of neurons with nearest neighbor coupling. Primarily, we study phase models which use the interaction functions (or approximations of them) derived from the Wang-Buszaki model. Our models may be relevant to patterns of wave activity in the neonatal rat. As alluded to in the previous chapter, Peinado et al. was able to observe wave activity in gap-junction coupled interneurons in rat neocortex prior to day twelve of development[72]. Furthermore, he was able to enhance these waves by applying halothane and picrotoxin. Picrotoxin blocks

inhibitory synapses while halothane reduces the potassium conductance. In general, he observed that the reduction in potassium directly led to the formation of waves. Since our intermediate stable phase-locked states can occur in gap junction coupled neurons by reducing the potassium conductance, this may be experimental evidence that this effect plays a role in wave formation in a two-dimensional network.

We focus on a specific type of solution to the phase equations known as anti-waves. Anti-waves (or kinked waves) were first studied in two papers by Ermentrout and Kopell[85][84]. Similar phenomena have been examined by Strogatz et al., (uniformly twisted waves) and Blasius et al., (1D quasiregular concentric waves)[88][89]. [1] Physically, anti-waves can be thought of as multiple waves emanating from various points in the neural chain. These waves propagate in both directions from the neuron of origin. When two waves collide on the same neuron, that neuron enters a refractory period and the propagation terminates. The cycle repeats itself periodically. Anti-waves have been experimentally observed in the spinal cords of dogfish [91] and may well be present in other neural networks. For instance, similar patterns of electrical activity have been observed in the muscle of the colon of a cat. If one considers these muscular contractions to be controlled by a central pattern generator, then this wave of electrical activity in muscles may correspond to activity patterns in a central pattern generator[92]. Central pattern generators in electric fish have also been known to produce anti-waves[84]. These animals are able to produce a variety of complex waves in which the "kink" or lead oscillator in the wave is able to shift[84]. Spindle waves can collide and form anti-wave like patterns of activity. Since these waves, however, are generated primarily through post-inhibitory rebound, it seems unlikely that intermediate stable phase-locked states play a role in their formation.

The current work differs from the work of Ermentrout and Kopell in several respects. First, we demonstrate a different mechanism for generating anti-waves: intermediate stable phase-locked solutions. In previous work these waves were generated with purely sinusoidal coupling and a few distal connections. The distal connections set up a frequency gradient across the chain creating waves. In the current work, the anti-waves are generated from the stable phase-locked states (determined from the interaction function) between nearest

[1] These are not to be confused with fractured waves studied by Kopell (also known as s-waves) [90].

neighbor pairs of oscillators comprising the chain. As previously mentioned, historically, interaction functions used in these models consisted only of one odd Fourier mode. Near a super-critical pitchfork bifurcation, both the higher order odd and even modes become prominent. The even component of the interaction function effects the stability of the wave solution. Additionally, the even component can effect the probability, starting from uniformly distributed random initial conditions, that a particular wave solution will form. Finally, Ermentrout has shown [85] that the even component can allow one to have a larger distribution of natural frequencies and still obtain phase-locking. This is an important feature in a real network, where a completely homogenous system may be unrealistic.

The rest of this chapter is organized into several sections. We begin in section 4.2 by discussing the basic phase models and boundary conditions. This is followed by an analysis of both an ordinary traveling wave (4.3) and anti-wave solutions (4.4) (4.5) . In section 4.6, we demonstrate that the probability of obtaining a particular solution depends on the relative contribution of the even component of the interaction function. We show that starting from the anti-wave solution, if the even component is sufficiently large, perturbations initiated at one end of the chain can propagate down the chain and shift the position of the kink. Finally, in 4.13 we demonstrate that this analysis can be extended to higher dimensions and that a variety of anti-wave patterns are possible in a two dimensional oscillator arrays.

4.2 MODELS AND BOUNDARY CONDITIONS

The models we consider were introduced by Kopell and Ermentrout in a 1986 paper[85]. These models primarily describe networks of neurons with nearest neighbor coupling. In analyzing these equations we apply two types of boundary conditions: periodic boundary conditions and non-reflecting boundary conditions. For a system of $N+1$ neurons with

periodic boundary conditions, the system of phase equations may be written:

$$\begin{aligned}
\dot{\theta_1} &= \omega_1 + H_L(\theta_{N+1} - \theta_1) + H_R(\theta_2 - \theta_1) \\
\dot{\theta_2} &= \omega_2 + H_L(\theta_1 - \theta_2) + H_R(\theta_3 - \theta_2) \\
&\vdots \\
\dot{\theta}_{N+1} &= \omega_{N+1} + H_L(\theta_N - \theta_{N+1}) + H_R(\theta_1 - \theta_{N+1}).
\end{aligned} \tag{4.1}$$

In these equations, the ω_i represents the natural frequencies of the oscillators, and the interaction functions behave like "forcing" terms. We denote the coupling in the two possible directions as $H_L(\phi)$ and $H_R(\phi)$. In general, we assume that the coupling is isotropic, so that: $H_R(\phi) = H_L(\phi) = H(\phi)$. Ultimately, we are interested in phase-locking behavior, thus we make the change of variables: $\phi_j = \phi_{j+1} - \phi_j$. This results in a system of N phase equations:

$$\begin{aligned}
\dot{\phi_1} &= \Delta\omega_1 + H(\phi_2) + H(-\phi_1) - H(\sum_{j=1}^{N} \phi_j) - H(\phi_1) \\
\dot{\phi_2} &= \Delta\omega_2 + H(\phi_3) + H(-\phi_2) - H(-\phi_1) - H(\phi_2) \\
\dot{\phi_j} &= \Delta\omega_j + H(\phi_{j+1}) + H(-\phi_j) - H(-\phi_{j-1}) - H(\phi_j) \\
&\vdots \\
&\vdots \\
\dot{\phi_N} &= \Delta\omega_1 + H(-\phi_N) + H(-\sum_{j=1}^{N} \phi_j) - H(-\phi_{N-1}) - H(\phi_N).
\end{aligned} \tag{4.2}$$

In these equations $\Delta\omega_i$ is the frequency gradient between oscillators. In most of our simulations, we assume identical frequencies and $\Delta\omega_i = 0$

The second type of boundary conditions that we use is a variation of what are known as non-reflecting boundary conditions. Non- reflecting boundary conditions have been used in computational physics since the early 1970's to effectively simulate waves over a large domain [93]. Non-reflecting boundary conditions are implemented in order to attempt to eliminate reflections and to "trick" the neurons at the ends of the chains, neuron 1 and neuron $N+1$,

into behaving as though the chain is infinite. If one were to think of the chain as being a continuous system, then the boundary conditions are simply a statement that $\frac{d\phi(x,t)}{dx} = 0$ when evaluated at the ends of the chain. There is a precedent for using such boundary conditions in nonlinear oscillator problems, for an example, see [94] . Applying these boundary conditions to our phase equations, we have[2]:

$$\begin{aligned} \theta_0 &= \theta_2 \\ \theta_{N+1} &= \theta_{N-1}, \end{aligned} \tag{4.4}$$

and our phase equations become:

$$\begin{aligned} \dot{\phi_1} &= \Delta\omega_1 + H(\phi_2) + H(-\phi_1) - 2H(\phi_1) \\ \dot{\phi_2} &= \Delta\omega_2 + H(\phi_3) + H(-\phi_2) - H(-\phi_1) - H(\phi_2) \\ \dot{\phi_j} &= \Delta\omega_j + H(\phi_{j+1}) + H(-\phi_j) - H(-\phi_{j-1}) - H(\phi_j) \\ &\vdots \\ &\vdots \\ \dot{\phi_N} &= \Delta\omega_N + 2H(-\phi_N) - H(-\phi_{N-1}) - H(\phi_N). \end{aligned} \tag{4.5}$$

4.3 TRAVELING WAVES IN CHAINS OF COUPLED OSCILLATORS

The wave solution for the plane wave can be written:

$$\phi_j = j\phi^* + \Delta\omega t, \tag{4.6}$$

[2]To see that this is consistent with the preceding statement, start with the $H(-\phi_{j-1}) = H(\phi_j)$, using a Taylor series to expand out each side and evaluating at the wave solution, we have the expression:

$$H'(-\phi)\frac{d\phi}{dx} = 0 \tag{4.3}$$

Since $H'(\phi) \neq 0$, then it must be that $(\frac{d\phi}{dx}|_{x=0}) = 0$.

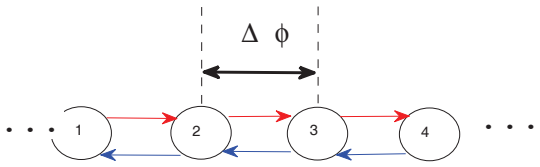

Figure 4.1: A chain of weakly coupled neurons. The phase locked solution between adjacent neurons in the chain defines the overall wavelength.

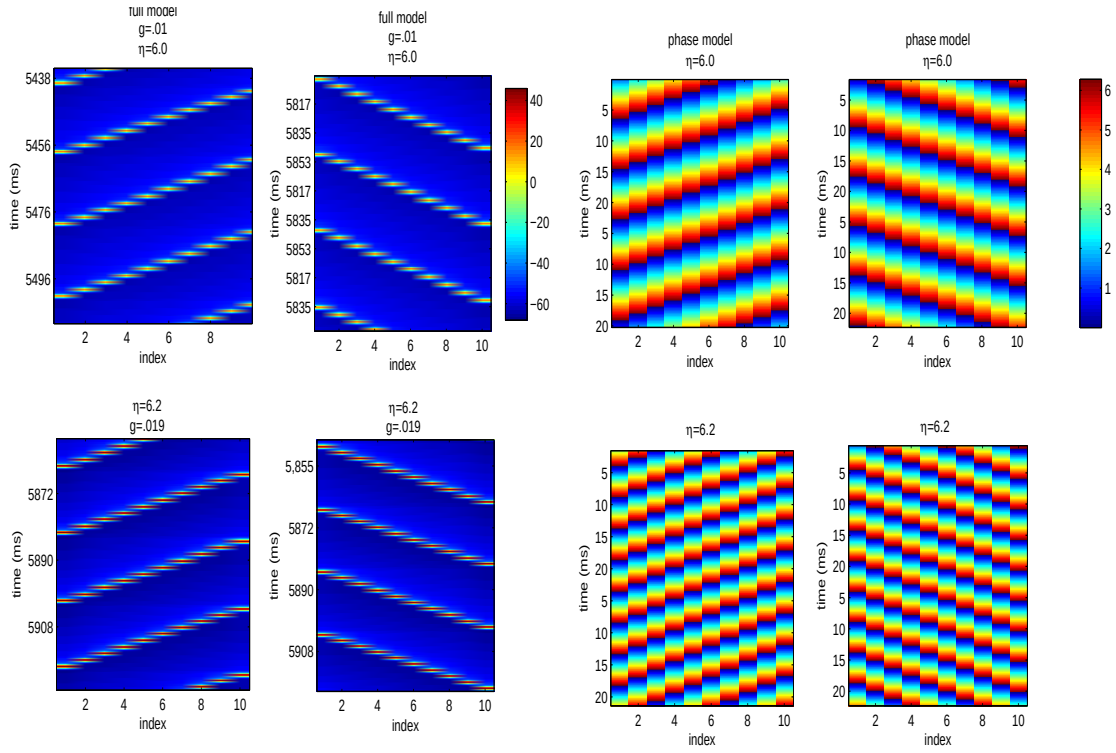

Figure 4.2: The four panels on the left are examples of traveling waves in the Wang-Buszaki model corresponding to four different values of the temperature dependent time constant η. The four panels on the right are four traveling waves obtained using the phase model for different values of η. The phase model reproduces the dynamics of the full model. Furthermore, it is clear from the phase model, that as one increases the constant η, the wavelength of the traveling waves decreases.

where j is the index of the oscillator or neuron and ϕ^* is the phase shift between adjacent oscillators. Substituting this solution into the equations with non-reflecting boundary conditions, we see that 4.6 is a solution provided that $H(\phi^*) = H(-\phi^*)$. Since our interaction function has both odd and even components, this statement is true only if ϕ^* is the root of $H(\phi)_{odd}$. Thus, the stable phase-locked states between oscillators determine the formation of a stable wave. In a continuum limit, we can consider $\theta(x,t)$ to be a function of both position and time. If we take the derivative of $\theta(x,t)$ with respect to t we obtain the expression[85]:

$$\frac{d\theta}{dt} + \frac{\partial\theta}{\partial x}\frac{\partial x}{\partial t} = 0, \tag{4.7}$$

which is equivalent to:

$$\begin{aligned} \omega + \phi^* v_\theta &= 0 \\ v_\theta &= \frac{\omega}{\phi^*}. \end{aligned} \tag{4.8}$$

This is an expression for the phase velocity of the wave. Therefore, we see that we may identify the wavenumber of the system as: $k_x = \phi^* = \frac{2\pi}{\lambda}$. Here λ is the wavelength of the system. The stable phase-locked state between pairs of oscillators defines the wavenumber of a traveling wave. In the last chapter we saw that as we we vary constants η and g_k in the Wang-Buszaki model, the stable fixed point changes. This translates to a change in wavelength in a chain of neurons. The phase model quantitatively reproduces the dynamics of the full model. Figure 4.2 shows a comparison between the phase model and full model for a variety of g_k and η. The four panels on the left correspond to the full model. The panels on the right correspond to the phase model. The phase model clearly demonstrates that the wavenumber increases for increasing η. Coupling strength in the full model is small. It must be on the order of 0.001 to ensure phase-locking.

4.4 ANTI-WAVES IN CHAINS OF COUPLED OSCILLATORS

The previous mechanisms for generating anti-waves rely on extremely long chains (essentially infinite) or chains with distal connections. Ermentrout and Kopell showed that by assuming a large chain and breaking the interaction function into even and odd components, they could derive a partial differential equation for the phase differences between oscillators in the chain:

$$\frac{d\phi(x,t)}{dt} = \Delta\omega(x) + 2f(\phi)_x + \frac{1}{N}g(\phi)_{xx}[85]. \tag{4.9}$$

In this equation, $f(\phi)$ is the even component of the interaction function and $g(\phi)$ represents the odd component ($H(\phi) = f(\phi) + g(\phi)$). The frequency gradient $\Delta\omega(x)$ is a smooth function in which x varies between $-1 \leq x \leq 1$[85]. "N" is the number of oscillators in the chain. The boundary conditions were defined as:

$$\begin{aligned} H(-\phi) &= 0 \quad at \;\; x = 0 \\ H(\phi) &= 0 \quad at \;\; x = 1 \end{aligned} \tag{4.10}$$

There were several major results in this paper, which sought to analyze the above system using a simple interaction function, $H(\phi) = A_1\cos(\phi) + B_1\sin(\phi)$. The authors proved that if the frequency gradient is zero, the coupling in the system is completely isotropic, and the equations use *cut-ends* boundary conditions[3], then anti-waves are possible solutions[85]. Assuming a finite chain, the shock will always form in the center of the chain. These solutions however, are extremely sensitive to perturbation and the shock will shift to either end if any there is any anisotropy introduced[85]. Ermentrout et al.[84] also showed that distal inhibitory connections projecting from the ends of the chain to the center can produce anti-waves. In this case the anti-waves are formed by increasing the frequency of the center oscillator. This central oscillator then acts as a "pacemaker": the frequency gradient between this oscillator and the oscillators in the rest of the chain forms a shock.

It should be emphasized that the mechanism of generating anti-waves through intermediate

[3]Cut ends boundary condtions refer to a chain in which the ends are coupled only to the interior of the chain (there is no weighting factor).

stable phase-locked solutions is fundamentally different than these previous works. For example, intermediate stable phase-locked states can generate anti-waves in which the shock is centered anywhere along the chain. These waves are also more robust against anisotropy and perturbations. Assuming an isotropic chain with no gradient in the natural frequencies, the intermediate stable phase-locked state defined by $H(\phi^*)_{odd} = 0$ will generate traveling waves. If the fixed point ϕ^* is identified as the wavenumber k, then the fractured wave solution can be written:

$$\begin{aligned} \phi_j &= kj + \omega t \qquad & j \leq N/2 \\ \phi_j &= -kj + \omega t \qquad & j \geq N/2. \end{aligned} \tag{4.11}$$

By substituting this into 4.5 we see again that the anti-wave is a solution provided that $H(k) = H(-k)$ (k is the root of $H_{odd}(k)$) . Figure 4.3 demonstrates examples of anti-waves obtained in the Wang-Buszaki model compared with a phase model. Figures 4.3A and 4.3C are waves generated in the full model with non-reflecting and periodic boundary conditions, respectively. Figures 4.3B and 4.3D are the equivalent phase models. Examining 4.3C there is a slight "distortion" in the kink between the 2nd and 3rd and 19th and 18th oscillators. This is most likely due to "competition" between the fractured solution and the solution $\theta_j = \frac{2\pi j}{N}$. Overall these comparisons show us that the phase model is a very good approximation to the full model and can be an extremely useful simplification for the analysis of more complex systems. The simulation of 4.3A involves sixty equations as opposed to the twenty used to simulate 4.3B.

4.5 ANTI-WAVES IN FIRING RATE MODELS

Anti-waves may be obtained in the types of firing rate models used in Chapter 2. For instance, consider a chain of oscillating neurons. In this coupling scheme, each oscillator is comprised of three asymmetric circulantly coupled neurons. It was shown in the previous chapter that by varying the coupling strength between such units, one can obtain intermediate stable phase-locked states in oscillator pairs. Figure 4.4 shows an example of an anti-wave in a chain

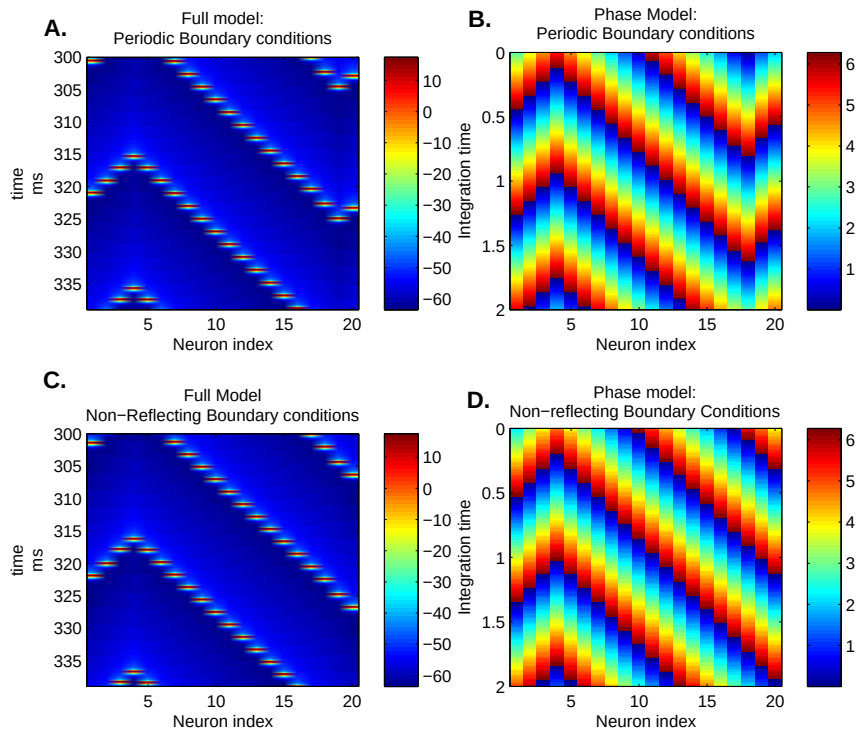

Figure 4.3: Four examples of anti-waves in both rings and chains of oscillators computed with $\eta = 6.0$. **A.** is a wave in a chain of Wang-Buszaki neurons with non-reflecting boundary conditions. **B.** is a wave in a chain of phase oscillators with non-reflecting boundary conditions. **C.** is a wave in a ring of Wang Buszaki neurons with periodic boundary conditions (full model). **D.** is the phase model reduction of panel C: It is a wave in a ring of phase oscillators with periodic boundary conditions.

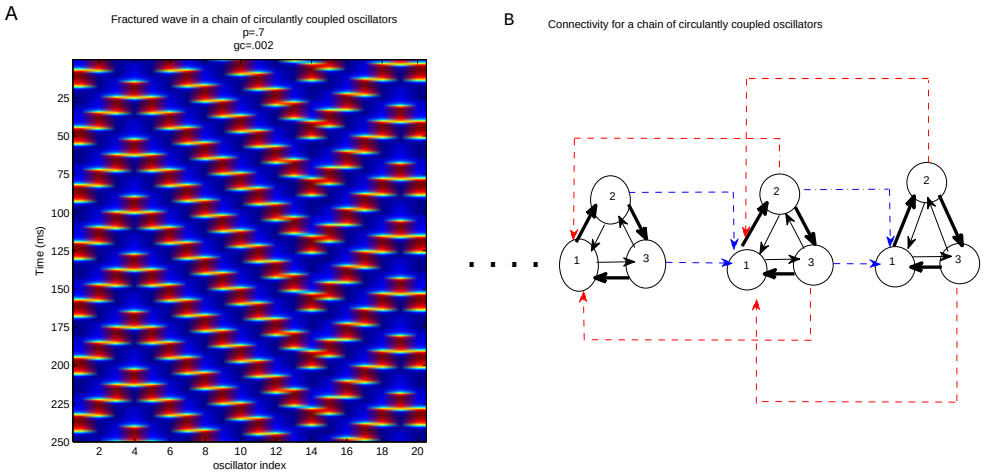

Figure 4.4: Example of an anti-wave in a chain of circulantly coupled Wilson-Cowan firing rate equations

of twenty Wilson-Cowan oscillators (sixty equations). These are the firing rate equations analyzed in Chapter 2. The plot shows the firing rate of the first neuron of each oscillator as a function of time. In order to produce these anti-waves, relatively weak coupling is needed, with coupling strength g_c on the order of $g_c = 0.001$. In the figure shown $g_c = 0.002$.

4.6 OBTAINING DIFFERENT WAVES FROM RANDOM INITIAL CONDITIONS

In order to simplify analysis, we assume that the interaction function may be approximated by only a few Fourier modes. We use only as many modes as are needed to produce the same effects as the full model. In many cases, using only the first two odd Fourier modes is

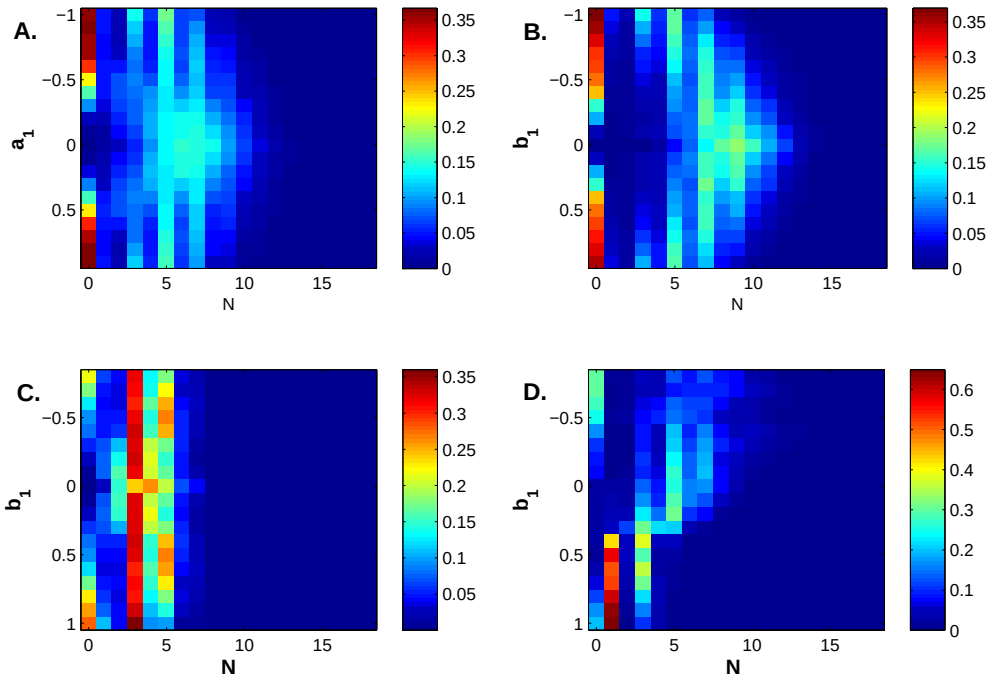

Figure 4.5: This is a plot of the probability of obtaining different solutions of 4.5 for twenty oscillators as a function of the Fourier coefficients of the interaction function. N designates the number of shocks in an anti-wave. $N = 0$ corresponds to a traveling wave. **A.** is a plot of the probability distribution with $H(\phi) = a_1 \cos(\phi) + b_1 \sin(\phi) + 0.75 \sin(2\phi)$ as a function of a_1 with $b_1 = 1$. **B.** is the probability distribution with $a_1 = 1$ and varying b_1. **C.** is the probability distribution calculated with an interaction function: $H(\phi) = -3 \cos(\phi) - .92 \cos(2\phi) + b_1 \sin(\phi) - 0.75 \sin(2\phi)$. **D.** is the probability distribution calculated using the interaction function: $H(\phi) = -3 \cos(\phi) + b_1 \sin(\phi) - 0.75 \sin(2\phi)$. For each parameter value the equations were solved from 10000 random initial conditions.

sufficient:[4].

$$\begin{aligned} H(\phi) &= a_1 \cos(x) + b_1 \sin(x) + b_2 \sin(2x). \\ b_2 &< 0 \end{aligned} \tag{4.12}$$

Such interaction functions will still produce anti-wave solutions. The behavior of the equations (4.5), using the function (4.12), will not be identical to the behavior obtained using the full interaction function. However, the approximation is close enough to infer some of the general properties of these waves.

Strogatz et al. has opined that while modeling and studying physical and biological systems, it is not sufficient to study only what solutions are possible to a set of differential equations, but also the probability of obtaining a particular solution starting from random initial conditions[88]. In particular, he applied this line of reasoning to try to understand the probability of synchronization in a ring of neurons, based on the number of connections in the network and the coupling strength[88]. This is akin to calculating the basin of attraction: the set of initial conditions that converges to a particular solution as $t \to \infty$. Strictly speaking, the interaction function we use (4.12) allows any number of shocks in the anti-wave, constrained only by the length of the chain. However, if we start the equations from random initial conditions, the probability of getting a certain number of shocks varies as we vary the size of the Fourier components. The main point is that even if the odd portion of the interaction function allows for a multiple shock solution, the probability of the system converging to this solution from random initial conditions may be extremely low and based on both the magnitude of the even and first odd Fourier modes. Figure 4.5 shows the probability distributions of obtaining various anti-wave and traveling wave solutions as a function of the magnitudes of both the even and odd Fourier terms of the interaction function. Panel 4.5A is a plot of the probability of obtaining either an N-shock anti-wave solution or a traveling wave solution as a function of a_1. From the plot, we see that the probability of obtaining a traveling wave solution approaches zero as $a_1 \to 0$. When $a_1 = 0$ the probability of obtaining a traveling wave is zero and the probability distribution shifts towards $N = 6$. As

[4]Kopell et al.[90] used a similar interaction function in her analysis of fractured waves, except her $b_2 > 0$. This is the difference between intermediate phase-locked states and bi-stability between synchrony and anti-phase states.

a_1 increases towards 1, the probability of obtaining the traveling wave solution increases as well. Near $a_1 = 1$ the traveling wave solution is the most probable one. Panel 4.5B is a plot of the probability distribution as a function of b_1 with $a_1 = 1$. Panel 4.5B shows a trend similar to 4.5A. For $b_1 = 0$ the probability of obtaining a traveling wave solution from random initial conditions is close to 0. The solution with the maximal probability corresponds to an anti-wave with $N = 9$ shocks or kinks. As b_1 is increased towards 1 or decreased towards -1 the probability distribution shifts towards $N = 0$. That is, solutions with fewer kinks become more probable as do traveling wave solutions. Panels 4.5C and 4.5D is an illustration of the effect of higher order even terms. Panel 4.5D demonstrates that using the interaction function with two even terms: $H(\phi) = \cos(\phi) + b_1 \sin(\phi) - \frac{3}{4}\sin(2\phi)$ results in a probability distribution in which the traveling wave solution is the most probable solution for $b_1 \to 1$ and the 1 kink anti-wave solution is the most probable for $b_1 \to -1$. If we do not include this second order term, as demonstrated in panel 4.5C the most probable solution corresponds to an ($N = 4$ shocks) anti-wave. The main point of this, is that even though the odd Fourier modes determine the solutions to equations 4.2 and 4.5, the even Fourier modes can drastically affect the basin of attraction of those solutions. In order to obtain a perfectly centered kink anti-wave solution, we must include a second order even term.

4.7 MOVING THE SHOCK POSITION WITH IMPULSES

Electric fish have been observed to produce complex anti-wave type patterns[84]. What is more, the lead oscillator or (kink) in these anti-waves has been observed to be able to shift position. We present a mechanism which shifts the position of the kink/shock in the anti-wave without changing its shape. Over the last fifteen years, Pikovsky and Rosenau have written several papers studying waves in oscillator lattices with purely even coupling ($H(\phi) = cos(\phi)$) . They showed that such interaction functions can be derived from networks of Josephson junctions and Van-der Pol oscillators[95][96][97]. Waves in such networks take the form of solitary pulses which retain their shape. Pikovsky and Rosenau have coined these waves "compactons"[95][96][97]. Collisions between different compactons have been studied

in detail. No one, however, has written about compactons colliding with a phase boundary (like our shock).

Compacton-like pulses are possible not only in systems with a purely even interaction function, but they can be observed in systems with odd terms, provided the even component is large enough[97]. The odd portion of the interaction function acts to dissipate the initial pulse, but a compacton-like wave may still travel large distances even with a substantial odd term. Compactons are possible in systems in which the interaction function generates anti-waves. For instance, Figure 4.6 illustrates a system of 200 phase-difference equations with non-reflecting boundary conditions. The interaction function used is $H(\phi) = \cos(\phi) + (\sin(\phi) - .75\sin(2\phi))$. The initial conditions are the one kink anti-wave solution with an extra pulse applied at the end. Thus we have the one kink/shock solution:

$$\begin{aligned} \phi_j &= k & j < \frac{N}{2} \\ \phi_j &= -k & j \geq \frac{N}{2}, \end{aligned} \tag{4.13}$$

with the addition of a pulse:

$$\phi_j = k + \frac{A}{2}(1 + \cos((j - x_0)\pi/\sigma)) \qquad |j - x_0| < \sigma. \tag{4.14}$$

Here A is the amplitude, x_0 is the position of the pulse and σ is the width of the pulse. This pulse is the form used by Pikovsky et al. to generate compactons, but square pulses may work as well[97]. Panel A shows a compacton, initiated from the right end of the chain, traveling on top of an anti-wave and colliding with the shock located at $N = 100$. Upon collsion, the shock shifts to the left but retains its shape. In this manner, multiple pulses initiated at the ends of the chain may be used to shift the shock back and forth. Panel B illustrates the same situation except the pulse is initiated from the left hand side of the chain. Larger amplitude pulses do not provide larger position shifts. If the pulse is too large, it will destroy the "perfect kink" solution. Thus, near the supercritical pitchfork bifurcation, not only can the shock of an anti-wave form anywhere along the the chain but precisely because of this property, it can be shifted around by an impulse (compacton). In this way, the additional

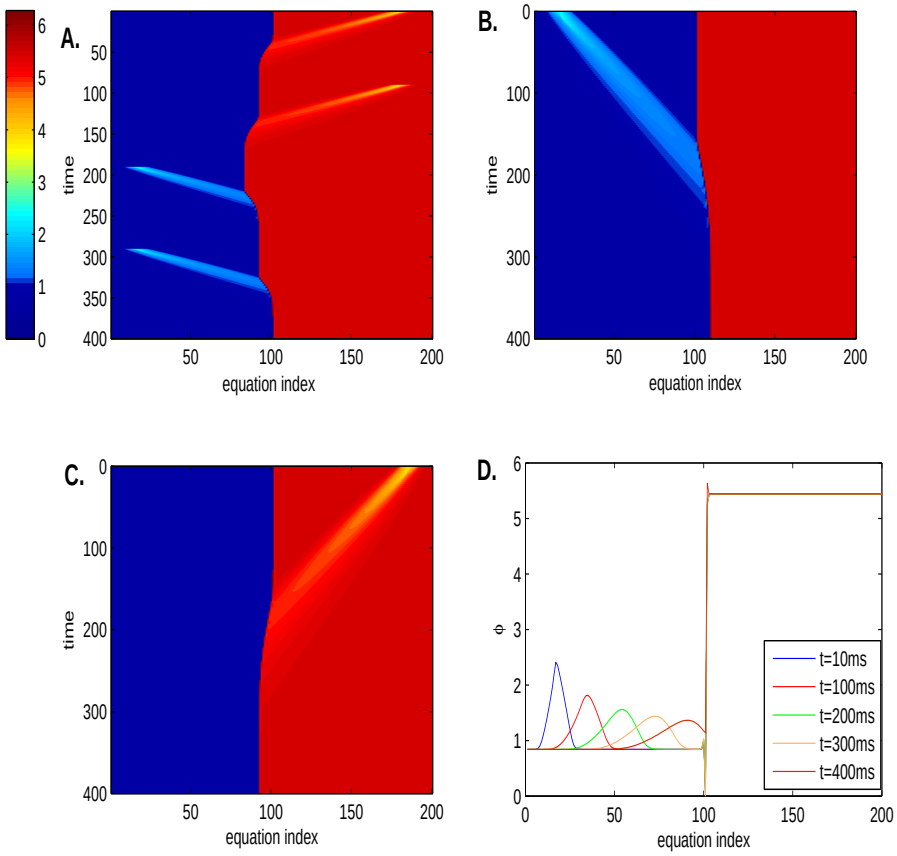

Figure 4.6: **A.** is a plot depicting pulses propagating on top of the anti-wave solution. At $t = 0$, a compacton pulse is initiated from the right hand side of the chain. This pulse collides with the other half of the anti-wave at the center. Upon impact the shock in the anti-phase solution shifts to the left. Multiple compactons can be used to shift the shock back and forth. The interaction function used was: $H(\phi) = \cos(\phi) + \sin(\phi) - 0.75\sin(2\phi)$ **B.** depicts the same situation as panel **A.** with one compacton eminating from the left of the wave. **C.** is an example of a pulse (compacton) emanating from the right to shift the shock. **D.** Is a plot of the compacton wave in **B.** at various instants in time. The wave dissipates as it approaches the shock.

even and odd Fourier terms produce a central pattern generator which is malleable. Perhaps this is a mechanism by which the hindbrain of a fish could send impulses to the rest of its spinal cord to modify the fish's swimming pattern.

4.8 STABILITY ANALYSIS

In analyzing the stability of anti-wave solutions, one of the main questions we want to address is how the relative contributions of each Fourier mode contributes to the stability of the solution. Additionally, we want to examine the importance of other parameters in the model, such as the length of the chain and the position of the kink. In these chain models there are four basic wave solutions which are of interest. Two of the solutions correspond to a traveling wave in either direction (left to right or right to left) and two correspond to anti-waves. The first anti-wave solution describes a wave emanating from the center of the chain and propagating in both directions outward. The second anti-wave solution corresponds to two waves emanating from the edges and colliding in the center of the chain. Using our simplified interaction function we begin by analyzing the simplest (shortest) chain possible, the three neuron system. The three phase equations (4.15) describing the neurons can be condensed to two by a change of variables. Linearizing these equations (4.16) about the anti-wave solution results in a 2x2 Jacobian. Thus, the problem is simple enough so that we can solve for the eigenvalues as a function of a_1 and subsequently show where and how the anti-wave solution loses stability. Once we have proved stability for this simple case, we discuss longer chains and specifically, we analyze the effects of the magnitude of the even component on the stability of various anti-wave solutions.

4.9 STABILITY ANALYSIS OF THE THREE OSCILLATOR SYSTEM

Our equations for the system with non-reflecting boundary conditions are:

$$\begin{aligned} \dot{\theta_1} &= 2H(\theta_2 - \theta_1) \\ \dot{\theta_2} &= H(\theta_3 - \theta_2) + H(\theta_1 - \theta_2) \\ \dot{\theta_3} &= 2H(\theta_2 - \theta_3). \end{aligned} \tag{4.15}$$

We then write them in terms of their phase differences:

$$\begin{aligned} \dot{\phi_1} &= 2H(-\phi_2) - H(-\phi_1) - H(\phi_2) \\ \dot{\phi_2} &= H(-\phi_1) + H(\phi_2) - 2H(\phi_1). \end{aligned} \tag{4.16}$$

Note that these equations are invariant under a reflection: $\phi_1 \to -\phi_2$
$\phi_2 \to -\phi_1$

Figure 4.7 is a plot of the nullclines of the system for various values of a_1. There are two anti-wave solutions indicated by the boxes and two traveling wave solutions denoted by the circles. One can see that when there is no even component the solutions to the system possesses perfect reflection symmetry. As the even component of the interaction is increased the system begins to lose this symmetry until roughly $a_1 = 1.1$. At this point the equations undergo a sub-critical pitchfork bifurcation and one of the solutions ($\phi_1 = k, \phi_2 = -k$) loses stability. (This is shown in appendix C) This bifurcation is depicted in Figure 4.7C. In this plot, the stable solution is represented by a solid line whereas the unstable solution is represented by the dotted lines. Figure 4.7D is an enlargement of the phase plane near the anti-wave solution. Both the nullclines and flow for $a_1 = 0$ and $a_1 = 1.2$ are plotted on top of one another. The flow corresponding to $a_1 = 0$ converges to the fixed point. This is in distinction with the flow corresponding to $a_1 = 1.2$, in which the stable node has been replaced with a saddle. We want to analyze the stability of the anti-wave analytically. Choosing $\phi_1 = k$ and $\phi_2 = -k$, we linearize our equations about this system and write down the Jacobian as follows:

$$M_0 = \begin{pmatrix} H'(-k) & -2H'(k) - H'(-k) \\ -H'(-k) - 2H'(k) & H'(-k) \end{pmatrix}, \tag{4.17}$$

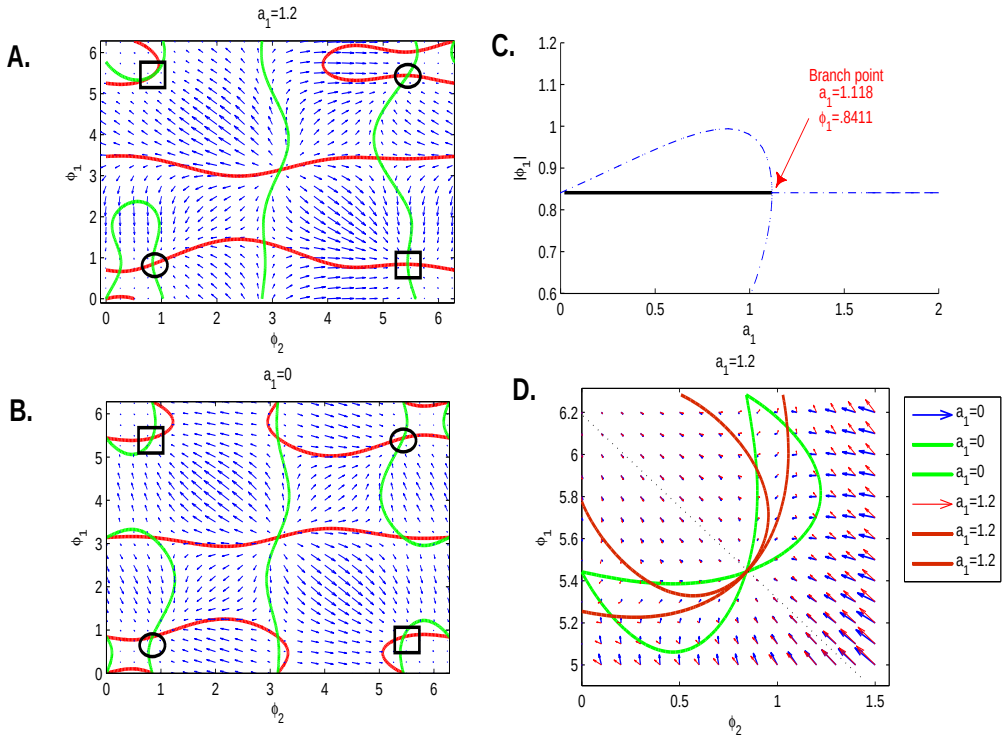

Figure 4.7: The nullclines of a three oscillator phase model system for varying values of a_1. **A.** is a plot of the nullclines and the flow for $a_1 = 0$. The fixed points corresponding to anti-waves are enclosed with boxes. The fixed points corresponding to traveling waves are circled. **B.** is a plot of the nullclines and the flow for $a_1 = 1.2$. **C.** is a bifurcation diagram computed with AUTO: The anti-wave solution loses stability near $a_1 = 1.118$. **D.** is a enlargement of the upper left hand corner of panels **A.** and **B.**. The red arrows correspond to $a_1 = 1.2$ whereas the blue arrows correspond to $a_1 = 0$.

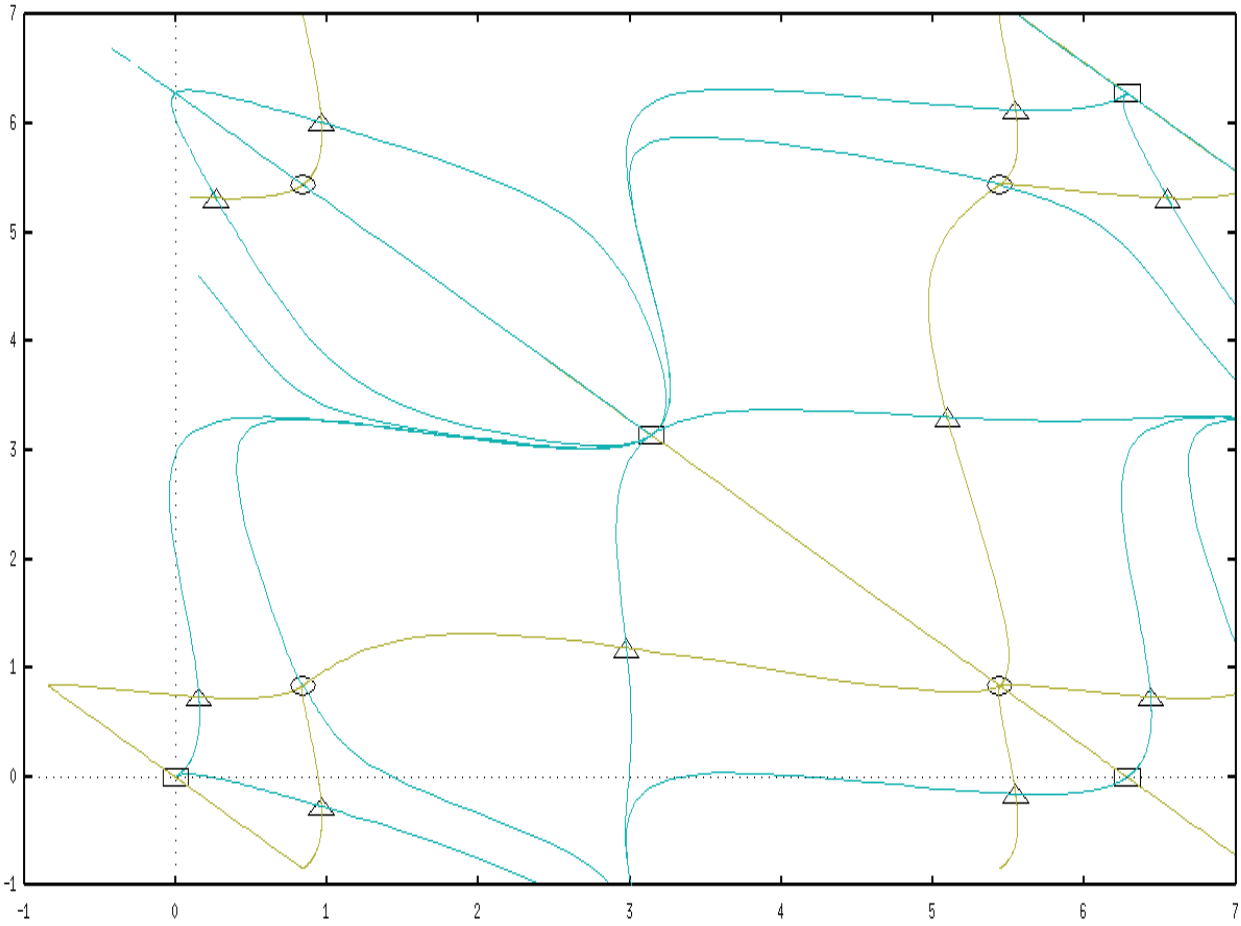

Figure 4.8: A plot of the fixed points as well as stable and unstable manifolds of equation 4.16. The x axis is ϕ_2 and the y axis is ϕ_1. The stable manifolds are the cyan colored curves. The unstable manifolds are the green curves. Squares are unstable nodes, circles are stable nodes and triangles are saddle points. This plot was generated using Ermentrout's XPP program: (www.math.pitt.edu/ bard/xpp/xpp.html).

Solving for the eigenvalues of this expression, we have

$$\lambda_{1,2} = -2H'(k), -2H'(-k) - 2H'(k). \tag{4.18}$$

As long as the derivative of these H functions evaluated at this solution is positive, then the solution will be stable. Substituting the simplified interaction function (4.19) and its derivative into equation 4.18. results in the eigenvalue expressions: equation 4.20.

$$\begin{aligned} H(\phi) &= b_1 \sin(\phi) + b_2 \sin(2\phi) + a_1 \cos(\phi) \\ H'(\phi) &= b_1 \cos(\phi) + 2b_2 \cos(2\phi) - a_1 \sin(\phi) \end{aligned} \tag{4.19}$$

$$\begin{aligned} \lambda_1 &= -2(b_1 \cos(k) + 2b_2 \cos(2k) - a_1 \sin(x)) \\ \lambda_2 &= -4(b_1 \cos(k) + 2b_2 \cos(2k)) \end{aligned} \tag{4.20}$$

At the critical value of the parameter $a_{critical} = -1.1$, the first eigenvalue vanishes. Beyond this point the fixed point becomes stable. The mirror symmetry of the equations, along with the bifurcation diagram in Figure 8, suggest that this is a subcritcal pitchfork bifurcation: this is verified in Appendix C. Applying the center manifold theorem to this system of equations results in the normal form equation:

$$\frac{du}{d\tau} = c_1 u + c_2 u^3. \tag{4.21}$$

The coefficients to this expression are found in Appendix C. It is shown that $c_2 > 0$, therefore the equation 4.21 is recognized as the normal form for the sub-critical pitchfork bifurcation.

4.10 STABILITY ANALYSIS FOR THE TRAVELING WAVE

Proving the stability of the traveling wave (with no kinks) is relatively straightforward. We begin by writing down the equations for the "jth" oscillator. Since the system is nearest neighbor coupling, the general expression is:

$$\dot{\phi_j} = H(\phi_{j+1}) + H(-\phi_j) - H(-\phi_{j-1}) - H(\phi_j). \tag{4.22}$$

Defining $a = H'(\phi)$, $b = H'(-\phi)$ and linearizing the equations about the wave solution, the equations for the phase are simply a discretized version of Laplace's equation:

$$\mathrm{a}\phi_{j+1} - (a+b)\phi_j + b\phi_{j-1} = \lambda\phi_j. \tag{4.23}$$

We may solve for the equations by assuming a general solution:

$$\phi_j = Ax_1^j + Bx_2^j, \tag{4.24}$$

and invoking the boundary conditions: $\phi_0 = \phi_1$ and $\phi_{N-1} = \phi_N$. Plugging our solution 4.24 into 4.23 and solving for x results in the quadratic expression:

$$x_{1,2} = \frac{(a+b+\lambda)}{2a} \pm \frac{1}{2a}\sqrt{(a+b+\lambda)^2 - 4ab}. \tag{4.25}$$

By multiplying the two solutions to the quadratic equation together, we obtain the expression:

$$x_1 x_2 = \frac{b}{a}. \tag{4.26}$$

This expression (4.26) can be used in conjunction with the boundary conditions to solve for the eigenvalues of the system of equations. Plugging our solution into the boundary conditions results in two equations for A and B.

$$\begin{aligned} (1+x_1)A + (1+x_2)B &= 0 \\ x_1^{N-1}(1+x_1)A + x_1^{N-1}(1+x_1)B &= 0 \end{aligned} \tag{4.27}$$

By forming a matrix from these equations and taking its determinant we are left with the expression:

$$\begin{aligned} \left(\frac{x_1}{x_2}\right)^{N-1} &= 1 \\ \frac{x_1}{x_2} &= e^{\frac{2\pi i m}{(N-1)}} \qquad\qquad m = 0, 1, 2..... \end{aligned} \tag{4.28}$$

Combining this expression with 4.26 yields:

$$x_1 = \sqrt{\frac{b}{a}} e^{\frac{i\pi m}{N-1}} \qquad x_2 = \sqrt{\frac{b}{a}} e^{-\frac{i\pi m}{N-1}}. \tag{4.29}$$

Substituting these into 4.23 and solving for the eigenvalues, λ results in the expression:

$$\Re\lambda = 2\sqrt{ba}\cos\frac{\pi m}{N-1} - (a+b). \tag{4.30}$$

This is the condition for stability. Therefore the wave solution will always be stable provided that

$$2\sqrt{ba} \leq a + b \tag{4.31}$$

Or alternately that $a, b > 0$. Stability is lost for $a, b < 0$.

4.11 STABILITY ANALYSIS FOR THE ANTI-WAVE (PURELY ODD COUPLING)

If our interaction function is purely odd, it is relatively easy to prove the stability of the anti-wave. Because the function is purely odd, its derivative will be purely even and $H'(\phi) = H'(-\phi)$. Therefore, equation 4.23 becomes

$$\mathrm{a}\phi_{j+1} - 2a\phi_j + a\phi_{j-1} = \lambda\phi_j. \tag{4.32}$$

We solve for the eigenvalues in exactly the same manner as the traveling wave case. This results in the solution:

$$\Re\lambda = 2a\left(\cos\frac{\pi m}{N-1} - 1\right). \tag{4.33}$$

The eigenvalues will be negative and the solution will be stable provided that $H'(\phi) > 0$. Proving the stability of a fractured wave is not as straightforward when the interaction function has an even component. In order to prove stability we must apply the Gershgorin Circle Theorem and/or calculate the eigenvalues numerically.

4.12 STABILITY FOR THE ANTI-WAVE UNDER MORE GENERAL CONDITIONS

We illustrate the use of Gershgorin Circle Theorem by applying it to a system of seven oscillators with a centrally located kink or shock. In this example, we use non-reflecting boundary conditions. The argument will be identical for periodic boundary conditions. The linearization for one element of the system of equations will be:

$$\dot{\phi_j} = H'(-\phi^*_{j-1})\phi_{j-1} - (H'(\phi^*_j) + H'(-\phi^*_j))\phi_j + H'(\phi^*_{j+1})\phi_{j+1}. \tag{4.34}$$

Now assume a 1-kink solution as given in Table 4.1:

We linearize our equations about this solution. If we define $a = H'(k)$, $b = H'(-k)$ the

Table 4.1: shock solution for a six neuron chain

ϕ_1	ϕ_2	ϕ_3	ϕ_4	ϕ_5	ϕ_6
k	k	k	$-k$	$-k$	$-k$

Jacobian matrix for a fractured solution will have the form:

$$\begin{pmatrix} -(2a+b) & a & 0 & 0 & 0 & 0 \\ b & -(a+b) & a & 0 & 0 & 0 \\ 0 & b & -(a+b) & b & 0 & 0 \\ 0 & 0 & b & -(a+b) & b & 0 \\ 0 & 0 & 0 & a & -(a+b) & b \\ 0 & 0 & 0 & 0 & a & -(2a+b) \end{pmatrix}. \tag{4.35}$$

The Gershgorin Circle Theorem is stated in Appendix**??**. It tells us that all of the eigenvalues of the matrix lay in the union of disks centered at the diagonal elements of the matrix with radii less than the absolute value of the sum of the row entries. If z is the eigenvalue of the matrix: $|z - a_{ii}| \leq \sum_{j \neq i} |a_{ij}| (i = 1...n)$.

If the Jacobian of the anti-wave is described by 4.35, then all eigenvalues will lie in the union of three disks: one centered at $-(a+b)$ with radius $a+b$, one centered at $-2a+b$ with radius a and one centered at $-(a+b)$ with radius $2b$. The latter disk corresponds to the equation at the shock. If we assume that the even term a_1 is positive and increasing, then $H'(-\phi) \geq H'(\phi)$

$$\begin{aligned} |b| &\geq |a|, \\ |2b| &> |a+b|. \end{aligned} \tag{4.36}$$

Thus the disks will extend beyond the origin, and we will not be able to say anything about stability using this theorem. On the other hand, if the solution is a shock oriented in the opposite direction, the Jacobian matrix is:

$$\begin{pmatrix} -(2b+a) & b & 0 & 0 & 0 & 0 \\ a & -(a+b) & b & 0 & 0 & 0 \\ 0 & a & -(a+b) & a & 0 & 0 \\ 0 & 0 & a & -(a+b) & a & 0 \\ 0 & 0 & 0 & b & -(a+b) & a \\ 0 & 0 & 0 & 0 & b & -(2b+a) \end{pmatrix} \tag{4.37}$$

In this case the disk corresponding to the equation at the shock is centered at $-|a+b|$ and extends out with radius $|2a|$. The disk will always lay in the left half of the imaginary plane for a_1. Therefore, this solution will always be stable.In the former case, in which the fractured wave is not necessarily stable, one must apply numerical methods to explicitly calculate the eigenvalues of the Jacobian. We want to study how variables such as the position of the shock and the length of the chain effect the stability of the solution as we vary the magnitude of the first even Fourier mode. We start by examining a fifty-one oscillator chain (described by fifty equations) in which we move the position of the shock. Figure 4.9A shows the critical value of a_1 at which the shock solution loses stability as a function of shock position where the position varies between site 4 and site 46. The parameter $a_{critical}$ is determined by calculating the eigenvalues of the Jacobian for various values of a_1 and determining when the eigenvalue with the maximal real part becomes positive. 4.9B plots the real part of the eigenvalue with maximal real part as a function of a_1

As we can see from the plot, as the position shifts, the eigenvalues lose stability at different values of a_1. The type of bifurcation by which they lose stability changes as well. For shocks located at even numbered sites, the system loses stability in a Hopf bifurcation as a complex conjugate pair of eigenvalues crosses the origin simultaneously. For shocks located at odd sites the system apparently loses stability in a sub-critical pitchfork bifurcation (This has not been proven). Figure 4.9C is a plot of $a_{critical}$ for the eigenvalues of the fifty-one oscillator Jacobian linearized about solutions corresponding to varying values of b_2. The plot

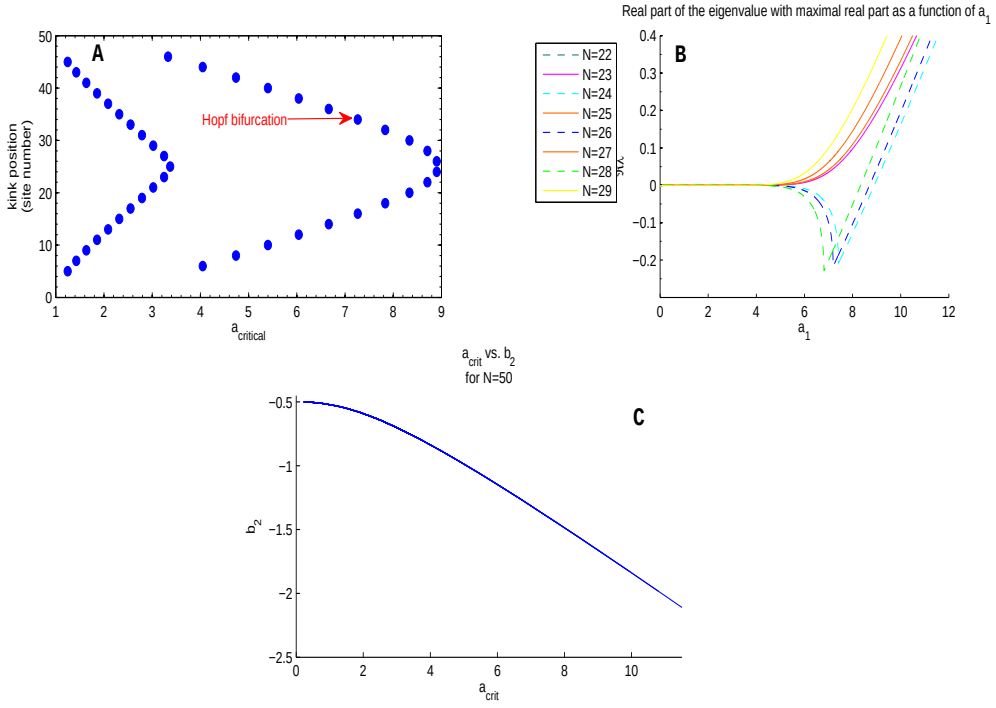

Figure 4.9: **A.** critical value of a_1 as a function of shock position. **B.** eigenvalue with the maximal real part as a function of a_1 for different shock positions. In this plot N denotes the location of the shock. **C.** is a plot demonstrating that an interaction function with a more negative b_2 can also possesses a larger a_1 before the solution becomes unstable.

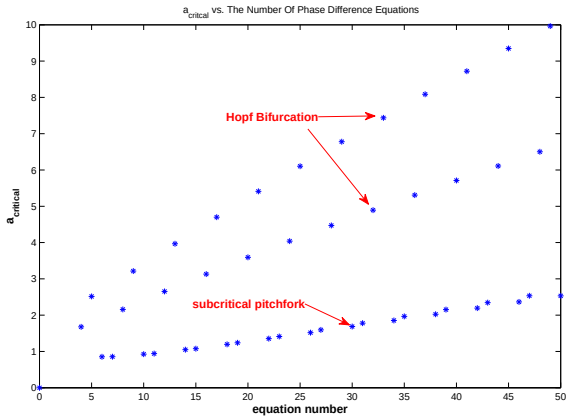

Figure 4.10: Critical value of a_1 as a function of chain length where N represents the number of phase difference equations ϕ_N. Depending on the length of the chain, the solution may lose stability in either a Hopf bifurcation or what is believed to be a subcritical pitchfork bifurcation.

clearly demonstrates that shock solutions corresponding to a larger value of b_2 can support a larger even component before becoming unstable.

Figure 4.10 is a plot of $a_{critical}$ vs. the number of phase difference equations (number of oscillators in a chain). It shows phenomena similar to Figure4.9. That is, a solution will lose stability for different a_1 dependent on the position of the shock in the solution as well as the number of oscillators in the chain. Since the solution is perfectly symmetric for the fifty oscillator chain, we expect this solution to loose stability in a sub-critical pitchfork. For relatively short chains, the anti-wave solution will be stable for a relatively large even component, whose magnitude is at least as large as the first odd Fourier mode. The manner in which the solution loses stability and the size of the even component it can support depends on both the position of the kink/shock and the length of the chain. The Gershgorin circle theorem tell us that one of the anti-wave solutions will always be stable, no matter how long the chain. It may be possible to say something more general about stability of long chains using the Ermentrout-Kopell continuum equation (4.9). This is currently being examined and may appear in future work.

4.13 PATTERN FORMATION IN TWO-DIMENSIONAL ARRAYS OF NEURONS

Anti-wave patterns can be observed in two-dimensional networks as well. Using nearest neighbor coupling, the differential equation for a single oscillator is:

$$\frac{d\theta_{x,y}}{dt} = H(\theta_{x+1,y} - \theta_{x,y}) + H(\theta_{x,y+1} - \theta_{x,y}) + H(\theta_{x,y-1} - \theta_{x,y}) + H(\theta_{x-1,y} - \theta_{x,y}), \quad (4.38)$$

where x, y are discrete indices describing the location of an oscillator. These indices run from 1 to N where N^2 is the number of differential equations in the array. As in the one dimensional case, we use both periodic boundary conditions and non-reflecting boundary conditions. Implementing periodic boundary conditions, we have $\theta_{N+1,y} = \theta_{1,y}$ and $\theta_{y,N+1} = \theta_{y,N}$. The non-reflecting boundary conditions are $\theta_{N+1,y} = \theta_{N-1,y}$ and $\theta_{x,N+1} = \theta_{x,N-1}$. We focus our analysis on three basic types of behavior in the two dimensional system: plane waves, shock waves and two dimensional fractured patterns. Other patterns may be possible as well. Examples of these patterns are are illustrated in Figure 4.11.

Analogous to the one-dimensional case, a plane wave may be represented by the solution:

$$\theta_{xy} = k_x x + k_y y + \omega t. \quad (4.39)$$

Whereas the shock solution may be written:

$$\begin{aligned} \theta_{xy} &= k_x x + k_y y \qquad x \leq x^* \\ \theta_{xy} &= -k_x x + k_y y \qquad x > x^*. \end{aligned} \quad (4.40)$$

In these equations x^* is the location of the shock. A shock may be thought of as a discontinuous boundary between the collision of two traveling waves. Fractured patterns are generated with random initial conditions where the phases are chosen between 0 and 2π.[5] The fractured pattern is composed of many small waves of varying k_x and k_y which form shocks where they collide. An example of a random pattern may be seen in Figure 4.12. One may also observe spiral-like waves in these patterns. As in the one dimensional case, we approximate our interaction functions as a Fourier series. Of course, the more Fourier terms

[5] All equations in this section were integrated with Euler's method. The step size used is .01.

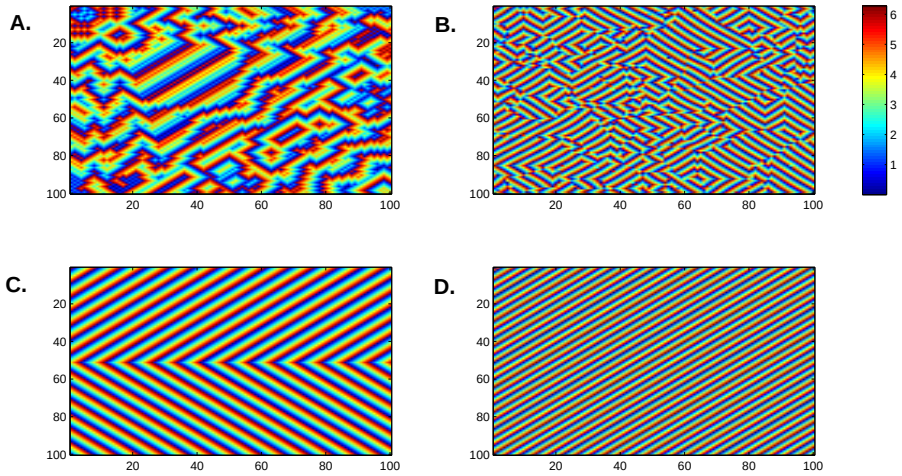

Figure 4.11: Examples of two-dimensional patterns. The horizontal and vertical axis are the oscillator indices. **A.** is a quasi-stationary wave pattern obtained from compacton-like initial conditions: a 2-dimensional pulse is initiated in the upper left-hand corner of the array. The interaction function used is $H(\phi) = \cos(\phi) - \sin(\phi) + .75\sin(2\phi)$ **B.** is a fractured pattern obtained from random initial conditions and interaction function:$-2\cos(\phi) - 0.518\sin(\phi) - 1.31\sin(2\phi) - .933\sin(3\phi)$ **C.** is an anti-wave generated with $H(\phi) = \cos(\phi) - \sin(\phi) + .75\cos(\phi)$. **D.** is a traveling wave generated with the same interaction function as **C.**

we use, the better the approximation to the true interaction function. In the interest of simplifying the analysis of the patterns, however, we try to use as few terms as are needed to produce the three patterns mentioned above. We find that interaction functions containing only several terms will suffice in order to produce patterns comparable to those produced with the full $H(\phi)$. Through trial and error, we eliminated Fourier components of the full model in order to obtain the interaction function with the fewest number of Fourier terms which would accurately yield the same fractured patterns as seen in Figure 12, as well as plane waves and colliding waves with one shock. The result is an interaction function with one even harmonic and three odd terms[6]:

$$H(\phi) = a_1 cos(\phi) + b_1 \sin(\phi) + b_2 \sin(2\phi) + b_3 \sin(3\phi) \tag{4.41}$$

An attracting class of fractured patterns can be generated from random initial conditions with: $a_1 = -2.0$, $b_1 = -0.518$, $b_2 = -1.31$ and $b_3 = -0.933$.

4.14 SPATIAL CORRELATION

One method we use to characterize these systems is the correlation between pairs of points in the array as a function of the distance between them. The correlation is essentially a measure of "how similar" two phase angles are. The correlation, $C(r,t)$, is computed by first taking $X_{ij} = \sin(\theta_{ij})$ for all of the phase angles in the array. We then compute the average over all sites in the array for all pairs of points with the same separation[7]:

$$C(r,t) = \frac{1}{N} \sum_{x'y'} X_{xy} X_{x'y'}, \tag{4.42}$$

subject to the constraint ; $(r-0.5)^2 < x'^2 + y'^2 < (r+0.5)^2$.

In this regard, if we measure this correlation as a distance between sites, then the distance at which the correlation is at a maximum may be thought of as a crude wavelength. For

[6]The Fourier terms used may or may not be calculated from the full model. For instance, an interaction function with an artificially inflated second odd mode will produce an interesting fractured pattern, whereas many interaction functions computed from the full model will not.

[7]Similar methods were used by [98].

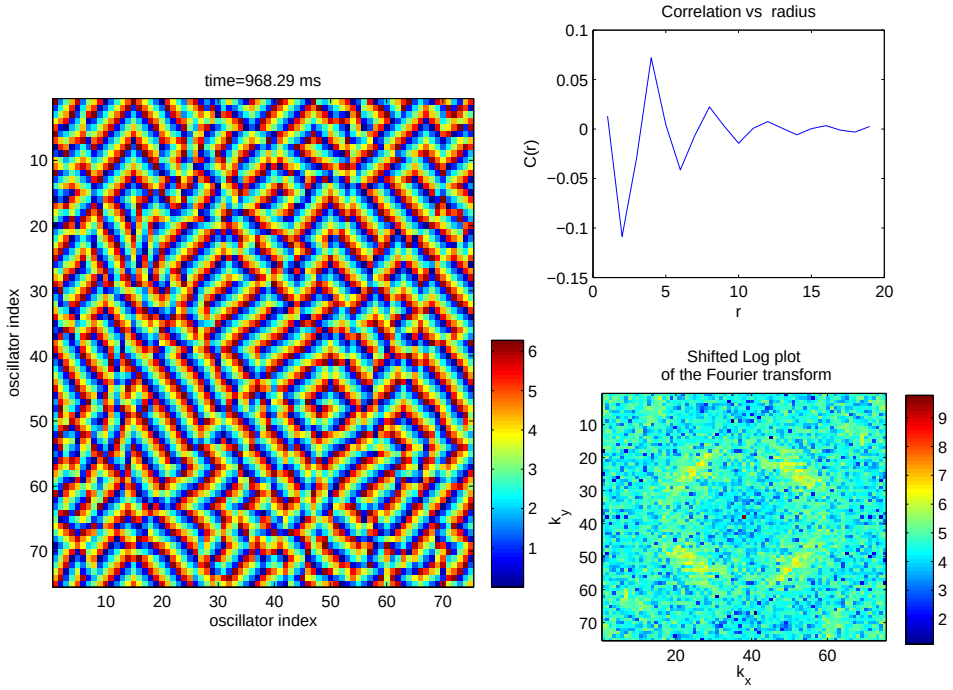

Figure 4.12: **A.** Steady state fractured wave pattern in two dimensions, this pattern was generated using the Fourier terms listed in 3.1 and random initial conditions. **B.** Spatial correlation calculated out to twenty sites. The maximum of the correlation corresponds approximately to a wavelength. The maximum occurs at $r = 4$. **C.** Fast Fourier transform (FFT) of the two dimensional pattern seen in A with the zero frequency component shifted to the center. The yellow ring with a radius of approximately 20 corresponds to a preferred wave number.

instance, Figure 4.12 A shows a fractured wave pattern generated with random initial conditions in a sheet of 75x75 neurons. The correlation for the fractured pattern generated with random initial conditions is shown in Figure 4.12B as a function of radius out to twenty sites. The maximum of the correlation occurs at about $r = 4$ which corresponds roughly to a "wavelength" at which the pattern repeats itself. In order to generate a stationary pattern we subtract θ_{11} from every phase in the network. Figure 4.12C was computed by taking the magnitude of the fast Fourier transform and shifting the zero frequency component to the center of the plot. One can see a "yellow ring" with a radius of about 20 sites in the plot corresponding to preferred wavenumbers. This simply illustrates that our box of length 75 neurons contains about 20 waves, thus validating the shape of $C(r)$. The spatial correlation may be used as a measure of the relative stability of different patterns and solutions obtained with different boundary conditions. To this end we add noise to the system and measure the spatial correlation as a function of noise strength for both traveling waves and anti-waves [98]. When the magnitude of the noise is large enough that the pattern is destroyed, the correlation drops to zero. The 2-dimensional anti-wave and traveling wave patterns using both sets of boundary conditions are plotted in Figure 4.13. All of the patterns were generated using the simplified interaction function $H(\phi) = a_1 \cos(\phi) + b_1 \sin(\phi) + b_2 \sin(2\phi) + b_3 \sin(3\phi)$. The maximum of the spatial correlation for both waves occurs at $r = 3$. Thus, we use $C(r = 3)$ as an order parameter to measure when the pattern loses stability due to the addition of noise. Adding a noise term γ to equation 4.38 results in the expression:

$$\dot{\theta}_{x,y} = H(\theta_{x+1,y} - \theta_{x,y}) + H(\theta_{x,y+1} - \theta_{x,y}) + H(\theta_{x,y-1} - \theta_{x,y}) + H(\theta_{x-1,y} - \theta_{x,y}) + \sigma\gamma. \quad (4.43)$$

This is a Langevin equation. The noise use is Gaussian distributed and characterized by:

$$\begin{aligned} < \gamma(t) > &= 0 \\ < \gamma_i(t)\gamma_j(t') > &= 2\delta_{ij}\delta(t - t')[99]. \end{aligned} \quad (4.44)$$

Discretization of this equation leads to a noise term $\sigma\sqrt{\Delta t}n$ where n is a normally distributed random number between 0 and 1[65]. Niebur et al. used a similar system of equations to study pattern formation in two dimensional arrays of oscillators with time lags[99]. They argued that the additive noise is like the "temperature" of the system [99]. They find that

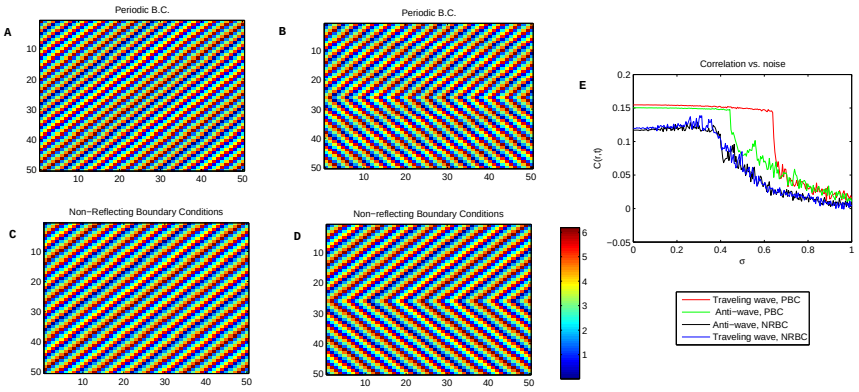

Figure 4.13: Examples of patterns obtained with a variety of boundary conditions and initial conditions. Figure 4.13E is a plot of the correlation as a function of noise for the different patterns. The abbreviations in the key: Non-reflecting boundary conditions (NRBC), Periodic boundary conditions (PBC).

as they increase the magnitude of this noise term, the system jumps from a state characterized by high frequency oscillations (called the metastable state) to one of low frequency oscillations[99]. We start with $\sigma = 0.0$ and simulate the equations with initial conditions corresponding to either the traveling wave or anti-wave solutions.[8] When the system of oscillators has reached a stationary pattern after $20,000$ time steps, we begin to increase the value of the noise in increments of 0.005 . We let the system settle down over a period of 50 seconds (500 time steps) of integration time before calculating the correlation and incrementing the noise again. Since the patterns examined are stationary, we did not time average the correlation. The results are plotted in Figure 4.13E. This correlation plot shows that in general, the traveling wave is more robust than the anti-wave.

These simulations show a 50x50 grid of neurons (phase oscillators). Figure 4.13 illustrates that using periodic boundary conditions, one cannot obtain the above "perfect" shock solution, nor can one obtain a perfect traveling wave. Using periodic boundary conditions

[8]Actually additive noise for this system is not strictly correct. If the original system of Wang-Buszaki equations was noisy then the noise term should be multiplicative. Additive noise suits our purposes of perturbing the system (see for instance:[98] [99]).

one obtains a ripple effect in the phase differences. The ripples can be qualitatively understood as competition between the anti-wave solution and the solution $\theta_{xy} = \frac{2\pi(x+y)}{N}$. The ripples are most evident in Figure 4.13B as dark areas running orthogonally to the direction of propagation of the wave.

4.15 STABILITY ANALYSIS OF THE TWO DIMENSIONAL PATTERNS

Ermentrout's theorem for stability in an array of oscillators provides a sufficient condition for the stability of our patterns. It can also be used to explain why we observe fractured patterns for some interaction functions and not others. According to this theorem, stability is ensured if all the derivatives of the interaction, when evaluated at the stationary solution are positive:

Ermentrout's Theorem for Oscillator Arrays:
Suppose $\theta_j = \sum_{k=1}^{N} \dot{H}(\lambda, j, k, \theta_k - \theta_j)$ *has a solution* θ_j^0 *for* $\lambda = 0$ *and suppose that* $a_{jk} = H_\theta(\lambda, j, k, \theta_k^0 - \theta_j^0) \geq 0$ *Suppose that the matrix* a_{jk} *is completely indirectly connected. Then there is a unique branch of solutions containing* θ_j^0 *for all* λ. *If* $a_{jk} \geq 0$ *this solution is orbitally asymptotically stable.*[87]

Figure 4.14A shows a plot of the derivatives of the interaction functions. The derivative of the interaction function corresponding to $a_1 = -2$, $b_1 = -0.518$, $b_2 = -1.31$ and $b_3 = -0.933$, is positive over a range of phases denoted by the black arrows. By contrast, the interaction function computed from the full model with $\eta = 6.0$ is only positive for values of phase difference between 0 and π. Now consider the random fractured pattern: the stationary solution for this pattern consists of a range of phase differences between different adjacent oscillators in the sheet. The distribution of phase differences in the "x" direction is shown in 4.14 B. Comparing this distribution with the plot of the derivatives of the various interaction functions, we see that the peaks of the distribution match perfectly with the range of positive H'. Therefore, since the derivatives of H evaluated at all these phase differences is positive, Ermentrout's theorem proves the stability of the solution. If one assumes that this same pattern is a solution to the array with the interaction function corresponding to $\eta = 6.0$, it

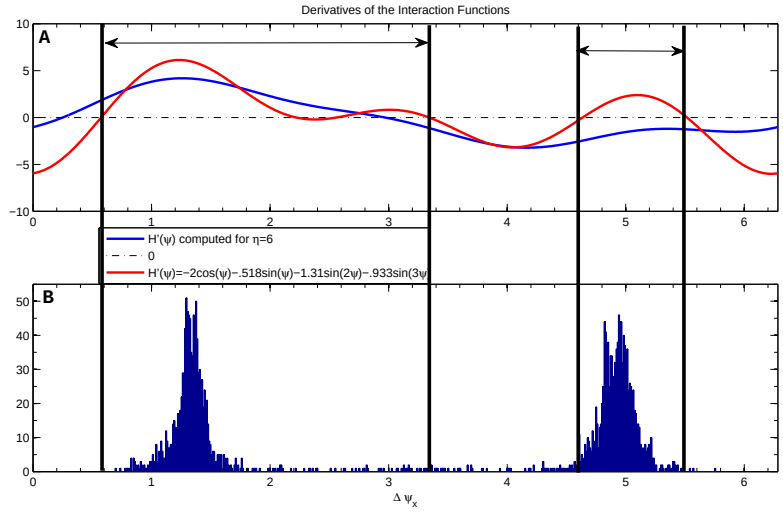

Figure 4.14: **A.** is a plot of the derivatives of two interaction functions evaluated over a range of phase differences. The blue curve represents the interaction functions are computed from $\eta = 6.0$ and the red curve is the interaction function used to generate the fractured pattern. The derivative of this interaction function (for the fractured pattern) is positive over a larger region than that computed for $\eta = 6.0$.

cannot meet the same stability criteria. This is because the derivative of H near the peak at $3\pi/2$ is negative. Therefore, we conclude the formation of stable patterns is critically dependent on the shape of the interaction function. In other words, in order to generate a stable pattern we need negative higher order terms that ensures the derivative of H is positive over the necessary range of phase differences.

4.15.1 Stability Analysis of the Two Dimensional Plane Wave

Generally speaking, the traveling wave is not a stable solution in systems which have beyond nearest neighbor coupling. In order to demonstrate this, we start with a continuum model where the interaction function is convolved with a Gaussian kernel. For instance, take the equation:

$$\begin{aligned} \frac{\partial u}{\partial t} &= \int_{-\infty}^{\infty} G(x'^2 + y'^2) H(u(x+x', y+y') - u(x,y)) dx' dy' \\ G(x,y) &= e^{-x^2-y^2}. \end{aligned} \tag{4.45}$$

Linearizing about the plane wave solution, we obtain an expression for the eigenvalues.

$$\lambda = \int_{-\infty}^{\infty} \int_{-\infty}^{\infty} G(x'^2 + y'^2) H'(\vec{k} \cdot \vec{r'}) (e^{\vec{q} \cdot \vec{r'}} - 1) dx' dy' \tag{4.46}$$

Calculating the integral with our simple interaction function and taking the real part of the eigenvalues results in the expression:

$$\begin{aligned} \Re\lambda &= 2\pi b_1 \left(e^{-(\vec{k}+\vec{q})\cdot(\vec{k}+\vec{q})} + e^{-(\vec{k}-\vec{q})\cdot(\vec{k}-\vec{q})} \right) + 4\pi b_2 \left(e^{-(2\vec{k}+\vec{q})\cdot(2\vec{k}+\vec{q})} + e^{-(2\vec{k}-\vec{q})\cdot(2\vec{k}-\vec{q})} \right) \\ &+ 6\pi b_3 \left(e^{-(3\vec{k}+\vec{q})\cdot(3\vec{k}+\vec{q})} + e^{-(3\vec{k}-\vec{q})\cdot(3\vec{k}-\vec{q})} \right) - 4\pi b_1 e^{-\frac{\vec{k}\cdot\vec{k}}{2}} - 8\pi b_2 e^{-2\vec{k}\cdot\vec{k}} - 12\pi b_3 e^{\frac{-9\vec{k}\cdot\vec{k}}{2}} \end{aligned} \tag{4.47}$$

Assuming that $q_x = q_y = q$ as well as $k_x = k_y = k$. Figure 4.15 is a plot of the maximum of the eigenvalue for all values of q as a function of k. All of the eigenvalues are positive or zero, hence the wave is unstable.

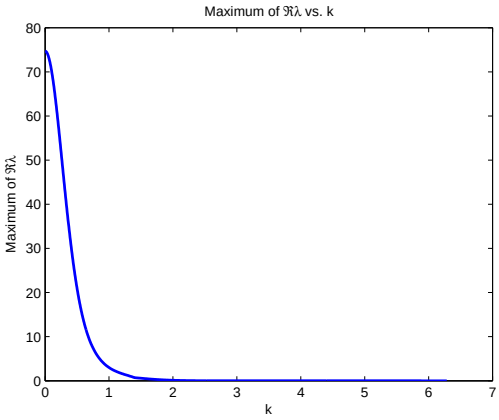

Figure 4.15: A plot of the real portion of the the maximum eigenvalue from 4.47 as a function of k. To obtain this plot it was assumed that $k_x = k_y$ and $q_x = q_y$. The magnitude of both vectors was varied between 0 and 2π. From the plot we see that the solution is unstable for all values of k.

4.16 CONCLUSION

In this Chapter, we showed how intermediate stable phase-locked states could produce wave behavior in one-dimensional chains of neurons. The mechanism for generating waves is preferable to past models, because it allows one to modulate the wavelength of the wave by adjusting properties such as the potassium conductance or temperature dependent time constant. It also does not require distal connections and the shock can form anywhere along the chain. The mechanism for generating these waves may have an experimental basis: Peinado et al. have shown that modulating the potassium conductance of gap junction coupled neurons in the neonatal mouse neocortex leads to wave behavior [72]. Furthermore, these intermediate phase-locked states are capable of producing a pattern of wave activity known as an anti-wave. This type of activity was first observed in the dogfish spinal cord by Grillner [91] and it may occur in other networks as well[92][77]. Reducing the full conductance based Wang-Buszaki model to a phase model results in interaction functions which have large higher order Fourier modes. Not only the odd modes are important, the even modes are very

important as well. The even modes affect the stability of the anti-wave solution. Varying the relative even component affects the basin of attraction of a particular solution, or the probability that the phases will converge to a particular anti-wave solution from random initial conditions. A second order even Fourier mode is required in order to generate a perfect 1 shock solution (as was observed in the dogfish spinal cord). This behavior is not only relevant to chains but to two dimensional arrays as well.

5.0 CONCLUDING REMARKS

In this dissertation, we have demonstrated that intermediate stable phase-locked states between nonlinear oscillators can occur in both conductance based models with electrical coupling and firing rate models describing inhibitory networks. These states emerge through a supercritical pitchfork bifurcation. We studied how pairs of oscillating inhibitory networks can stay phase-locked at any phase between 0 and π over a large range of frequencies. This makes these models attractive descriptions of central pattern generators. The oscillator models that we studied were largely inspired by central pattern generators in the lobster stomatogastric system as well as the spinal cords of fish. In Chapter 4 we demonstrated that intermediate stable phase-locked states can also be used to generate wave behavior in large networks. There may also be experimental evidence for this mechanism of wave formation in the neonatal rat neocortex [72]. In conclusion, intermediate stable phase-locked states are capable of generating a variety of robust patterns between pairs of oscillators and also in networks of oscillators. The interaction functions describing these generate a large waves in the phase model which are not obtainable in models which use simple *sin* terms.

APPENDIX A

THE WANG-BUSZAKI MODEL

$$
\begin{aligned}
&\mathrm{V}' = -g_L(V - E_L) - g_{Na}(M_\infty(V)^3)h(V - E_{Na}) - g_K(n^4)(V - E_K) + i(t) \\
&\mathrm{h}' = \eta(H_\infty(V) - h)/\tau_H(V) \\
&\mathrm{n}' = \eta(N_\infty(V) - n)/\tau_N(V) \\
&\mathrm{M}_\infty(V) = \tfrac{\alpha_m(V)}{(\alpha_m(V)+\beta_m(V))} \\
&\mathrm{N}_\infty(V) = \tfrac{\alpha_n(V)}{(\alpha_n(V)+\beta_n(V))} \\
&\mathrm{H}_\infty(V) = \tfrac{\alpha_h(V)}{(\alpha_h(V)+\beta_h(V))} \\
&\alpha_h(V) = 0.07\exp\left(-(V + 58.0)/20.0\right) \\
&\beta_h(V) = 1.0/(1.0 + \exp\left(-(V + 28.0)/10.0\right)) \\
&\tau_H(V) = 1.0/(\alpha_h(V) + \beta_h(v)) \\
&\alpha_n(V) = 0.01(V + 34.0)/(1.0 - exp(-(V + 34.0)/10.00)) \\
&\beta_n(V) = 0.125\exp\left(-(V + 44.0)/80.0\right) \\
&\tau_N(V) = 1.0/(\alpha_n(V) + \beta_n(V))
\end{aligned}
\tag{A.1}
$$

This model was introduced in 1996 in a paper by Wang and Buszaki [26]. V is the membrane potential, measured in millivolts. The variables denoted by"$g_{k,Na}$" are maximal conductances and have units of inverse ohms or Siemens. Time is in units of ms. The variables m and n are "activation variables" and h is an "inactivation variable". These are probabilities of channels being open or closed. The α and β functions represent voltage dependent rates of channels opening and closing. This model is identical to the Hodgkin-Huxley model discussed in Chapter 1 except that we assume that the "m" activation variable reaches its steady state value immediately. The parameters used are: $v_{syn} = -60.5$ mV $g_L = 0.1\mu$S $v_L = -65$mV, $g_{Na} = 35\mu$S, $V_{Na} = 55$mV, $g_K = 9\mu$S, $V_K = -90$mV, $a_{i0} = 4$ $\tau_i = 15$ and $i_0 = 0.63$ nA

APPENDIX B

DYNAMICAL SYSTEMS

Generally speaking, a dynamical system is a mathematical description of a deterministic physical process[100]. Normally, when modeling physical systems, dynamical systems are described in terms of differential equations. Any differential equation of arbitrary order can be described by a set of first order ordinary differential equations by a suitable change of variables:

$$\dot{\mathbf{x}} = F(\mathbf{x}). \tag{B.1}$$

The components of this vector $\mathbf{x}$ are the local coordinates of the state space, and so the time evolution of the system is given in terms of the velocities [100]. Thus, a system of ordinary differential equations describes a vector field and vice versa [101]. A point in the phase space is described by the vector:

$$\mathbf{x}(t) = \Big[x_1(t), x_2(t), x_3(t).....x_N(t)\Big]. \tag{B.2}$$

This vector corresponds to the state of the system at time t. The solution of equation (B.1) for a given initial condition describes a trajectory in phase space. The collection of all possible trajectories for all initial conditions corresponds to the complete phase portrait. This phase portrait is dependent on the parameters of the equation. In a system of ordinary differential equations describing a neural network these parameters may be the stimulus current, maximal ion channel conductance and so forth. Often times, we try to gain a qualitative understanding of the phase portrait by studying the stationary solutions or fixed

points of the system. A solution X^* corresponding to $F(X^*) = 0$ is known as a fixed point. As we vary parameters of these ordinary differential equations the topological structure of the phase portrait/vector field may change as fixed points lose stability or are created or destroyed. This change in topological structure (a qualitative change) of the phase portrait is referred to as a *bifurcation*. Bifurcations can be either local or global. Much of the material in this dissertation employs local bifurcation theory. Local bifurcation theory rests on analyzing the system based on the trajectories of the solutions (known as the flow) near the fixed points. The basic idea is to analyze the linearized system close to one of these fixed points. Assume that $X = X_0$ is a fixed point or limit cycle solution to our system of ordinary differential equations, i.e., $F(\mathbf{x_0}) = 0$. The linearized system is given by the following differential equation:

$$\dot{X} = D_X F(X_0) X. \tag{B.3}$$

The matrix $J = D_X F(X_0)$ is known as the Jacobian. The solution to this problem is $X(t)_n = C_n \exp(\lambda_n t)$. The subscript n corresponds to elements of the vector B.2. Thus, substituting this solution into the above problem results in the eigenvalue problem $\mathbf{J}X = \lambda \mathbf{X}$. The solution to the linear problem is specified by solving for the eigenvalues of the Jacobian. Close to the fixed point, the dynamics of the full nonlinear system are completely described by the linear system. In more formal terms, this is known as the Hartman-Grobman theorem. We can determine the nature of the flow in the phase portrait by analyzing the eigenvalues of the linearized system near the fixed points. When the real part of the eigenvalues are nonzero this fixed point is said to be hyperbolic[6]. The real part of the eigenvalues tells us about the stability of the point. For instance, if the eigenvalues are purely real and $\lambda > 0$, then the flow diverges outward from the fixed point, reminiscent of the electric field of a positive charge. In this case the fixed point is said to be unstable and behaves like a source. If the eigenvalues are purely real and negative then the flow converges inward. The fixed point acts like a sink and is said to be stable. If the eigenvalues are complex, the real part still determines the stability. The complex component causes the flow to have a curl such that it spirals inward or outward dependent on the sign of $\Re\lambda$.

B.0.1 Central Manifold Theorem and Normal Forms

As mentioned above, a bifurcation is said to have occurred when there is a topological change in the phase portrait. In terms of the linearized system, we know that a bifurcation has occurred if, by varying some parameter which is intrinsic to the model, the real part of one or more of the eigenvalues change sign. When this happens, there is an accompanying change in the stability of the solution. When $\lambda = 0$ the eigenvalue is said to be critical. The fixed point is said to be non-hyperbolic. The eigenvectors corresponding to the critical eigenvectors span a space known as the critical eigenspace. There exists an invariant manifold which is tangent to this eigenspace such that as $t \to \pm\infty$. All trajectories in the phase space flow to this manifold. Therefore regardless of the dimensionality of the full nonlinear system, near the bifurcation point the bifurcation will occur in a manner identical to a lower dimensional (one or two dimensional) system. At criticality the dimensionality of the system may be drastically reduced as the dynamics are constrained to the center manifold. The dynamics on the central manifold (and associated bifurcation) is described by a normal form equation. These equations can be obtained by projecting the original system of ordinary differential equations ($\dot{x} = F(X)$) onto the critical subspace. This procedure will be demonstrated in Chapter 4. In this dissertation we deal with primarily three types of bifurcations, the super-critical Andronov-Hopf bifurcation, the super-critical pitchfork bifurcation and the saddle node on an invariant circle bifurcation. They are described in the following subsections.

B.0.2 Hopf Bifurcation

The super-critical Andronov-Hopf bifurcation is associated with the emergence of periodic behavior. The phase portrait corresponding to the normal form of this bifurcation is shown in Figure B.0.2. The normal form for the Andronov-Hopf is:

$$\dot{z} = (a + i\omega)z + (\sigma + i\gamma)z|z|^2 \tag{B.4}$$

In order to obtain a Hopf bifurcation, the Jacobian of the system linearized about some fixed point must have a pair of complex conjugate eigenvalues. For $\Re\lambda < 0$, the fixed point is a stable spiral node, meaning that all solutions spiral inward to the fixed point. Now, if we

vary a parameter which increases λ The bifurcation occurs when the complex conjugate pair of eigenvalues cross the imaginary axis simultaneously. When this happens, the stable spiral becomes an unstable spiral, and the trajectories all flow out to a stable limit cycle. Near the bifurcation point, the frequency of the limit cycle is given approximately by $\omega = Im\lambda$[102].

B.0.3 SNIC Bifurcation

The saddle node bifurcation corresponds to the creation and annihilation of fixed points. The normal form for the saddle node bifurcation in one dimension is:

$$\dot{x} = a + x^2. \tag{B.5}$$

If the parameter a is less than zero, there exists both a saddle point and a node. As a is increased the two fixed points move closer and closer until $a = 0$. When $a = 0$, the fixed points collide and annihilate one another. For $a > 0$ there are no fixed points.

B.0.4 Super-Critical Pitchfork Bifurcation

The pitchfork bifurcation, like the Hopf bifurcation can be either subcritical or supercritical. The normal form for the supercritical pitchfork bifurcation is

$$\dot{x} = \alpha x - x^3 \tag{B.6}$$

The normal form for the subcritical pitchfork is obtained by changing the sign on the cubic term. This Equation (B.6) has three fixed points: $x = 0$ and $x = \pm\sqrt{\alpha}$. If we linearize this equation about these fixed points, we find that $x = 0$ is a stable point for $\alpha < 0$ and that $x = \pm\sqrt{\alpha}$ are stable for $\alpha > 0$. Thus for $\alpha < 0$ we have one stable fixed point at the origin as we increase α this fixed point loses stability and gives rise to two stable nodes. If we plot x vs α the graph looks like a two-tined pitchfork.

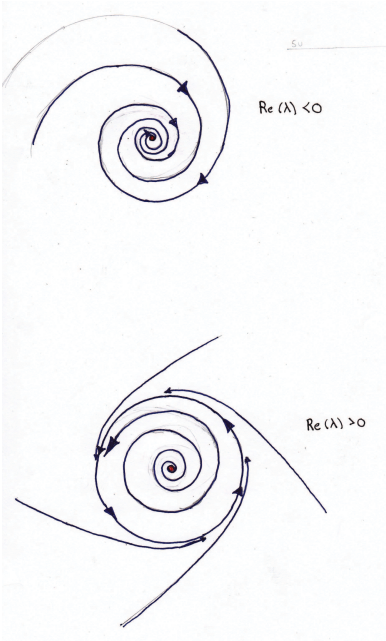

Figure B1: Phase space plot illustrating a supercritical Hopf bifurcation. If $\lambda < 0$ all trajectories flow into the fixed point. When $\lambda > 0$ the fixed point loses stability and trajectories flow outward to a new stable limit cycle.

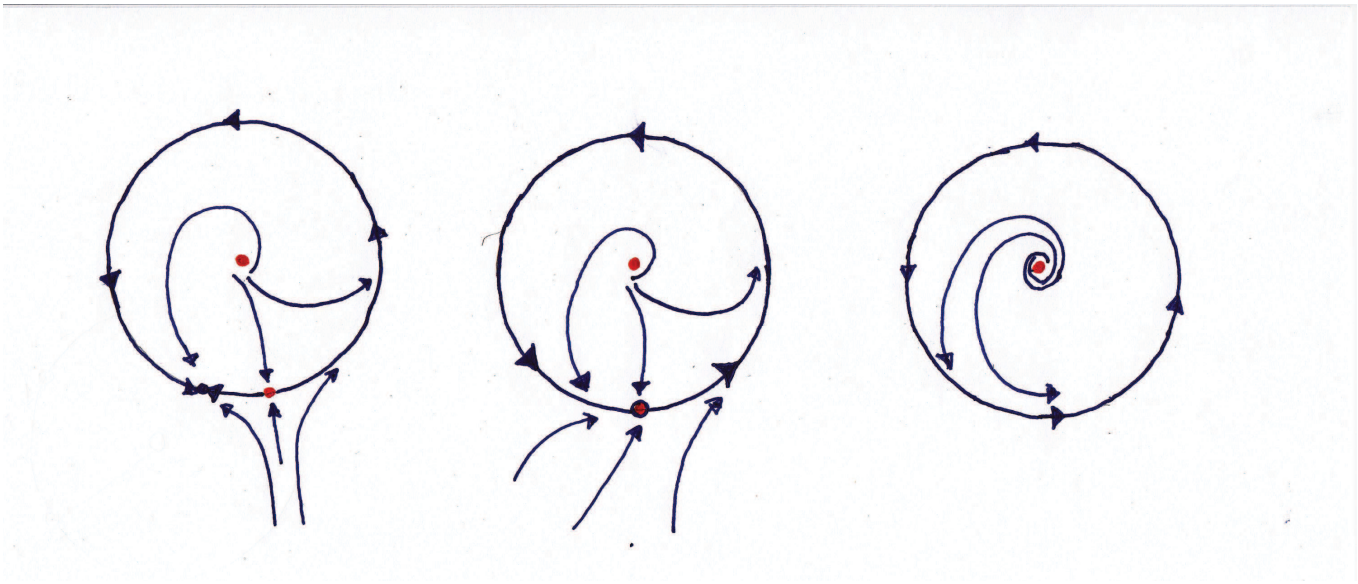

Figure B2: Phase space plot illustrating a saddle node on an invariant circle bifurcation.

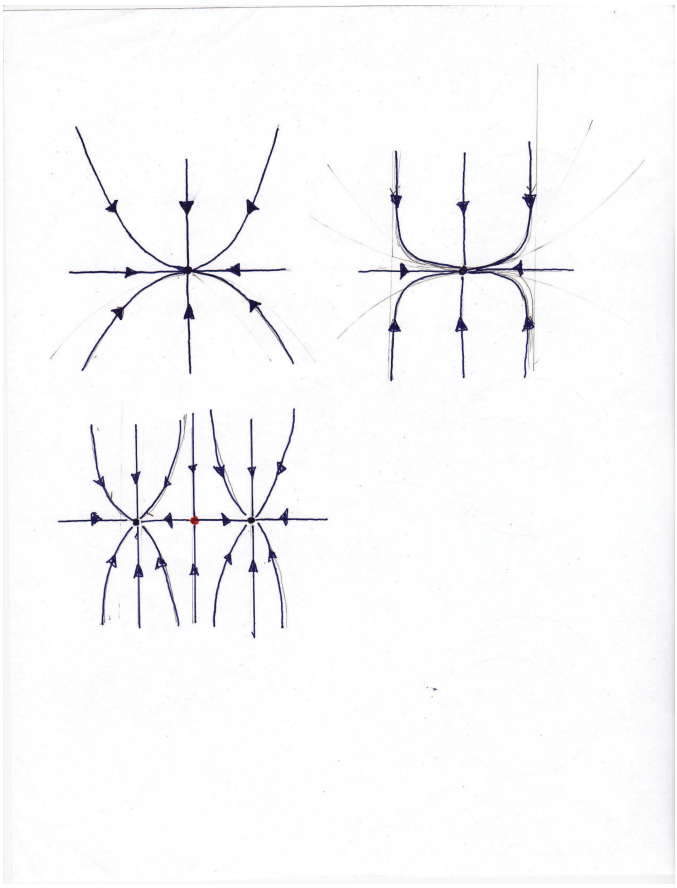

Figure B3: Phase space plot illustrating a Saddle node on an Invariant Circle Bifurcation.

APPENDIX C

CENTER MANIFOLD CALCULATION FOR THE THREE OSCILLATOR SYSTEM

In order to calculate the center manifold we apply a projection method which makes use of a perturbation expansion of our original equations. Since our Jacobian has a simple zero eigenvalue, the eigenspace is one-dimensional and spanned by the nullspace vector $\vec{n}$, where $An = 0$. There is another 1-dimensional eigenspace corresponding to the non-zero eigenvalue, call it $\vec{v}$. Ultimately, one wants to exapnd out the phases and bifurcation parameter in orders of ϵ and use the null vector to project the components of the resulting expression onto the critical eigenspace. The result is an equation for the normal form of the center manifold [103]. Start by examining the right hand side of our phase equations:

$$\begin{aligned} f(\phi_1, \phi_2) &= 2H(-\phi_2) - H(-\phi_1) - H(\phi_2), \\ g(\phi_1, \phi_2) &= H(-\phi_1) + H(\phi_2) - 2H(\phi_1). \end{aligned} \tag{C.1}$$

We can write down a multi-dimensional Taylor series such as the following:

$$\begin{pmatrix} \dot{\phi}_1 \\ \dot{\phi}_2 \end{pmatrix} = \begin{pmatrix} \partial_{\phi_1} f & \partial_{\phi_2} f \\ \partial_{\phi_1} g & \partial_{\phi_2} g \end{pmatrix} \begin{pmatrix} \phi_1 \\ \phi_2 \end{pmatrix} + \begin{pmatrix} \partial^2_{\phi_1} f & \partial^2_{\phi_2} f \\ \partial^2_{\phi_1} g & \partial^2_{\phi_2} g \end{pmatrix} \begin{pmatrix} \phi_1^2 \\ \phi_2^2 \end{pmatrix} + \begin{pmatrix} \partial^3_{\phi_1} f & \partial^3_{\phi_2} f \\ \partial^3_{\phi_1} g & \partial^3_{\phi_2} g \end{pmatrix} \begin{pmatrix} \phi_1^3 \\ \phi_2^3 \end{pmatrix} \tag{C.2}$$

Calculating the derivatives and evaluating terms at the fractured solution $\phi_1 = k, \phi_2 = -k$ we obtain the equation:

$$\dot{\phi} = \beta p(k) A_0 \phi + q(k) A_1 \phi + \frac{s(k)}{2} A_3 \phi^2 + \frac{r(k)}{2} \beta A_2 \phi^2 + \frac{U(k)}{3!} A_1 \phi^3 + \frac{w(k)}{3!} \beta A_0 \phi^3, \tag{C.3}$$

where:

$$\begin{aligned} f(k) &= H(k)_{even} \;\; g(k) = H(k)_{odd} \\ p(k) &= H'(k)_{even} \;\; q(k) = H'(k)_{odd} \\ r(k) &= H''(k)_{even} \;\; s(k) = H''(k)_{odd} \\ U(k) &= H'''(k)_{even} \;\; w(k) = H'''(k)_{odd}. \end{aligned} \tag{C.4}$$

The term β is a parameter used to adjust the magnitude of the even term. A_0,A_1,A_2,A_3 are matrices:

$$A_0 = \begin{pmatrix} 1 & 1 \\ 1 & 1 \end{pmatrix}, \quad A_1 = \begin{pmatrix} -3 & 1 \\ 1 & -3 \end{pmatrix}, \quad A_2 = \begin{pmatrix} -1 & 1 \\ -1 & 1 \end{pmatrix}, \quad A_3 = \begin{pmatrix} -3 & 1 \\ 1 & -3 \end{pmatrix}. \tag{C.5}$$

The term β_c is the critical value of β for which the eigenvalue is 0. We proceed by using perturbation theory and the Fredholm Alternative to solve for the normal form equation. Begin by expanding out the phase and parameter λ and introducing slow time:

$$\begin{aligned} \phi &= \epsilon x_1 + \epsilon^2 x_2 + \epsilon^3 x_3 + \epsilon^4 x_4 .... \\ \beta &= \beta_c + \epsilon^2 \lambda_2 + \epsilon^3 \lambda_3 + \epsilon^4 \lambda_4 .... \\ \tau &= \epsilon^2 t. \end{aligned} \tag{C.6}$$

This leads to a system of algebraic equations up to third order in ϵ, the first of which provides us with an equation relating the null vector and the first term in our perturbation expansion.

$$\begin{aligned} (\beta_c p(k) A_0 + q(k) A_1) x_1 &= 0 \\ (\beta_c p(k) A_0 + q(k) A_1) x_2 &= \lambda_1 p(k) A_0 x_1 + \frac{s(k)}{2} A_3 x_1^2 + \frac{r(k)}{2} \beta_c A_2 x_1^2 \\ (\beta_c p(k) A_0 + q(k) A_1) x_3 &= x_1' - \lambda_1 p A_o x_2 - \lambda_2 p A_0 x_1 - s A_3 x_1 x_2 \\ &- r \beta_c A_2 x_1 x_2 - \frac{r \lambda_1}{2} A_2 x_1^2 - \frac{U(k)}{3} A_5 x_1^3 - \frac{w(k) \beta_c}{3} A_0 x_1^3 \end{aligned} \tag{C.7}$$

The first of the three expressions implies:

$$x_1 = u(\tau)\mathbf{n}. \tag{C.8}$$

We then want to find the null vector $\mathbf{n}$. Due to the form of our linearization matrix the null vector is

$$\mathbf{n} = \frac{1}{\sqrt{2}} \begin{pmatrix} 1 \\ 1 \end{pmatrix} \tag{C.9}$$

Once we have solved for the lowest order we move to the 2nd equation which comprised terms in ϵ^2. In solving this equation we must apply a transversality condition which is simply an assumption that as we vary the parameter a_1 the eigenvalue passes directly through the origin. It does not asymptotically approach it or slow down. This condition is valid for the three oscillator case, but breaks down for larger chains of oscillators. Applying this condition is the equivalent of setting $\lambda_1 = 0$. this gives us an matrix equation for x_2. It can be shown that:

$$x_2 = \frac{-s(k)}{\sqrt{2}q(k)} u^2(\tau) \begin{pmatrix} 1 \\ 2 \end{pmatrix} \tag{C.10}$$

satisfies this equation. Finally, going to third order and applying the adjoint to both sides of the equation yields a differential equation for the normal form:

$$\frac{du}{d\tau} = \lambda_2 p(k) A_0 u + \left(\frac{2w(k)q(k)}{3p(k)} + \frac{s(k)^2}{\sqrt{2}q(k)} - \frac{r(k)s(k)}{\sqrt{2}p(k)} - \frac{U(k)}{3} \right) u^3. \tag{C.11}$$

Immediately we see that since the coefficient on the cubic term is positive that it is the normal form for the well known subcritical pitchfork bifurcation.

APPENDIX D

GERSHGORIN CIRCLE THEOREM

Let:$A = [a_{ij}]$ be an arbitrary n x n matrix with elements that may be complex and let:

$$\Lambda_i = \sum_{j=1, i \neq j}^{n} |a_{ij}| \qquad for \;\; i = 1, 2, ...n \tag{D.1}$$

Then all of the eigenvalues λ_i of A lie in the union of n disks Γ_i where:

$$\Gamma_i : |\lambda - a_{ii}| \leq \lambda_i \qquad for \;\; i = 1, 2, ...n \tag{D.2}$$

This wording of the Gershgorin Circle theorem was taken from:

Tables of Integrals, Series, and Products by I.S.Gradshteyn and I.M. Ryzhik[104].

APPENDIX E

CODE FOR FIGURES

The following subsections contain the XPP-AUT, MATLAB and C code for the figures for which they are labeled.

E.0.5 Figure 2.2

Matlab code for generating random matrices:

```
%N is the dimension of your random matrix
N=50;
a=rand(N,N);
for i=1:5
    b=sum(a,2);
    a(i,:)=a(i,:)./b(i);
end
eig(a)

L=eig(a);

scatter(real(L),imag(L),'.')
% you have to manually delete the "1" eigenvalue
% reshape the matrix it can be pasted into a lookup table
```

```
M=reshape(a,N*N,1)
```

E.0.6 Figure 2.3

This is code for a twenty oscillator system with random coupling. The weights are generated from a lookup table which is a column of numbers whose entries were generated by the above matlab file.

```
table c 20_oscillators_may15.tab
@ autoeval=0


f(x)=1/(1+exp(-x))
fp(x)=exp(-x)/(1+exp(-x))^2
special k=mmult(20,20,c,u0)
)u[0..19]'=-u[j]+f(I-g*k([j])
par I=10,g=1
done
```

E.0.7 Figure 2.4

The same code was used as in the previous figure, just different random matrices.

E.0.8 Figure 2.6

Same code as the anti-wave in a twenty oscillator chain (see below)

E.0.9 Figure 2.7

XPP file for the three neuron circulantly coupled Ermentrout-Cowan model

```
x1'=-x1+f(I-g*(a*x1+b*x2+c*x3))
x2'=-x2+f(I-g*(a*x2+b*x3+c*x1))
x3'=-x3+f(I-g*(a*x3+b*x1+c*x2))


par b=.6 a=.1 c=.3
f(x)=1/(1+exp(-x))
aux FF=1/(1+exp(I-g*(a*x1+b*x2+c*x3)))
FP(x)= (F(x+.001)-F(x-.001))/(.002)

par I=2
par g=52
init x1=0.3579
init x2=0.0
init x3=0.0216
done
```

E.0.10 Figure 2.9

Interaction function computed using xpp and the previous ode file.

E.0.11 Figure 2.13

The following four figures were computed in xpp with two ode files, one to compute the phase difference between two wang buszaki models and the other to compute a bifurcation diagrams.

```
# ode to calculate phase differences in the full wlc model of two coupled
# oscillators
global 0 t {x1=ran(1);x2=ran(1);x3=ran(1);y1=.1;y2=ran(1); y3=ran(1)}
global 1 x1-xt {t1=t}
```

```
global 1 y1-xt {phase=(t-t1)/(t-t2);t2=t}

par xt=.2
t1'=0
t2'=0
#period'=0
phase'=0
p'=0
init p=0
init t2=0
init t1=0
x[1..3](0)=ran(1)
y[1..3](0)=ran(1)
x1'=-x1+f(I-g*(a*x1+b*x2+c*x3)-gc*(p*y2+(1-p)*y3))
x2'=-x2+f(I-g*(a*x2+b*x3+c*x1))
x3'=-x3+f(I-g*(a*x3+b*x1+c*x2))

y1'=-y1+f(I-g*(a*y1+b*y2+c*y3)-gc*(p*x2+(1-p)*x3))
y2'=-y2+f(I-g*(a*y2+b*y3+c*y1))
y3'=-y3+f(I-g*(a*y3+b*y1+c*y2))
f(x)=1/(1+exp(-x))
fp(x)=exp(-x)/(1+exp(-x))^2
par gc=.25
par g=50,I=2
par a=.1,b=.3,c=.6
done
```

Here is the second ode file

```
x1'=-x1+f(I-g*(a*x1+b*x2+c*x3)-gc*(p*y2+(1-p)*y3))
x2'=-x2+f(I-g*(a*x2+b*x3+c*x1))
```

```
x3'=-x3+f(I-g*(a*x3+b*x1+c*x2))


y1'=-y1+f(I-g*(a*y1+b*y2+c*y3)-gc*(p*x2+(1-p)*x3))
y2'=-y2+f(I-g*(a*y2+b*y3+c*y1))
y3'=-y3+f(I-g*(a*y3+b*y1+c*y2))
f(x)=1/(1+exp(-x))
fp(x)=exp(-x)/(1+exp(-x))^2
par gc=.25,p=0
par g=50,I=2
par a=.1,b=.3,c=.6
done
```

E.0.12 Figure 2.14

An Ode File For Two Coupled Systems Of Twenty Neurons

```
table c 20_oscillators_may15.tab
#!n[0..19]=sum(0,19)of(c(20*[j]+i'))
@ autoeval=0
f(x)=1/(1+exp(-x))
fp(x)=exp(-x)/(1+exp(-x))^2
special k=mmult(20,20,c,u0)
special m=mmult(20,20,c,x0)
par p0=1
par q0=1
par eps=0
u[0..19]'=-u[j]+f(I-g*k([j])-eps*([j]==p0)*shift(x0,q0))
x[0..19]'=-x[j]+f(I-g*m([j])-eps*([j]==q0)*shift(u0,p0))
par I=10,g=1
done
```

E.0.13 Figure 3.1

```
The following is an ode file for use with XPP it is the Wang Buszaki model
:\\
par vt=0\\
par phi=5\\
par i0=.63\\
V1'=-gL*(V1-EL)-gNa*(Minf(V1)^3)*h1*(V1-ENa)-gK*(n1^4)*(V1-EK)+i0\\
h1'=phi*(Hinf(V1)-h1)/tauH(V1)  \\
n1'=phi*(Ninf(V1)-n1)/tauN(V1)  \\
s1'=ai(V1)*(1-s1)-s1/taui \\
aux y=ai0/(1+exp(-(v1-vst)/vss))  \\
auz q=ai(V1)/(1+ai(V1))*(1-exp(-(1+ai(V1))*t/taui)) \\
ai(v)=ai0/(1+exp(-(v-vst)/vss))  \\

alpham(V) = 0.1*(V+35.0)/(1.0-exp(-(V+35.0)/10.0))  \\
betam(V)  = 4.0*exp(-(V+60.0)/18.0)  \\
Minf(V) = alpham(V)/(alpham(V)+betam(V))\\
alphah(V) = 0.07*exp(-(V+58.0)/20.0)  \\
betah(V)  = 1.0/(1.0+exp(-(V+28.0)/10.0))\\
Hinf(V) = alphah(V)/(alphah(V)+betah(V))  \\
tauH(V) = 1.0/(alphah(V)+betah(v))  \\
alphan(V) = 0.01*(V+34.0)/(1.0-exp(-(V+34.0)/10.00))  \\
betan(V)  = 0.125*exp(-(V+44.0)/80.0)  \\
Ninf(V) = alphan(V)/(alphan(V)+betan(V)) \\
tauN(V) = 1.0/(alphan(V)+betan(V))  \\
aux th=1.0/(alphah(V1)+betah(v1)) \\
aux tn=1.0/(alphan(V1)+betan(V1))  \\
aux M=alpham(V1)/(alpham(V1)+betam(V1))\\
V1(0)=-64  \\
```

```
h1(0)=0.78  \\
n1(0)=0.09  \\
@ DT=0.01,bound=10000  \\
@ METH=qualrk  \\
@ MAXSTOR=2000000\\
init V1=17.0595 H1=0.0732798 N1=0.543615 S1=0.533686 \\
par esyn=-60.5  ip=0 ton=20 toff=60  gL=0.1 EL=-65 \\
par gNa=35 ENa=55 gK=9 EK=-90 ai0=4 taui=15 vst=0 vss=5\\
par eps=1 \\
done
```

E.0.14 Figure 3.2

Same ode used file as the previous figure.

E.0.15 Figure 3.3

The following ode was used for calculating the phase differences in the full model.

```
This is the ode file used for computing the phase diference as a function of
phi. the file for computing phase difference vs. gk is nearly identical
global 1 v1 {t1=t}
global 1 v2 {period=t-t2;phase=(t-t1)/(t-t2);t2=t}
par vt=0
t1'=0
t2'=0
period'=0
phase'=0
#i0'=0
#init i0=.63
#gk'=0
#init gk=2
```

```
phi'=0
init phi=5
par i0=.63
V1'=-gL*(V1-EL)-gNa*(Minf(V1)^3)*h1*(V1-ENa)-gK*(n1^4)*(V1-EK)+i(t)+gc*(V2-V1)
h1'=phi*(Hinf(V1)-h1)/tauH(V1)
n1'=phi*(Ninf(V1)-n1)/tauN(V1)
s1'=ai(V1)*(1-s1)-s1/taui
aux tm=tauH(V1)
aux tm2=tauN(V1)
aux fast=v1-v2
V2'=-gL*(V2-EL)-gNa*(Minf(V2)^3)*h2*(V2-ENa)-gK*(n2^4)*(V2-EK)+i(t)+gc*(V1-V2)
h2'=phi*(Hinf(V2)-h2)/tauH(V2)
n2'=phi*(Ninf(V2)-n2)/tauN(V2)
s2'=ai(V2)*(1-s2)-s2/taui
par gc=.01
aux y=ai0/(1+exp(-(v1-vst)/vss))
auz q=ai(V1)/(1+ai(V1))*(1-exp(-(1+ai(V1))*t/taui))
ai(v)=ai0/(1+exp(-(v-vst)/vss))
i(t)=i0
alpham(V) = 0.1*(V+35.0)/(1.0-exp(-(V+35.0)/10.0))
betam(V)  = 4.0*exp(-(V+60.0)/18.0)
Minf(V) = alpham(V)/(alpham(V)+betam(V))
alphah(V) = 0.07*exp(-(V+58.0)/20.0)
betah(V)  = 1.0/(1.0+exp(-(V+28.0)/10.0))
Hinf(V) = alphah(V)/(alphah(V)+betah(V))
tauH(V) = 1.0/(alphah(V)+betah(v))
alphan(V) = 0.01*(V+34.0)/(1.0-exp(-(V+34.0)/10.00))
betan(V)  = 0.125*exp(-(V+44.0)/80.0)
Ninf(V) = alphan(V)/(alphan(V)+betan(V))
tauN(V) = 1.0/(alphan(V)+betan(V))
```

```
v1(0)=-64
v2(0)=-40
h1(0)=0.78
n1(0)=0.09
@ XP=T
@ YP=V
@ TOTAL=1500
@ DT=0.01,bound=10000
@ METH=qualrk
@ TOLER=0.00001
@ XLO=0.0, XHI=30.0, YLO=-90.0, YHI=30.0
@ rangeover i0, rangestep=.1, rangelow=.6, rangehigh=20
@ range=1,rangereset=yes
@ MAXSTOR=2000000
@ OUTPUT=phase_data
@ transient 1499.999
#init V1=17.0595 H1=0.0732798 N1=0.543615 S1=0.533686
par esyn=-60.5  ip=0 ton=20 toff=60  gL=0.1 EL=-65
par gNa=35 ENa=55 gK=9 EK=-90 ai0=4 taui=15 vst=0 vss=5
par eps=1
done
```

E.0.16 Figure 4.2

```
function dv=wang_chain2(t,v)
dv=zeros(40,1);
esyn=-60.5;
 i0=0.63 ;
 phi=6.0 ;
```

```
 gL=0.1 ;
 EL=-65 ;
 gNa=35 ;
 ENa=55 ;
 gK=9 ;
 EK=-90;
taui=15;
g=.01;
% neuron 1
dv(1)=-gL*(v(1)-EL)-gNa*(Minf(v(1))^3)*v(2)*(v(1)-ENa)
-gK*(v(3)^4)*(v(1)-EK)+i0+g*2*(v(5)-v(1))  ;
dv(2)=phi*(Hinf(v(1))-v(2))/tauH(v(1));
dv(3)=phi*(Ninf(v(1))-v(3))/tauN(v(1));
dv(4)=ai(v(1))*(1-v(4))-v(4)/taui ;

% neuron 2
dv(5)=-gL*(v(5)-EL)-gNa*(Minf(v(5))^3)*v(6)*(v(5)-ENa)
-gK*(v(7)^4)*(v(5)-EK)+i0+g*((v(9)-v(5))+(v(1)-v(5)));
dv(6)=phi*(Hinf(v(5))-v(6))/tauH(v(5)) ;
dv(7)=phi*(Ninf(v(5))-v(7))/tauN(v(5))  ;
dv(8)=ai(v(5))*(1-v(8))-v(8)/taui ;


% neuron 3
dv(9)=-gL*(v(9)-EL)-gNa*(Minf(v(9))^3)*v(10)*(v(9)-ENa)
-gK*(v(11)^4)*(v(9)-EK)+i0+g*((v(5)-v(9))+(v(13)-v(9))) ;
dv(10)=phi*(Hinf(v(9))-v(10))/tauH(v(9)) ;
dv(11)=phi*(Ninf(v(9))-v(11))/tauN(v(9))  ;
dv(12)=ai(v(9))*(1-v(12))-v(12)/taui ;
```

```
% neuron 4
dv(13)=-gL*(v(13)-EL)-gNa*(Minf(v(13))^3)*v(14)*(v(13)-ENa)
-gK*(v(15)^4)*(v(13)-EK)+i0+g*((v(9)-v(13))+(v(17)-v(13)))  ;
dv(14)=phi*(Hinf(v(13))-v(14))/tauH(v(13)) ;
dv(15)=phi*(Ninf(v(13))-v(15))/tauN(v(13))  ;
dv(16)=ai(v(13))*(1-v(16))-v(16)/taui ;


% neuron 5
dv(17)=-gL*(v(17)-EL)-gNa*(Minf(v(17))^3)*v(18)*(v(17)-ENa)
-gK*(v(19)^4)*(v(17)-EK)+i0+g*((v(13)-v(17))+(v(21)-v(17))) ;
dv(18)=phi*(Hinf(v(17))-v(18))/tauH(v(17)) ;
dv(19)=phi*(Ninf(v(17))-v(19))/tauN(v(17))  ;
dv(20)=ai(v(17))*(1-v(20))-v(20)/taui ;



% neuron 6
dv(21)=-gL*(v(21)-EL)-gNa*(Minf(v(21))^3)*v(22)*(v(21)-ENa)
-gK*(v(23)^4)*(v(21)-EK)+i0+g*((v(17)-v(21)) +(v(25)-v(21))) ;
dv(22)=phi*(Hinf(v(21))-v(22))/tauH(v(21)) ;
dv(23)=phi*(Ninf(v(21))-v(23))/tauN(v(21))  ;
dv(24)=ai(v(21))*(1-v(24))-v(24)/taui ;


% neuron 7
dv(25)=-gL*(v(25)-EL)-gNa*(Minf(v(25))^3)*v(26)*(v(25)-ENa)
-gK*(v(27)^4)*(v(25)-EK)+i0+g*((v(21)-v(25)) +(v(29)-v(25))) ;
dv(26)=phi*(Hinf(v(25))-v(26))/tauH(v(25)) ;
dv(27)=phi*(Ninf(v(25))-v(27))/tauN(v(25))  ;
```

```
dv(28)=ai(v(25))*(1-v(28))-v(28)/taui ;




% neuron 8
dv(29)=-gL*(v(29)-EL)-gNa*(Minf(v(29))^3)*v(30)*(v(29)-ENa)
-gK*(v(31)^4)*(v(29)-EK)+i0+g*((v(25)-v(29)) +(v(33)-v(29))) ;
dv(30)=phi*(Hinf(v(29))-v(30))/tauH(v(29)) ;
dv(31)=phi*(Ninf(v(29))-v(31))/tauN(v(29))  ;
dv(32)=ai(v(29))*(1-v(32))-v(32)/taui ;


% neuron 9
dv(33)=-gL*(v(33)-EL)-gNa*(Minf(v(33))^3)*v(34)*(v(33)-ENa)
-gK*(v(35)^4)*(v(33)-EK)+i0+g*((v(29)-v(33)) +(v(37)-v(33)));
dv(34)=phi*(Hinf(v(33))-v(34))/tauH(v(33)) ;
dv(35)=phi*(Ninf(v(33))-v(35))/tauN(v(33))  ;
dv(36)=ai(v(33))*(1-v(36))-v(36)/taui ;


% neuron 10
dv(37)=-gL*(v(37)-EL)-gNa*(Minf(v(37))^3)*v(38)*(v(37)-ENa)
-gK*(v(39)^4)*(v(37)-EK)+i0+g*2*(v(33)-v(37));
dv(38)=phi*(Hinf(v(37))-v(38))/tauH(v(37)) ;
dv(39)=phi*(Ninf(v(37))-v(39))/tauN(v(37))  ;
dv(40)=ai(v(37))*(1-v(40))-v(40)/taui ;


 end
```

```
     function output1=ai(v)
ai0=4 ;
 vst=0 ;
 vss=5 ;
output1=ai0/(1+exp(-(v-vst)/vss));



     end
function [output2]= alpham(v)

[output2] = 0.1*(v+35.0)/(1.0-exp(-(v+35.0)/10.0));
end
function [output3]=betam(v)


[output3]= 4.0*exp(-(v+60.0)/18.0);
end
function [output4]=Minf(v)

[output4]=alpham(v)/(alpham(v)+betam(v));

end
function [output5]=alphah(v)
[output5] = 0.07*exp(-(v+58.0)/20.0);
end
    function [output6]=betah(v)
 [output6] = 1.0/(1.0+exp(-(v+28.0)/10.0));
    end
```

```
        function [output7]=Hinf(v)
 [output7]= alphah(v)/(alphah(v)+betah(v));
        end
            function [output8]=tauH(v)
[output8] = 1.0/(alphah(v)+betah(v));
            end
                function  [output9]=alphan(v)
[output9] = 0.01*(v+34.0)/(1.0-exp(-(v+34.0)/10.00));
                end
                    function [output10]=betan(v)
 [output10] = 0.125*exp(-(v+44.0)/80.0);
                    end
                        function [output11]=Ninf(v)
[output11] = alphan(v)/(alphan(v)+betan(v)) ;
                        end
    function output12=tauN(v)
 output12=1.0/(alphan(v)+betan(v));


       end
```

This m file integrates and plots the equations in the previous function.

```
% integrating a chain of ten wang buszaki neurons with cut ends
% image the chain using imagesc
% getting the correct intial conditions

% these are initial conditions for phi around 6.5 ( function wang_chain_2)
% I got them by trial and error. they seem to work
% they seem to work at phi=6.2 as well
%v=[-58.7288  0.6580  0.1145 0 -52.3385 0.5064 0.1642 0 -62.1667 0.6403
 0.1226 0 -57.3763  0.5944  0.1342   0 -56.6688   0.5466   0.1018 0
```

```
-53.8326 0.4338   0.1398 0 -51.1567 0.1583   0.1020 0   -63.8017  0.6644
  0.1088 0 -61.0615 0.5692   0.1472 0  -58.9623   0.1808 0.2637 0];

%v=[-58.9623 0.1808 0.2637 0 -61.0615 0.5692 0.1472 0 -63.8017 0.6644
 0.1088 0 -51.1567 0.1583 0.102 0 -53.8326 0.4338 0.1398 0 -56.6688
 0.5466 0.1018 0 -57.3763 0.5944 0.1342 0 -62.1667 0.6403 0.1226 0
-52.3385 0.5064 0.1642 0 -58.7288 0.658 0.11450 0]
% flip the initial conditions to get a wave in the opposite direction.

  % these are initial conditions for phi around 6
%v=[-62.9123  0.7827  0.2362  0 -58.7906 0.6757  0.1526 0 -54.8587 0.5212
 0.0083 0 -63.9619  0.7269   0.2858 0 -60.6145  0.7253 0.1718 0 -58.1171
0.6056 .1351 0 -37.4739 0.1255  0.3783 0  -10.6370  0.7637  0.2300 0 2.2193
 0.6644  0.1401 0 -57.0656  -0.0886 0.5272 0];
  % I fit the V n and h to fourier series to try and find the right ic.
  % evaluating these functions at multiples of the fixed point of the odd
  % H. In the end  I just played around to get these, they seem to work
%w=v';
%v=rand(40,1);
%
 % activation variable initial conditions.
 v=[-57.065 -0.0886 0.5272 0 2.2193 0.66440 0.14010 0 -10.637
0.7637   0.23  0 -37.4739  0.1255   0.3783   0 -58.1171  0.6056
 0.1351   0 -60.6145  0.7253   0.1718   0 -63.9619  0.7269   0.2858
   0 -54.8587  0.5212   0.0083  0 -58.7906  0.6757   0.1526   0
 -62.9123  0.7827  0.2362 0]

% v= [-58.2071    0.6299    0.1315    0.3492  -56.4706    0.5744
  0.1472    0.3020  -53.3596    0.4905    0.1734    0.2535   13.4219
  0.1095    0.4521    0.4108  -63.1118    0.5065    0.1994    0.6779
```

```
 -61.7699    0.6866    0.1117    0.5824  -60.3391    0.6822 -58.2071
  0.6299    0.1315    0.3492  -56.4706    0.5744    0.1472    0.3020
 -53.3596    0.4905    0.1734    0.2535 0.1 0.3];
%w=fliplr(v);
 %?? whether or not the straight wave seems stable seems to depend upon the
 %dont use ode15s

 [T,X] = ode45(@wang_chain2,[0 6000],v);




Matrix=[X(:,1) X(:,5) X(:,9) X(:,13) X(:,17)
 X(:,21) X(:,25) X(:,29) X(:,33),X(:,37)];

figure
imagesc(Matrix)
```

E.0.17 Figure 4.3

This is the ODE file for a twenty oscillator chain with periodic boundary conditions.

```
# wang buszaki fsu
p i0=.6,ip=0,ton=20,toff=60
p phi=6.0
p gL=0.1
p EL=-65.0
p gNa=35.0
p ENa=55.0
p gK=9.0
p EK=-90.0
```

```
p c=0

# a twenty oscillator chain
#

v1'=-gL*(v1-EL)-gNa*(Minf(V1)^3)*h1*(v1-ENa)
-gK*(n1^4)*(v1-EK)+i(t)+c*(v2-v1)+c*((v20-v1))
v2'=-gL*(v2-EL)-gNa*(Minf(V2)^3)*h2*(v2-ENa)
-gK*(n2^4)*(v2-EK)+i(t)+c*((V3-v2)+(V1-v2))
v3'=-gL*(v3-EL)-gNa*(Minf(V3)^3)*h3*(v3-ENa)
-gK*(n3^4)*(v3-EK)+i(t)+c*((V4-v3)+(V2-v3))
v4'=-gL*(v4-EL)-gNa*(Minf(V4)^3)*h4*(v4-ENa)
-gK*(n4^4)*(v4-EK)+i(t)+c*((V5-v4)+(V13-v4))
v5'=-gL*(v5-EL)-gNa*(Minf(V5)^3)*h5*(v5-ENa)
-gK*(n5^4)*(v5-EK)+i(t)+c*((V6-v5)+(V4-v5))
v6'=-gL*(v6-EL)-gNa*(Minf(V6)^3)*h6*(v6-ENa)
-gK*(n6^4)*(v6-EK)+i(t)+c*((V7-v6)+(V5-v6))
v7'=-gL*(v7-EL)-gNa*(Minf(V7)^3)*h7*(v7-ENa)
-gK*(n7^4)*(v7-EK)+i(t)+c*((V8-v7)+(V6-v7))
v8'=-gL*(v8-EL)-gNa*(Minf(V8)^3)*h8*(v8-ENa)
-gK*(n8^4)*(v8-EK)+i(t)+c*((V9-v8)+(V7-v8))
v9'=-gL*(v9-EL)-gNa*(Minf(V9)^3)*h9*(v9-ENa)
-gK*(n9^4)*(v9-EK)+i(t)+c*((V10-v9)+(V8-v9))
v10'=-gL*(v10-EL)-gNa*(Minf(V10)^3)*h10*(v10-ENa)
-gK*(n10^4)*(v10-EK)+i(t)+c*((V11-v10)+(V9-v10))
v11'=-gL*(v11-EL)-gNa*(Minf(V11)^3)*h11*(v11-ENa)
-gK*(n11^4)*(v11-EK)+i(t)+c*((V12-v11)+(V10-v11))
v12'=-gL*(v12-EL)-gNa*(Minf(V12)^3)*h12*(v12-ENa)
-gK*(n12^4)*(v12-EK)+i(t)+c*((V13-v12)+(V11-v12))
v13'=-gL*(v13-EL)-gNa*(Minf(V13)^3)*h13*(v13-ENa)
```

```
-gK*(n13^4)*(v13-EK)+i(t)+c*((V14-v13)+(V12-v13))
v14'=-gL*(v14-EL)-gNa*(Minf(V14)^3)*h14*(v14-ENa)
-gK*(n14^4)*(v14-EK)+i(t)+c*((V15-v14)+(V13-v14))
v15'=-gL*(v15-EL)-gNa*(Minf(V15)^3)*h15*(v15-ENa)
-gK*(n15^4)*(v15-EK)+i(t)+c*((V16-v15)+(V14-v15))
v16'=-gL*(v16-EL)-gNa*(Minf(V16)^3)*h16*(v16-ENa)
-gK*(n16^4)*(v16-EK)+i(t)+c*((V17-v16)+(V15-v16))
v17'=-gL*(v17-EL)-gNa*(Minf(V17)^3)*h17*(v17-ENa)
-gK*(n17^4)*(v17-EK)+i(t)+c*((V18-v17)+(V16-v17))
v18'=-gL*(v18-EL)-gNa*(Minf(V18)^3)*h18*(v18-ENa)
-gK*(n18^4)*(v18-EK)+i(t)+c*((V19-v18)+(V17-v18))
v19'=-gL*(v19-EL)-gNa*(Minf(V19)^3)*h19*(v19-ENa)
-gK*(n19^4)*(v19-EK)+i(t)+c*((V20-v19)+(V18-v19))
v20'=-gL*(v20-EL)-gNa*(Minf(V20)^3)*h20*(v20-ENa)
-gK*(n20^4)*(v20-EK)+i(t)+c*((v19-v20))+c*((v19-v1))


h1'=phi*(Hinf(V1)-h1)/tauH(V1)
h2'=phi*(Hinf(V2)-h2)/tauH(V2)
h3'=phi*(Hinf(V3)-h3)/tauH(V3)
h4'=phi*(Hinf(V4)-h4)/tauH(V4)
h5'=phi*(Hinf(V5)-h5)/tauH(V5)
h6'=phi*(Hinf(V6)-h6)/tauH(V6)
h7'=phi*(Hinf(V7)-h7)/tauH(V7)
h8'=phi*(Hinf(V8)-h8)/tauH(V8)
h9'=phi*(Hinf(V9)-h9)/tauH(V9)
h10'=phi*(Hinf(V10)-h10)/tauH(V10)
h11'=phi*(Hinf(V11)-h11)/tauH(V11)
h12'=phi*(Hinf(V12)-h12)/tauH(V12)
h13'=phi*(Hinf(V13)-h13)/tauH(V13)
```

```
h14'=phi*(Hinf(V14)-h14)/tauH(V14)
h15'=phi*(Hinf(V15)-h15)/tauH(V15)
h16'=phi*(Hinf(V16)-h16)/tauH(V16)
h17'=phi*(Hinf(V17)-h17)/tauH(V17)
h18'=phi*(Hinf(V18)-h18)/tauH(V18)
h19'=phi*(Hinf(V19)-h19)/tauH(V19)
h20'=phi*(Hinf(V20)-h20)/tauH(V20)

n1'=phi*(Ninf(V1)-n1)/tauN(V1)
n2'=phi*(Ninf(V2)-n2)/tauN(V2)
n3'=phi*(Ninf(V3)-n3)/tauN(V3)
n4'=phi*(Ninf(V4)-n4)/tauN(V4)
n5'=phi*(Ninf(V5)-n5)/tauN(V5)
n6'=phi*(Ninf(V6)-n6)/tauN(V6)
n7'=phi*(Ninf(V7)-n7)/tauN(V7)
n8'=phi*(Ninf(v8)-n8)/tauN(V8)
n9'=phi*(Ninf(V9)-n9)/tauN(V9)
n10'=phi*(Ninf(V10)-n10)/tauN(V10)
n11'=phi*(Ninf(V11)-n11)/tauN(V11)
n12'=phi*(Ninf(V12)-n12)/tauN(V12)
n13'=phi*(Ninf(V13)-n13)/tauN(V13)
n14'=phi*(Ninf(V14)-n14)/tauN(V14)
n15'=phi*(Ninf(V15)-n15)/tauN(V15)
n16'=phi*(Ninf(V16)-n16)/tauN(V16)
n17'=phi*(Ninf(V17)-n17)/tauN(V17)

n18'=phi*(Ninf(V18)-n18)/tauN(V18)
n19'=phi*(Ninf(V19)-n19)/tauN(V19)
n20'=phi*(Ninf(V20)-n20)/tauN(V20)
```

```
#
ai(v)=ai0/(1+exp(-(v-vst)/vss))
par ai0=4,taui=6,vst=0,vss=5
#

i(t)=i0+ip*heav(t-ton)*heav(toff-t)
alpham(V) = 0.1*(V+35.0)/(1.0-exp(-(V+35.0)/10.0))
betam(V)  = 4.0*exp(-(V+60.0)/18.0)
Minf(V) = alpham(V)/(alpham(V)+betam(V))
#
alphah(V) = 0.07*exp(-(V+58.0)/20.0)
betah(V)  = 1.0/(1.0+exp(-(V+28.0)/10.0))
Hinf(V) = alphah(V)/(alphah(V)+betah(V))
tauH(V) = 1.0/(alphah(V)+betah(V))
#
alphan(V) = 0.01*(V+34.0)/(1.0-exp(-(V+34.0)/10.00))
betan(V)  = 0.125*exp(-(V+44.0)/80.0)
Ninf(V) = alphan(V)/(alphan(V)+betan(V))
tauN(V) = 1.0/(alphan(V)+betan(V))

par eps=1
#
#
V[1..20](0)=-64*ran(1)
h[1..20](0)=0.78*ran(1)
n[2..20](0)=ran(1)
#
#global 1 v1-vt {t1=t}
#global 1 v2-vt {period=t-t2;phase=(t-t1)/(t-t2);t2=t}
```

```
#par vt=1
#t1'=0
#t2'=0
#period'=0
#phase'=0
#g'=0
#init g=0

@ DT=0.01,bound=10000
@ METH=qualrk
@ TOLER=0.00001
@ dt=.01, total=1500,transient=1499.99
@ xlo=80, xhi=100,ylo=0, nplot=2, yp2=v2
@ MAXSTOR 500000
# gap junction coupling
done
```

This is xpp code for a 20 oscillator phase model.

```
a0=5.1974931
a1=-2.9970722
a2=-0.92187762
a3=-0.44113794
a4=-0.25482759
a5=-0.16416954
a6=-0.11295291
a7=-0.080749117
a8=-0.058964562
```

```
b1=0.47408548
b2=-0.36833799
b3=-0.2577318
b4=-0.15762125
b5=-0.09083201
b6=-0.048487604
b7=-0.022178065
b8=-0.0061888532

H(x)=a0+a1*cos(x)+b1*sin(x)+a2*cos(2*x)+b2*sin(2*x)+a3*cos(3*x)
+b3*sin(3*x)+a4*cos(4*x)+b4*sin(4*x)+a5*cos(5*x)+b5*sin(5*x)
+a6*cos(6*x)+b6*sin(6*x)+a7*cos(7*x)+b7*sin(7*x)

x1'=H(x20-x1)+H(x2-x1)
x[2..19]'=H(x[j+1]-x[j])+H(x[j-1]-x[j])
x20'=H(x19-x20)+H(x1-x20)
done
```

Another ode file for the phase model (different way to compute the same thing)

```
#table h_ test.tab
#table h_ H_phi_5.7.tab
#table h_ H_phi_6.2.tab
#table h_ H_phi_6.5.tab
table h_ H_phi_6.tab
h(x)=h_(mod(x,1))

x1'=h(x2-x1)+h(x20-x1)
```

```
x[2..19]'=h(x[j+1]-x[j])+h(x[j-1]-x[j])
x20'=h(x19-x20)+h(x1-x20)


y1'=-h(y1)+h(-y1)
```

E.0.18 Figure 4.4

Ode File for an anti-wave in a chain of twenty neural oscillators using the Ermentrout-Cowan Model.

```
aux w1=2*gc*(p*y2+(1-p)*z2)

x1'=-x1+f(I-g*(a1*x1+a2*y1+a3*z1))-2*gc*(p*y2+(1-p)*z2)
y1'=-y1+f(I-g*(a1*y1+a2*z1+a3*x1))
z1'=-z1+f(I-g*(a1*z1+a2*x1+a3*y1))

x2'=-x2+f(I-g*(a1*x2+a2*y2+a3*z2))-gc*(p*y1+(1-p)*z1)-gc*(p*y3+(1-p)*z3)
y2'=-y2+f(I-g*(a1*y2+a2*z2+a3*x2))
z2'=-z2+f(I-g*(a1*z2+a2*x2+a3*y2))


x3'=-x3+f(I-g*(a1*x3+a2*y3+a3*z3))-gc*(p*y2+(1-p)*z2)-gc*(p*y4+(1-p)*z4)
y3'=-y3+f(I-g*(a1*y3+a2*z3+a3*x3))
z3'=-z3+f(I-g*(a1*z3+a2*x3+a3*y3))


x4'=-x4+f(I-g*(a1*x4+a2*y4+a3*z4))-gc*(p*y5+(1-p)*z5)-gc*(p*y3+(1-p)*z3)
y4'=-y4+f(I-g*(a1*y4+a2*z4+a3*x4))
z4'=-z4+f(I-g*(a1*z4+a2*x4+a3*y4))
```

```
x5'=-x5+f(I-g*(a1*x5+a2*y5+a3*z5))-gc*(p*y6+(1-p)*z6)-gc*(p*y4+(1-p)*z4)
y5'=-y5+f(I-g*(a1*y5+a2*z5+a3*x5))
z5'=-z5+f(I-g*(a1*z5+a2*x5+a3*y5))

x6'=-x6+f(I-g*(a1*x6+a2*y6+a3*z6))-gc*(p*y7+(1-p)*z7)-gc*(p*y5+(1-p)*z5)
y6'=-y6+f(I-g*(a1*y6+a2*z6+a3*x6))
z6'=-z6+f(I-g*(a1*z6+a2*x6+a3*y6))

x7'=-x7+f(I-g*(a1*x7+a2*y7+a3*z7))-gc*(p*y8+(1-p)*z8)-gc*(p*y6+(1-p)*z6)
y7'=-y7+f(I-g*(a1*y7+a2*z7+a3*x7))
z7'=-z7+f(I-g*(a1*z7+a2*x7+a3*y7))

x8'=-x8+f(I-g*(a1*x8+a2*y8+a3*z8))-gc*(p*y9+(1-p)*z9)-gc*(p*y7+(1-p)*z7)
y8'=-y8+f(I-g*(a1*y8+a2*z8+a3*x8))
z8'=-z8+f(I-g*(a1*z8+a2*x8+a3*y8))

x9'=-x9+f(I-g*(a1*x9+a2*y9+a3*z9))-gc*(p*y10+(1-p)*z10)-gc*(p*y8+(1-p)*z8)
y9'=-y9+f(I-g*(a1*y9+a2*z9+a3*x9))
z9'=-z9+f(I-g*(a1*z9+a2*x9+a3*y9))

x10'=-x10+f(I-g*(a1*x10+a2*y10+a3*z10))-gc*(p*y11+(1-p)*z11)-gc*(p*y9+(1-p)*z9)
y10'=-y10+f(I-g*(a1*y10+a2*z10+a3*x10))
z10'=-z10+f(I-g*(a1*z10+a2*x10+a3*y10))

x11'=-x11+f(I-g*(a1*x11+a2*y11+a3*z11))-gc*(p*y10+(1-p)*z10)-gc*(p*y12+(1-p)*z12)
y11'=-y11+f(I-g*(a1*y11+a2*z11+a3*x11))
z11'=-z11+f(I-g*(a1*z11+a2*x11+a3*y11))
```

```
x12'=-x12+f(I-g*(a1*x12+a2*y12+a3*z12))-gc*(p*y11+(1-p)*z11)-gc*(p*y13+(1-p)*z13)
y12'=-y12+f(I-g*(a1*y12+a2*z12+a3*x12))
z12'=-z12+f(I-g*(a1*z12+a2*x12+a3*y12))


x13'=-x13+f(I-g*(a1*x13+a2*y13+a3*z13))-gc*(p*y12+(1-p)*z12)-gc*(p*y14+(1-p)*z14)
y13'=-y13+f(I-g*(a1*y13+a2*z13+a3*x13))
z13'=-z13+f(I-g*(a1*z13+a2*x13+a3*y13))


x14'=-x14+f(I-g*(a1*x14+a2*y14+a3*z14))-gc*(p*y13+(1-p)*z13)-gc*(p*y15+(1-p)*z15)
y14'=-y14+f(I-g*(a1*y14+a2*z14+a3*x14))
z14'=-z14+f(I-g*(a1*z14+a2*x14+a3*y14))

x15'=-x15+f(I-g*(a1*x15+a2*y15+a3*z15))-gc*(p*y14+(1-p)*z14)-gc*(p*y16+(1-p)*z16)
y15'=-y15+f(I-g*(a1*y15+a2*z15+a3*x15))
z15'=-z15+f(I-g*(a1*z15+a2*x15+a3*y15))

x16'=-x16+f(I-g*(a1*x16+a2*y16+a3*z16))-gc*(p*y15+(1-p)*z15)-gc*(p*y17+(1-p)*z17)
y16'=-y16+f(I-g*(a1*y16+a2*z16+a3*x16))
z16'=-z16+f(I-g*(a1*z16+a2*x16+a3*y16))

x17'=-x17+f(I-g*(a1*x17+a2*y17+a3*z17))-gc*(p*y16+(1-p)*z16)-gc*(p*y18+(1-p)*z18)
y17'=-y17+f(I-g*(a1*y17+a2*z17+a3*x17))
z17'=-z17+f(I-g*(a1*z17+a2*x17+a3*y17))

x18'=-x18+f(I-g*(a1*x18+a2*y18+a3*z18))-gc*(p*y17+(1-p)*z17)-gc*(p*y19+(1-p)*z19)
y18'=-y18+f(I-g*(a1*y18+a2*z18+a3*x18))
z18'=-z18+f(I-g*(a1*z18+a2*x18+a3*y18))
```

```
x19'=-x19+f(I-g*(a1*x19+a2*y19+a3*z19))-gc*(p*y18+(1-p)*z18)-gc*(p*y20+(1-p)*z20)
y19'=-y19+f(I-g*(a1*y19+a2*z19+a3*x19))
z19'=-z19+f(I-g*(a1*z19+a2*x19+a3*y19))

x20'=-x20+f(I-g*(a1*x20+a2*y20+a3*z20))-2*gc*(p*y19+(1-p)*z19)
y20'=-y20+f(I-g*(a1*y20+a2*z20+a3*x20))
z20'=-z20+f(I-g*(a1*z20+a2*x20+a3*y20))



x[1..3](0)=ran(1)



par gc=.25,p=0
par g=50,I=2
par a1=.1,a2=.3,a3=.6

par eps=.1

f(x)=1/(1+exp(-x))

FP(x)= (F(x+.001)-F(x-.001))/(.002)

done
```

E.0.19 Figure 4.5

This code was used to compute the probability of various anti-wave solutions starting from random initial conditions.

E.0.20 Figure 4.6

This code was used to generate the Compacton Figures.

```
/
# include <ctype.h>
# include <stdio.h>
# include <stdlib.h>
# include <math.h>

#define step .01
#define pi 3.1416



double correlation;
double radius;
double sum;
double c3;
double integer;
double r;

double mean;



int rand(void);
void srand(unsigned seed);




int T;
int N;
```

```
int i;
int j;
int q;
int im;
int ip;
int k;
int l;
int ir;



//char fname[1234];


FILE  *ifp;



double h( double x){

  return cos(x)+(sin(x)-.75*sin(2*x));

}
```

```
double integrate(double *x, double *rhs,int N){
int n;

double zip;



  for(i=0;i<N;i++){

ip=i+1;
im=i-1;


if(ip>(N-1)) ip=im;
if(im<0) im=ip;



// subtract off x[i][j] from all guys in the matrix
 rhs[i]=h(x[ip])+h(-x[i])-h(-x[im])-h(x[i]);


  }


  }



FILE *fp;
```

```
FILE *ifp;
FILE *ph;
int main(){
char name[10];
printf("\n%s\n","Input n for the length of a chain of neurons.");
scanf("%d",&N);

double x[N];

double rhs[N];



i=0;


 int  s;
 int  nout;
 ph=fopen("phases.dat","w");
 ifp=fopen("histogram.dat","w");
 s=0;
 nout=50;

double v;
double np;
double w;
double A;
double z;
z=0;
//v=1.9065;
```

```
//v=1.675427;
v=.84106;
np=15;
w=10;
A=1.5;
/*
for (i=0;i<N;++i){
x[i]=v;
z=i-np;
if (abs(z)<w){
x[i]=v+(A/2)*(1+cos((i-np)*pi/w));

}

}
*/


for (i=0;i<N;++i){
x[i]=v;
//if (i<N/2){
//x[i]=v;
//}

//if (i>N/2){
//x[i]=-v;
//}
z=i-np;
if (abs(z)<w){
x[i]=(v+(A/2)*(1+cos((i-np)*pi/w)));
```

```
}

}

for(q=0;q<7000;++q){



integrate(x,rhs,N);


fp=fopen(name,"w");
for(i=0;i<N;++i){
x[i]+=step*rhs[i];
x[i]=fmod(x[i],2*pi);
if(x[i]<=0) x[i]=2*pi+x[i];

fprintf(ph,"%g ",x[i]);

}


fprintf(ph,"\n ");
 }
fclose(ph);

}
```

E.0.21 Figure 4.7

```
function nullclines
function output=h(x,beta)
output=sin(x)-.75*sin(x*2)+beta*cos(x);
end

x2=0:.01:2*pi;
x1=0:.01:2*pi;
beta=.6;


x=2*h(-x2,beta)-h(x2,beta)-h(-x1,beta);

y=h(x2,beta)+h(-x1,beta)-2*h(x1,beta);

%plot(x,y,'b')


h1= @(x1,x2)  2*h(-x2,beta)-h(x2,beta)-h(-x1,beta);
h2= @(x1,x2)  h(x2,beta)+h(-x1,beta)-2*h(x1,beta);
figure;
hold

ezplot(h1)
```

```
ezplot(h2)
end
```

Here is the code in XPP for three oscillators to produce a bifurcation diagram in AUTO:

```
H(x)=sin(x)-k*sin(2*x)+beta*(1-cos(x))
par k=.75
par beta=1

x1'=-2*H(x1)+H(-x1)+H(x2)
x2'=2*H(-x2)-H(-x1)-H(x2)
done
```

E.0.22 Figure 4.9

```
function beta_critical
% define the wave vector phi
phi=-.841068;
% a program for computing beta critical for chains of phase oscillators
%H(x)=sin(x)-3/4*sin(2*x)+b*cos(x)
function [output]=dh(x,b)
[output]=cos(x)-3/2*cos(2*x)-b*sin(x);
end
%Nmax the maximal number of oscillators in a chain
figure;
hold
Nmax=50;

mmax=6000;
% initialize b
bcrit=zeros(1,Nmax);
Nvec=zeros(1,Nmax);
```

```
pmaximalv=zeros(1,Nmax);
figure;
hold
for N=4:1:Nmax
% loop through values of N
%N=95;
bv=0;
J=zeros(N,N);
x=zeros(1,N);
% now, create a kink solution
for j=1:floor(N/2)
x(1,j)=-phi;
end
for j=floor(N/2+1):N
    x(1,j)=phi;
end
%plot(x)
%hold
b=zeros(1,mmax);
maximalv=zeros(1,mmax);
for m=1:mmax
bv=.005+bv;
b(m)=bv;
% now linearize about the stable solution and solve for the eigenvalues


% the first row of the Jacobian

J(1,1)=-1*(2*dh(x(1),bv)+dh(-x(1),bv));
J(1,2)=dh(x(2),bv);
```

```
% now compute all the tridiagonal elements up to row N
for i=2:N-1
J(i,i)=-1*(dh(-x(i),bv)+dh(x(i),bv));
J(i,i+1)=dh(x(i+1),bv);
J(i,i-1)=dh(-x(i-1),bv);
% Now fill in row N
end
J(N,N-1)=dh(-x(N-1),bv);
J(N,N)=-1*(2*dh(-x(N),bv)+dh(x(N),bv));

%if (N==5)
%J
%end
v=eig(J,'nobalance');

v=real(v);
mv=max(v);
maximalv(m)=mv;
if (bcrit(N)==0);
if m>2
if ( maximalv(m)>1e-6 && maximalv(m-1)>1e-7 )
    bcrit(N)=b(m);


%bcrit
end
end
end
end
```

```
Nvec(N)=N;
pmaximalv(N)=maximalv(mmax);
disp(N)

plot(b,maximalv)

end
figure
plot(Nvec,bcrit)
```

E.0.23 Figure 4.10

```
function beta_criticalvskinkposition
% a program for computing beta critical for chains of phase oscillators
%H(x)=sin(x)-3/4*sin(2*x)+b*cos(x)


function [output]=dh(x,b)
[output]=cos(x)-3/2*cos(2*x)-b*sin(x);
end


figure;
hold
N=50;

mmax=6000;
phi=-.841068;
```

```
% now, create a kink solution that moves
% f is the fraction of the chain where the kink starts.
%let f go from 2:10;

start=4;
fmax=(N-2*start);
% compute a critical value of beta for every kink position
bcrit=zeros(1,fmax);
position=zeros(1,fmax);

for f=1:fmax
b=zeros(1,mmax);
maximalv=zeros(1,mmax);
disp(f)
   bv=0;
J=zeros(N,N);
x=zeros(1,N);



for j=1:start+f
x(1,j)=-phi;
end
for j=(1+f+start):N
    x(1,j)=phi;
end

position(f)=start+f;
%hold

for m=1:mmax
```

```
bv=.002+bv;
b(m)=bv;
% now linearize about the stable solution and solve for the eigenvalues


% the first row of the Jacobian

J(1,1)=-1*(2*dh(x(1),bv)+dh(-x(1),bv));
J(1,2)=dh(x(2),bv);

% now compute all the tridiagonal elements up to row N
for i=2:N-1
J(i,i)=-1*(dh(-x(i),bv)+dh(x(i),bv));
J(i,i+1)=dh(x(i+1),bv);
J(i,i-1)=dh(-x(i-1),bv);
% Now fill in row N
end
J(N,N-1)=dh(-x(N-1),bv);
J(N,N)=-1*(2*dh(-x(N),bv)+dh(x(N),bv));


v=eig(J);

%if f==6
 %   disp(max(real(v)))
%end
    v=real(v);
mv=max(v);
maximalv(m)=mv;
if (bcrit(f)==0) % Im not sure if this should be here or not.
```

```
if m>2
if (maximalv(m-1)<1e-5 && maximalv(m)>1e-6)
    % determines the critical beta as a function of the kink position
    bcrit(f)=b(m);


end
end
end
end
plot(b,maximalv)
end
figure;
%disp(bcrit)
%disp(position)
plot(bcrit,position)
end
```

E.0.24 Figure 4.13,4.11,4.12

```
# include <ctype.h>
# include <stdio.h>
# include <stdlib.h>
# include <math.h>

// these are the fourier coefficients for the H-function
// This program is a sheet with nearest neighbor coupling.
// I want to study plane waves with our H function in this sheet.
#define step .01
#define pi 3.1416
```

```
 // these are the good fourier terms phi=6.4
# define a0 7.0926414
# define a1 -4.8928847
# define a2 -1.5865817
# define a3 -0.55360311
# define a4 -0.17344333
# define a5 -0.033863876
# define a6 0.014845844
# define a7 0.028762558
# define a8 0.029549792


#define b1 -0.5182156
#define b2 -1.3124702
#define b3 -0.93395054
#define b4 -0.57600337
#define b5 -0.33628672
#define b6 -0.18798296
#define b7 -0.098594636
#define b8 -0.045613445

/* H function phi=6
#define a0 5.19535640000000
#define a1 -2.99568370000000
#define a2 -0.921286340000000
#define a3 -0.440974560000000
#define a4 -0.254829260000000
#define a5  -0.164220840000000
#define a6  -0.113010170000000
#define a7 -0.113010170000000
```

```
#define b1 0.474202630000000
#define b2 -0.367749870000000
#define b3 -0.257242530000000
*/



double correlation;
double radius;
double sum;
double c3;
double integer;
double r;

double mean;



int rand(void);
void srand(unsigned seed);




int N3;
int p;
int jr;
int kr;
int ir;
int lr;
```

```
int T;
int N;
int i;
int j;
int q;
int im;
int ip;
int jm;
int jp;
int k;
int l;
 int ir;
 int jr;
 int kr;
 int lr;
double **x;
double **y;
double **rhs;
double xx;

//char fname[1234];


FILE  *ifp;
double c(double **y,double r, int N){
//take the array and compute the correlations
int i;
int j;
int k;
int l;
```

```
int ip;
int jp;
int im;
int jm;
double kl;
double ave;
 double C;
 double Ncount;
i=0;
j=0;
k=0;
l=0;
C=0;

// pick points a distance r away in the sheet.
// periodic boundary conditions
 ave=0;
// visit all sites in the lattice
 for(i=0;i<N;i++){
for(j=0;j<N;j++){
           Ncount=0;
   C=0;

  for(k=1;k<=r;k++){
     for(l=1;l<=r;l++){

      ip=i+k;
      jp=j+l;
      im=i-k;
      jm=j-l;
```

```
if(jm<0)  jm=(N-1);
if(jp>(N-1)) jp=0;
if(ip>(N-1)) ip=0;
if(im<0) im=(N-1);
if( (l*l+k*k)<=(r+.5)*(r+.5) &&(l*l+k*k)>=(r-.5)*(r-.5)){
Ncount+=1;
double b;
b=.25*(y[i][j]*y[ip][jp]+y[i][j]*y[ip][jm]+y[i][j]*y[im][jm]+y[i][j]*y[im][jp]);
C+=.25*y[i][j]*(y[ip][jp]+y[ip][jm]+y[im][jm]+y[im][jp]);

 }
     }

  }
 ave+=C/Ncount;
}
 }

return ave/pow(N,2);
}

double H( double x){

  return -2*cos(x)+b1*sin(x)+b2*sin(2*x)+b3*sin(3*x);


}
double BoxMuller;
int BoxMullerFlag=0;
```

```
double normal()
{
 double fac,r,v1,v2;
 if(BoxMullerFlag==0){
  do {
    v1=2.0*drand48()-1.0;
    v2=2.0*drand48()-1.0;
    r=v1*v1+v2*v2;
  } while(r>=1.0);
  fac=sqrt(-2.0*log(r)/r);
  BoxMuller=v1*fac;
  BoxMullerFlag=1;
  return(v2*fac);
 }
 else {
  BoxMullerFlag=0;
  return(BoxMuller);
 }
}
```

```
double integrate(double **x, double **rhs,int N){
int n;
```

```
 double zip;
 x[0][0]=0;
 zip=(H(x[1][0]-x[0][0])+H(x[N-1][0]-x[0][0])
+H(x[0][N-1]-x[0][0])+H(x[0][1]-x[0][0]));


  for(i=0;i<N;i++){

ip=i+1;
im=i-1;
for(j=0;j<N;j++){
// sum up all contributions

jp=j+1;
jm=j-1;
// periodic boundary conditions
/*
if(jm<0)  jm=(N-1);
if(jp>(N-1)) jp=0;
if(ip>(N-1)) ip=0;
if(im<0) im=(N-1);
*/
// we may also have cut ends boundary conditions
// use these for the perfect kink.

// Implement cut ends boundary conditions.

if(jm<0)  jm=jp;
if(jp>(N-1)) jp=jm;
if(ip>(N-1)) ip=im;
```

```
if(im<0) im=ip;




xx=x[i][j];

//if(jm<0)  printf("%d",jm);

// subtract off x[i][j] from all guys in the matrix
 rhs[i][j]=(H(x[ip][j]-xx)+H(x[im][j]-xx)+H(x[i][jp]-xx)+H(x[i][jm]-xx))-zip;


//printf("%s","test");
}}
}


FILE *fp;
FILE *ifp;
FILE *cor;
// *************************************************************
// *************************************************************

// PROGRAM STARTS HERE

//! you have to enter the name of the file you want to print the correlation
//data to
// ***********************************************************
int main(){
```

```
char name[10];
char cname[10];
printf("\n%s\n","Input n for the dimension of an nxn sheet of neurons.");
scanf("%d",&N);




x=calloc(N, sizeof(double*));
for(i=0;i<N;++i){
x[i]=calloc(N,sizeof(double));
}



y=calloc(N, sizeof(double*));
for(i=0;i<N;++i){
y[i]=calloc(N,sizeof(double));
}

rhs=calloc(N, sizeof(double*));
for(i=0;i<N;++i){
rhs[i]=calloc(N,sizeof(double));
}

// INTIAL CONDTIONS
```

```
// we focus on three types of intial conditions
// use these wave vectors in the x and y directions.
double kx=1.6336;
double ky=1.6336;



// traveling wave
//Do this for a 50x 50
/*
for (i=0;i<N;++i){
for(j=0;j<N;++j){
  x[i][j]=i*kx+j*ky;

}}

*/
/*
// 1 2D (perfect) kink
// DO THIS FOR A 50 X 50 SHEET
// These i.c.s give a perfect kink (or very close to it)

for (i=0;i<N/2;++i){
for(j=0;j<N;++j){
  x[i][j]=i*kx+j*ky;

}}
for (i=N/2;i<N;++i){
for(j=0;j<N;++j){
 x[i][j]=-i*kx+j*ky;
```

```
 }}

*/

// random initial conditions

for (i=0;i<N;++i){
for(j=0;j<N;++j){
  x[i][j]=2*pi*drand48();

  }}



T=1;



i=0;
j=0;
 double sigma=0;
 int  s;
 int  nout;
nout=50;
 int sp=0;
 cor=fopen("correlation.dat","w");
  //ifp=fopen("histogram.dat","w");
 s=0;
 nout=500;
```

```
 // i want to compute the correlation for the plane wave system
  // the initial conditions are for the plane wave solution
  // I slowly increase noise from zero until I loose the plane wave

 for(sp=0;sp<250;sp++){
 sigma=sigma+.005;
 // seems like a good combination of stepsize for simple h patterns
 // may need to go finer for full H

 //sprintf(cname,"c%d.dat",sp);
//cor=fopen(cname,"w");
for(q=0;q<150000;++q){
N3=0;
 mean=0;
integrate(x,rhs,N);
for(j=0;j<N;++j){
for(i=0;i<N;++i){

   x[i][j]+=step*rhs[i][j]+sqrt(step)*sigma*normal();

  //  x[i][j]+=step*rhs[i][j];
// step through time, incrementally add noise and compute the correlation.



x[i][j]=fmod(x[i][j],2*pi);
if(x[i][j]<=0) x[i][j]=2*pi+x[i][j];
}
}
```

```
// print the phase angles to a file every 500 time steps

if(q==s){


sprintf(name,"x%d.dat",q);
//ifp=fopen("histogram","w");
fp=fopen(name,"w");
for(i=0;i<N;++i){
for(j=0;j<N;++j){


  // every 500 time steps
   fprintf(fp,"%g;",x[i][j]);
 }
fprintf(fp,"\n ");
 }
fclose(fp);
 s=s+nout;
 }
//now compute the mean of the phase angles.

for(i=0;i<N;++i){
for(j=0;j<N;++j){

  x[i][j]=x[i][j];

//take the sin of all the phase angles
```

```
   y[i][j]=sin(x[i][j]);

  mean+=y[i][j];

  //printf("%g\n",mean);
 }}
mean=mean/(N*N);
// printf("%g",mean);
 // now, subtract the mean off of the y

for(i=0;i<N;++i){
for(j=0;j<N;++j){


  y[i][j]=y[i][j]-mean;

  //  fprintf(cor,"%g;",sin(x[i][j]));
  //printf("%g",mean);
}
//fprintf(cor,"\n");
}

// c(y,2,N);
//int w=0;
//for(w=1;w<10;w++){
   // make this bigger for random i.c.
  //fprintf(cor,"%g;",c(y,w,N));

if(q==4900){
```

```
  //fprintf(cor,"%g;",c(y,3,N));


//printf("%g;",c(y,3,N));
}
//}

if(q==4901){
  //fprintf(cor,"\n");
 }
 }
// }
 fclose(cor);

}
```

E.0.25 Figure 4.15

```
function wave_instability

% I want to show that the plane wave is an unstable solution
% for coupling which is beyond nearest neighbor.
N=1000;
%kx=0:1/(N-1):1;
%q=0.01;
k=0:1/(N-1):1;
q=0:1/(N-1):1;
b1=-0.5182156;
b2= -1.3124702;
b3=-0.93395054;
```

```
%a1=-2;


%ky=0:1/(N-1):1;
%kx=kx*2*pi;
%ky=2*pi*ky;

k=2*pi*k;
q=2*pi*q;
% add a small peturbation

kx=k;
ky=k;
qx=q;
qy=q;
lambda=zeros(N,N);
for i=1:length(q)
    for j=1:length(k)
sum1=2*b1*pi*(exp(-.5*((kx(j)+qx(i))^2+(ky(j)+qy(i))^2)
+exp(-.5*((kx(j)-qx(i))^2+(ky(j)-qy(i))^2))));

sum2=4*pi*b2*(exp(-.5*((2*kx(j)+qx(i))^2+(2*ky(j)+qy(i))^2))
+exp(-.5*((2*kx(j)-qx(i))^2+(2*ky(j)-qy(i))^2)));


sum3=6*pi*b3*(exp(-.5*((3*kx(j)+qx(i))^2+(3*ky(j)+qy(i))^2))
+exp(-.5*((3*kx(j)-qx(i))^2+(3*ky(j)-qy(i))^2)));


sum4=-4*pi*b1*exp(-.5*(kx(j)*kx(j)+ky(j)*ky(j)))
```

```
-8*pi*b2*exp(-2*(kx(j)*kx(j)+ky(j)*ky(j)))
-12*pi*b3*exp(-(9/2)*(kx(j)*kx(j)+ky(j)*ky(j)));
lp(i,j)=sum1+sum2+sum3+sum4;
lambda(i,j)=sum1+sum2+sum3+sum4;

    end
end
pt=max(lp);

plot(k,pt)
%figure;
%contour(kx,ky,lambda);
figure;
imagesc(kx,q,lambda)
%surfc(kx,ky,lambda,'FaceColor','interp','EdgeColor','none','FaceLighting','phong')
%[C h]=contourc(kx,ky,lambda);
%clabel(C,h)
```

BIBLIOGRAPHY

[1] S Grillner. Neurobiological bases of rhythmic motor acts in vertebrates. *Science*, 228(4696):143–149, 1985.

[2] Frank C. Hoppensteadt and Eugene Izhikevich. *Weakly Connected Neural Networks*. Spinger-Verlag New York Inc, 1997.

[3] Gyrgy Buzski and Andreas Draguhn. Neuronal oscillations in cortical networks. *Science*, 304(5679):1926–1929, 2004.

[4] Steven H. and Strogatz. From kuramoto to crawford: exploring the onset of synchronization in populations of coupled oscillators. *Physica D: Nonlinear Phenomena*, 143(1-4):1 – 20, 2000.

[5] W. K. Rose. Relaxation oscillations in helium shell-burning stars of low mass and evolution into the white-dwarf state. *apj*, 146:838, dec 1966.

[6] Eugene Izhikevich. *Dynamical Systems in Neuroscience: The Geometry of Excitabilty and Bursting*. MIT press: Cambridge, Massachusetts, 2007.

[7] W O Friesen and G S Stent. Neural circuits for generating rhythmic movements. *Annual Review of Biophysics and Bioengineering*, 7(1):37–61, 1978.

[8] Avis H. Cohen, Philip J. Holmes, and Richard H. Rand. The nature of the coupling between segmental oscillators of the lamprey spinal generator for locomotion: A mathematical model. *Journal of Mathematical Biology*, 13:345–369, 1982. 10.1007/BF00276069.

[9] Ole Kiehn and Matthew C. Tresch. Gap junctions and motor behavior. *Trends in Neurosciences*, 25(2):108 – 115, 2002.

[10] Stephanie R. Jones, Brian Mulloney, Tasso J. Kaper, and Nancy Kopell. Coordination of cellular pattern-generating circuits that control limb movements: The sources of stable differences in intersegmental phases. *The Journal of Neuroscience*, 23(8):3457–3468, 2003.

[11] Nicholas Minorsky. *Nonlinear Oscillations*. D. Van Nostrand Company, Inc., 1962.

[12] Stephen T Thorton Jerry B. Marion. *Classical dynamics of particles and systems.* Saunders College Publishers, 1995.

[13] Richard and FitzHugh. Impulses and physiological states in theoretical models of nerve membrane. *Biophysical Journal*, 1(6):445 – 466, 1961.

[14] Richard Fitzhugh. Thresholds and plateaus in the hodgkin-huxley nerve equations. *The Journal of General Physiology*, 43(5):867–896, 1960.

[15] R. V. Johnson and J. H. Marburger. Relaxation oscillations in stimulated raman and brillouin scattering. *Phys. Rev. A*, 4:1175–1182, Sept 1971.

[16] Peter Dayan and L.F. Abbott. *Theoretical Neuroscience.* The MIT Press, 2001.

[17] Thomas M. Jessell Eric R. Kandell, James H. Schwartz. *Principles of Neural Science.* McGraw-Hill, 1991.

[18] David J. Pinto, Joshua C. Brumberg, Daniel J. Simons, G. Bard Ermentrout, and Roger Traub. A quantitative population model of whisker barrels: Re-examining the wilson-cowan equations. *Journal of Computational Neuroscience*, 3:247–264, 1996. 10.1007/BF00161134.

[19] Gyorgy Buszaki Xiao-Jing Wang. Gamma oscillation by synaptic inhibition in a hippocampal interneuronal network model. *The Journal of Neuroscience*, 16(20):6402–6413, October 1996.

[20] Andrew V. Poliakov, Randall K. Powers, and Marc D. Binder. Functional identification of the input-output transforms of motoneurones in the rat and cat. *The Journal of Physiology*, 504(2):401–424, 1997.

[21] H. R. Wilson and J. D. Cowan. A mathematical theory of the functional dynamics of cortical and thalamic nervous tissue. *Biological Cybernetics*, 13:55–80, 1973. 10.1007/BF00288786.

[22] Bard Ermentrout. Neural networks as spatio-temporal pattern-forming systems. *Reports on Progress in Physics*, 61(4):353, 1998.

[23] J J Hopfield. Neural networks and physical systems with emergent collective computational abilities. *Proceedings of the National Academy of Sciences*, 79(8):2554–2558, 1982.

[24] Catherine Morris and Harold Lecar. Voltage oscillations in the barnacle giant muscle fiber. *Biophysical Journal*, 35:193–213, October 1981.

[25] James T. Buchanan. Commissural interneurons in rhythm generation and intersegmental coupling in the lamprey spinal cord. *Journal of Neurophysiology*, 81(5):2037–2045, 1999.

[26] Xiao-Jing Wang and John Rinzel. Alternating and synchronous rhythms in reciprocally inhibitory model neurons. *Neural Comput.*, 4:84–97, January 1992.

[27] Donald H. Perkel and Brian Mulloney. Motor pattern production in reciprocally inhibitory neurons exhibiting postinhibitory rebound. *Science*, 185(4146):181–183, 1974.

[28] B. L. McNaughton, C. A. Barnes, and P. Andersen. Synaptic efficacy and epsp summation in granule cells of rat fascia dentata studied in vitro. *Journal of Neurophysiology*, 46(5):952–966, 1981.

[29] RJ Sayer, MJ Friedlander, and SJ Redman. The time course and amplitude of epsps evoked at synapses between pairs of ca3/ca1 neurons in the hippocampal slice. *The Journal of Neuroscience*, 10(3):826–836, 1990.

[30] James A. Murdock. *Perturbations : Theory and Methods*. John Wiley and Sons Inc., 1991.

[31] Roberto F. Galán, G. Bard Ermentrout, and Nathaniel N. Urban. Efficient estimation of phase-resetting curves in real neurons and its significance for neural-network modeling. *Phys. Rev. Lett.*, 94:158101, Apr 2005.

[32] Robert J Prill, Pablo A Iglesias, and Andre Levchenko. Dynamic properties of network motifs contribute to biological network organization. *PLoS Biol*, 3(11):e343, 10 2005.

[33] O. Sporns and R. Kotter. Motifs in brain networks. *PLoS Biol.*, 2:e369, Nov 2004.

[34] Marder E Prinz A, Bucher D. Similar network activity from disparate circuit parameters. *Nature Neuroscience*, 12:1345–1352, 2004.

[35] A. L. Weaver and S. L. Hooper. Relating network synaptic connectivity and network activity in the lobster (Panulirus interruptus) pyloric network. *J. Neurophysiol.*, 90:2378–2386, Oct 2003.

[36] A. G. Bulloch and N. I. Syed. Reconstruction of neuronal networks in culture. *Trends Neurosci.*, 15:422–427, Nov 1992.

[37] A. Shilnikov, R. Gordon, and I. Belykh. Polyrhythmic synchronization in bursting networking motifs. *Chaos*, 18:037120, Sep 2008.

[38] J. Collins and I. Stewart. Coupled nonlinear oscillators and the symmetries of animal gaits. *J. Nonlinear Science*, 3:349–392, 1993.

[39] Carla M. A. Pinto and Martin Golubitsky. Central pattern generators for bipedal locomotion. *J. Math. Biol.*, 53(3):474–489, 2006.

[40] J. E. Rubin, N. A. Shevtsova, G. B. Ermentrout, J. C. Smith, and I. A. Rybak. Multiple rhythmic states in a model of the respiratory central pattern generator. *J. Neurophysiol.*, 101:2146–2165, Apr 2009.

[41] D. Terman, S. Ahn, X. Wang, and W Just. Reducing neuronal networks to discrete dynamics. *Physica D*, 237:324–338, 2010.

[42] M. S. Goldman. Memory without feedback in a neural network. *Neuron*, 61:621–634, Feb 2009.

[43] B. K. Murphy and K. D. Miller. Balanced amplification: a new mechanism of selective amplification of neural activity patterns. *Neuron*, 61:635–648, Feb 2009.

[44] Mikhail I. Rabinovich, Pablo Varona, Allen I. Selverston, and Henry D. I. Abarbanel. Dynamical principles in neuroscience. *Rev. Mod. Phys.*, 78(4):1213–1265, Nov 2006.

[45] Maria da Conceição A Leite and Martin Golubitsky. Homogeneous three-cell networks. *Nonlinearity*, 19(10):2313–2363, 2006.

[46] Martin Golubitsky, Ian Stewart, and Andrei Török. Patterns of synchrony in coupled cell networks with multiple arrows. *SIAM J. Appl. Dyn. Syst.*, 4(1):78–100 (electronic), 2005.

[47] Kanaka Rajan and L. F. Abbott. Eigenvalue spectra of random matrices for neural networks. *Phys. Rev. Lett.*, 97(18):188104, Nov 2006.

[48] R. Ben-Yishai, D. Hansel, and H. Sompolinsky. Traveling waves and the processing of weakly tuned inputs in a cortical network module. *J Comput Neurosci*, 4:57–77, Jan 1997.

[49] A. Szucs, R. Huerta, M. I. Rabinovich, and A. I. Selverston. Robust microcircuit synchronization by inhibitory connections. *Neuron*, 61:439–453, Feb 2009.

[50] George Bard Ermentrout and Nancy Kopell. Frequency plateaus in a chain of weakly coupled oscillators. I. *SIAM J. Math. Anal.*, 15(2):215–237, 1984.

[51] Kuramoto Y. *Chemical Oscillations, Waves, and Turbulence*. Springer Verlag, New York, 1984.

[52] G. B. Ermentrout and N. Kopell. Parabolic bursting in an excitable system coupled with a slow oscillation. *SIAM Journal on Applied Mathematics*, 46(2):233–253, 1986.

[53] S. R. Jones, B. Mulloney, T. J. Kaper, and N. Kopell. Coordination of cellular pattern-generating circuits that control limb movements: the sources of stable differences in intersegmental phases. *J. Neurosci.*, 23:3457–3468, Apr 2003.

[54] J. H. Kotaleski, S. Grillner, and A. Lansner. Neural mechanisms potentially contributing to the intersegmental phase lag in lamprey.I. Segmental oscillations dependent on reciprocal inhibition. *Biol Cybern*, 81:317–330, Oct 1999.

[55] P. L. Varkonyi, T. Kiemel, K. Hoffman, A. H. Cohen, and P. Holmes. On the derivation and tuning of phase oscillator models for lamprey central pattern generators. *J Comput Neurosci*, 25:245–261, Oct 2008.

[56] U. Rutishauser, R. Douglas, and J-J. Slotine. Collective stability of networks of winner-take-all circuits. *Neural Computation, in press*, 2010.

[57] G Orosz, P Ashwin, and S Townley. Learning of spatiotemporal codes in a coupled oscillator system. *IEEE TRANSACTIONS ON NEURAL NETWORKS*, 20:1135–1147, 2009.

[58] Z. Chen, M. Zheng, W. O. Friesen, and T. Iwasaki. Multivariable harmonic balance analysis of the neuronal oscillator for leech swimming. *J Comput Neurosci*, 25:583–606, Dec 2008.

[59] Carl Vreeswijk, L. F. Abbott, and G. Bard Ermentrout. When inhibition not excitation synchronizes neural firing. *Journal of Computational Neuroscience*, 1:313–321, 1994. 10.1007/BF00961879.

[60] Bard Ermentrout, Matthew Pascal, and Boris Gutkin. The effects of spike frequency adaptation and negative feedback on the synchronization of neural oscillators. *Neural Computation*, 13(6):1285–1310, 2001.

[61] Gennady S. Cymbalyuk, Girish N. Patel, Ronald L. Calabrese, Stephen P. DeWeerth, and Avis H. Cohen. Modeling alternation to synchrony with inhibitory coupling: A neuromorphic vlsi approach. *Neural Computation*, 12(10):2259–2278, 2000.

[62] Jaime G. Mancilla, Timothy J. Lewis, David J. Pinto, John Rinzel, and Barry W. Connors. Synchronization of electrically coupled pairs of inhibitory interneurons in neocortex. *The Journal of Neuroscience*, 27(8):2058–2073, 2007.

[63] Nancy Kopell Amitabha Bose and David Terman. Almost-synchronous solutions for mutually coupled excitatory neurons. *PHYSICA D*, 140:69–94, 2000.

[64] Benjamin Pfeuty, Germn Mato, David Golomb, and David Hansel. Electrical synapses and synchrony: The role of intrinsic currents. *The Journal of Neuroscience*, 23(15):6280–6294, 2003.

[65] G. Bard Ermentrout and David Terman. *Mathematical Foundations of Neuroscience*. Springer-Verlag, 2010.

[66] Sten Grillner, Henry Markram, Erik De Schutter, Gilad Silberberg, and Fiona E.N. LeBeau. Microcircuits in action from cpgs to neocortex. *Trends in Neurosciences*, 28(10):525 – 533, 2005.

[67] Michael V. L Bennett. Gap junctions as electrical synapses. *Journal of Neurocytology*, 26:349–366, 1997. 10.1023/A:1018560803261.

[68] M. P. Nusbaum and M. P. Beenhakker. A small-systems approach to motor pattern generation. , 417:343–350, May 2002.

[69] Cline Bou-Flores and Albert J. Berger. Gap junctions and inhibitory synapses modulate inspiratory motoneuron synchronization. *Journal of Neurophysiology*, 85(4):1543–1551, 2001.

[70] Louis Saint-Amant and Pierre Drapeau. Synchronization of an embryonic network of identified spinal interneurons solely by electrical coupling. *Neuron*, 31(6):1035 – 1046, 2001.

[71] Matthew C. Tresch Ole Kiehn, Ole Kjaerrulff and Ronald M. Harris-Warrick. Contributions of intrinsic motor neuron properties to the production of rhythmic motor output in the mammalian spinal cord. *Brain Research Bulletin*, 53(5):649–659, 2000.

[72] Alejandro Peinado. Immature neocortical neurons exist as extensive syncitial networks linked by dendrodendritic electrical connections. *Journal of Neurophysiology*, 85(2):620–629, 2001.

[73] Hans G. Eder Kris Smith Sam P. Javedan, Robert S. Fisher and Jie Wu. Cooling abolishes neuronal network synchronization in rat hippocampal slices. *Epilepsia*, 46(6):574–580, 2002.

[74] Zachary P. Kilpatrick and G. Bard Ermentrout. Sparse gamma rhythms arising through clustering in adapting neuronal networks. University of Pittsburgh Department of Mathematics, Pittsburgh, PA 15260, 2011.

[75] Sharon M. Crook, G. Bard Ermentrout, and James M. Bower. Dendritic and synaptic effects in systems of coupled cortical oscillators. *Journal of Computational Neuroscience*, 5:315–329, 1998. 10.1023/A:1008839112707.

[76] A. Gelperin. Oscillatory dynamics and information processing in olfactory systems. *Journal of Experimental Biology*, 202(14):1855–1864, 1999.

[77] U. Kim, T. Bal, and D. A. McCormick. Spindle waves are propagating synchronized oscillations in the ferret lgn in vitro. *Journal of Neurophysiology*, 74(3):1301–1323, 1995.

[78] G.Bard Ermentrout and David Kleinfeld. Traveling electrical waves in cortex: Insights from phase dynamics and speculation on a computational role. *Neuron*, 29(1):33 – 44, 2001.

[79] Yoko Momose-Sato, Katsushige Sato, and Masae Kinoshita. Spontaneous depolarization waves of multiple origins in the embryonic rat cns. *European Journal of Neuroscience*, 25(4):929–944, 2007.

[80] Bard Ermentrout, Jorge Flores, and Alan Gelperin. Minimal model of oscillations and waves in the limax olfactory lobe with tests of the model's predictive power. *Journal of Neurophysiology*, 79(5):2677–2689, 1998.

[81] M. Diesmann, M.-O. Gewaltig, and A. Aertsen. Stable propagation of synchronous spiking in cortical neural networks. *nature*, 402:529–533, December 1999.

[82] Moshe Abeles, Gaby Hayon, and Daniel Lehmann. Modeling compositionality by dynamic binding of synfire chains. *Journal of Computational Neuroscience*, 17(2):179–201, 2004.

[83] J. Rinzel, D. Terman, X.-J. Wang, and B. Ermentrout. Propagating activity patterns in large-scale inhibitory neuronal networks. *Science*, 279(5355):1351–1355, 1998.

[84] G. B. Ermentrout and N. Kopell. Inhibition-produced patterning in chains of coupled nonlinear oscillators. *SIAM Journal on Applied Mathematics*, 54(2):pp. 478–507, 1994.

[85] N. Kopell and G. B. Ermentrout. Symmetry and phaselocking in chains of weakly coupled oscillators. *Communications on Pure and Applied Mathematics*, 39(5):623–660, 1986.

[86] G. B. Ermentrout. The behavior of rings of coupled oscillators. *Journal of Mathematical Biology*, 23:55–74, 1985. 10.1007/BF00276558.

[87] G. Bard Ermentrout. Stable periodic solutions to discrete and continuum arrays of weakly coupled nonlinear oscillators. *SIAM Journal on Applied Mathematics*, 52(6):pp. 1665–1687, 1992.

[88] Daniel A. Wiley, Steven H. Strogatz, and Michelle Girvan. The size of the sync basin. *CHAOS*, 16(1):015103, 2006.

[89] Bernd Blasius and Ralf Tönjes. Quasiregular concentric waves in heterogeneous lattices of coupled oscillators. *Phys. Rev. Lett.*, 95:084101, Aug 2005.

[90] David Somers and Nancy Kopell. Waves and synchrony in networks of oscillators of relaxation and non-relaxation type. *Physica D: Nonlinear Phenomena*, 89(1-2):169 – 183, 1995.

[91] S Grillner. On the generation of locomotion in spinal dogfish. *Experimental Brain Research*, 20:459–470, 1974.

[92] J Christensen and RL Hauser. Circumferential coupling of electric slow waves in circular muscle of cat colon. *American Journal of Physiology – Legacy Content*, 221(4):1033–1037, 1971.

[93] Kevin W Thompson. Time dependent boundary conditions for hyperbolic systems. *Journal of Computational Physics*, 68(1):1 – 24, 1987.

[94] Bruce Denardo, Brian Galvin, Alan Greenfield, Andres Larraza, Seth Putterman, and William Wright. Observations of localized structures in nonlinear lattices: Domain walls and kinks. *Phys. Rev. Lett.*, 68:1730–1733, Mar 1992.

[95] Arkady Pikovsky and Philip Rosenau. Phase compactons. *Physica D: Nonlinear Phenomena*, 218(1):56 – 69, 2006.

[96] Karsten Ahnert and Arkady Pikovsky. Compactons and chaos in strongly nonlinear lattices. *Phys. Rev. E*, 79:026209, Feb 2009.

[97] K. Ahnert and A. Pikovsky. Traveling waves and compactons in phase oscillator lattices. *Chaos*, 18(3):037118–+, September 2008.

[98] Ernst Niebur, Heinz G. Schuster, Daniel M. Kammen, and Christof Koch. Oscillator-phase coupling for different two-dimensional network connectivities. *Phys. Rev. A*, 44:6895–6904, Nov 1991.

[99] Daniel Kammen Ernst Niebur, Heinz G.Shuster. Collective frequencies and metastability in networks of limit-cycle oscillators with time delay. *Physical Review Letters*, 67(20):2753–2756, November 1991.

[100] Yuri A. Kuznetsov. *Elements Of Applied Bifurcation Theory*. Number 112 in Applied Mathematical Sciences. Springer-Verlag, 1998.

[101] John David Crawford. Introduction to bifurcation theory. *Rev. Mod. Phys.*, 63:991–1037, Oct 1991.

[102] Steven Strogatz. *Nonlinear Dyanmics and Chaos*. Westview Press, 2000.

[103] Yuri A Kuznetsov. *Elements of Applied Bifurcation Theory*. Springer, 1998.

[104] I.S. Gradshteyn and I.M Ryzhik. *Tables of Integrals, Series and Products*. Academic Press, 2000.